Cell-type specific responses to antidepressants – the epigenetic makeup of the glia-neuron interface

DISSERTATION ZUR ERLANGUNG DES
DOKTORGRADES DER NATURWISSENSCHAFTEN (DR. RER. NAT.)
DER FAKULTÄT FÜR BIOLOGIE UND VORKLINISCHE MEDIZIN
DER UNIVERSITÄT REGENSBURG

vorgelegt von

Victoria Malik

aus Freising

im Jahr

2016

Das Promotionsgesuch wurde eingereicht am
10.06.2016

Die Arbeit wurde angeleitet von
Prof. Dr. Inga D. Neumann und Dr. Barbara Di Benedetto

_____

Unterschrift

Table of contents

Abstract

Understanding the neurobiological underpinnings of major depressive disorder (MDD) is of utmost importance. Recently, it was shown in post-mortem tissue of MDD patients that the number of glia cells is reduced, accompanied by atrophy of neuronal cells and a decreased volume of the prefrontal cortex (PFC). Following the observation that morphological deficits are present in both cell-types, it is likely that a misregulation in the communication between glia and neuronal cells might be one of the key factors underlying the development of MDD. Furthermore, the coverage of blood vessels by astrocytic endfeet has been shown to be reduced in MDD, implicating a misregulation also at the level of the glia-vasculature interface. A well-established approach to understand these deficits is the investigation of the molecular responses of neuronal cells to antidepressants (AD) in a cell-type specific manner. ADs have been shown to influence astrocytes as well as neurons and have been implicated in the regulation of gene expression via modulation of epigenetic modifications, like posttranslational histonemodifications (PTM).

To understand these molecular changes, I first investigated the expression pattern of several PTMs (H3K4me3, H3K27me3 and H3K27ac) both, on global and cell-type specific levels before and after treatment with fluoxetine (FLX), one of the most commonly used ADs, in high anxiety-related behavior (HAB) rats, serving as a well-established model for comorbid depressive-like behavior. I focused on the PFC, hence this brain area is known to be highly involved in depression in humans and animal models, although not much is known about epigenetic modifications in this area. For examining deeper cell-type specific changes and responses to ADs, I used both *in vitro* and *in vivo* models. In the present study I demonstrated that under baseline conditions, HAB rats resumed not only the human loss of glia cells in the PFC, but they also showed a putatively upregulated gene expression indicated by a 2-3 fold increase of H3K4me3, an activating PTM. I further showed that increased activation of H3K4me3 was specific of astrocytes and was targeted by FLX treatment. I additionally demonstrated that H3K27me3, a repressive mark which is supposed to be a counteracting partner of H3K4me3, is downregulated in HAB animals. Moreover, it decreased even further after FLX treatment, whereas H3K27ac, a permissive mark, was also decreased in HAB animals, which suggested that it might be a target of FLX, but after long term treatment. Together these data indicate a unique code of epigenetic modification in HAB rats under baseline

conditions that presumably can be altered by AD treatment. In course of this study, I was further able to identify, for the first time, an aberrantly high gene expression of ephrinA1, regulated by a high accumulation of H3K4me3 at its promoter, in HAB astrocytes as well as in the PFC of HAB rats, thus suggesting that this might represent a novel target of AD therapy in MDD. In view of the crucial role that the ephrin/Eph system plays at the glia-neuron interface to modulate synaptic transmission, its misregulation may very well lead to the development of depressive symptoms.

In addition, I identified GDF15, a neurotrophic factor, as a target of AD treatment *in vitro* and *in vivo*. My findings indicated that the ADs desipramine and FLX might induce increased expression of GDF15, leading to altered astrocytic morphology both in cell culture and around blood vessels of the PFC. An in-depth analysis revealed that FLX was specifically able to increase the sprouting of new processes as well as the elongation of preexisting ones, after a prolonged treatment in normal cells (derived from non-selectively bred animals, NAB), thereby also rescuing the morphology of the diseased HAB astrocytes, which showed a lack of processes with respect to NAB cells. These data corresponded to the *in vivo* findings in HAB rats, which show a reduced coverage of blood vessels with astrocytic processes. This deficit could be reversed by AD treatment. Moreover, I investigated the effects of exogenous GDF15 on astrocytic processes. Application of GDF15 was able to restore in HAB astrocytes both the number and length of processes in a dose- and time-dependent manner. Taken together, these data suggested that GDF15 might be involved in recovering a proper glia-vasculature interface that is needed for the proper exchanges of substances at the blood-brain-barrier.

Zusammenfassung

Es ist äußert wichtig die neurobiologischen Grundlagen einer Depression zu verstehen. Erst kürzlich konnte in postmortalem Gewebe gezeigt werden, dass depressive Patienten eine geringere Anzahl an Gliazellen, neuronale Atrophie sowie ein vermindertes Volumen des präfrontalen Kortex aufweisen. Da morphologische Veränderungen in diesen beiden Zelltypen auftreten ist es sehr wahrscheinlich, dass eine fehlerhafte Kommunikation zwischen Glia- und neuronalen Zellen eine Schlüsselrolle in der Entstehung einer Depression spielen könnte. Des Weiteren konnte gezeigt werden, dass die Blutgefäße in depressiven Patienten zu einem geringeren Ausmaße mit den Fortsätzen von Astrozyten bedeckt sind, was eine Deregulierung in diesem System bedeuten könnte. Ein gängiger Ansatz diese Defizite zu untersuchen, besteht darin die Reaktion dieser Systeme nach Behandlung mit Antidepressiva auf molekularer sowie zellspezifischer Ebene zu untersuchen. Antidepressiva können Astrozyten und Neurone beeinflussen und wurden bereits mit der Regulation von Genexpression mittels epigenetischer Modifikationen, wie beispielsweise posttranslationaler Histonmodifikationen (PTM) in Zusammenhang gebracht. Um diese molekularen Veränderungen zu verstehen, habe ich die Expressionsmuster verschiedener PTMs (H3K4me3, H3K27me3 und H3K27ac), vor und nach Behandlung mit Fluoxetin (FLX), auf globaler sowie zell-spezifischer Ebene untersucht. Als Tiermodell für diese Analyse habe ich high anxiety-related behavior (HAB) Ratten genutzt, die ein bereits gut etabliertes Tiermodel für Depression darstellen. Ich konzentrierte mich auf den präfrontalen Kortex, da diese Gehirnregion in der Pathophysiologie dieser Erkrankung sehr stark involviert ist, obwohl in diesem Areal bisher nur wenig über epigenetische Veränderungen bekannt ist. Um eine bessere Vergleichbarkeit zu erzielen, nutzte ich sowohl *in vitro* als auch *in vivo* Modelle. Mit der vorliegenden Studie konnte ich zeigen, dass HAB Ratten den humanen Phänotyp, welcher eine verringerten Anzahl an Glia Zellen aufweist, widerspiegeln, sowie dass diese Tiere eine vermeintlich gesteigerte Geneexpression haben, welche durch ein 2-3 fach höheres H3K4me3 Vorkommen angedeutet wird. Des Weiteren, konnte ich zeigen, dass die gesteigerte H3K4me3-Aktivität spezifisch in Astrozyten vorkommt und durch FLX Behandlung beeinflusst werden kann. Außerdem konnte ich zeigen, dass H3K27me3, eine repressive PTM, welche zudem vermutlich ein Gegenspieler von H3K4me3 ist, in HAB Ratten unter basalen Bedingungen herunterreguliert ist und durch eine längere FLX Behandlung sogar noch weiter reduziert wird. H3K27ac, eine aktivierende PTM, hingegen ist in HAB Ratten ebenfalls herunterreguliert und scheint durch eine längere FLX

Behandlung beeinflussbar zu sein. Zusammenfassend weisen meine Daten darauf hin, dass in HAB Ratten eine einzigartige Kombination dieser PTMs existiert, welche sehr wahrscheinlich durch Antidepressiva verändert werden kann. Im Zuge dieser Studie konnte ich ephrinA1, als ein Gen identifizieren, welches in HAB Astrozyten sowie im präfrontalem Kortex von HAB Ratten aufgrund eines gesteigertem H3K4me3 Vorkommens in dessen Promoter abnorm stark exprimiert wird. Diese Daten weisen darauf hin, dass ephrinA1 ein neues therapeutisches Ziel für die Behandlung einer Depression sein könnte. Eine Fehlregulation des Eph/ephrin Systems, welches maßgeblich an der synaptischen Übertragung zwischen Glia und neuronalen Zellen beteiligt ist, könnte zu den morphologischen Defiziten dieser Schnittstellen beitragen und letztendlich zu depressiven Symptomen führen.

Zudem konnte ich GDF15, einen neurotrophen Faktor, identifizieren, welcher durch Antidepressiva beeinflussbar ist. Meine Ergebnisse deuten darauf hin, dass die Expression von GDF15 in Astrozyten durch die Gabe von Antidepressiva gesteigert werden kann, was zu einer morphologischen Veränderung dieser Zellen führt. Eine detaillierte Analyse hat gezeigt, dass FLX das Entstehen neuer, sowie die Verlängerung bereits bestehender Astrozyten-Fortsätze in „gesunden“ Zellen begünstigt. In HAB Zellen scheint FLX die aberrante Morphologie der Astrozyten so zu verändern, dass sie dem „gesunden“ Phänotyp gleichen. Diese Daten korrespondieren zu den *in vivo* Experimenten, in denen gezeigt wurde, dass eine verringerter Abdeckung der Blutgefäße mit Astrozyten-Fortsätzen in HAB Ratten durch FLX Behandlung verbessert werden kann. Weiterführend habe ich zudem die Effekte von exogen verabreichtem GDF15 untersucht. Die Behandlung von Astrozyten mit exogenem GDF15 führt dazu, dass neue Fortsätze entstehen und bestehende verlängert werden. Dieser Effekt scheint von der Dosis und der Behandlungsdauer abhängig zu sein. Aufgrund dieser Daten lässt sich spekulieren, dass GDF15 vermutlich daran beteiligt ist die funktionelle Schnittstelle zwischen Gliazellen und den Blutgefäßen wiederherzustellen, um damit einen angemessen Austausch von Substanzen zwischen dem Blutstrom und dem Hirnparenchym zu gewährleisten.

1. Introduction

1.1. Major depressive disorder (MDD)

According to a recently published new data set by the world health organization (WHO [7]), unipolar disorder, also known as major depressive disorder (MDD), has become the leading cause of disability worldwide. Globally, over 350 million people of all ages are estimated to be affected by depression. MDD is a polygenic and multifactorial disease with a high lifetime prevalence, hence it is considered that one out of three people may suffer from depressive episodes during the life [8-10]. This disease is characterized by core symptoms of depressed mood and anhedonia, often accompanied by changes in body weight, loss of energy or pleasure, disturbances in sleep and cognitive functions [11, 12]. Especially the lack of specific biomarkers which might help to properly define the state of depression makes it very complicated to get a precise diagnosis. Moreover, the high comorbidity with other psychiatric illnesses, especially anxiety-related disorders, complicate a proper diagnosis even further [13]. Patients suffering from MDD also exhibit a markedly reduced lifespan, not necessarily due to concomitant suicide, but rather due to a well-documented increased risk of other life-threatening diseases, such as diabetes or cardiovascular disease [14]. Unfortunately, to date the most reliable criterion to diagnose/ categorize the state and severity of depression is based on questionnaires for the patients (DSM-Ⅴ, 2013), making a definite diagnosis dependent on subjective perceptions rather than on concrete pathophysiological evidences. Therefore, it is of utmost importance to understand the etiology and pathophysiology of MDD, its underlying molecular and additionally cell-type specific mechanisms to distinguish early on time people who might be prone to develop depression and to eventually being able to formulate a clearer diagnosis using specifically identified biomarkers. To approach these questions it is highly important to open new ways to identify novel targets and develop better and faster-acting therapeutics. Unfortunately, some of the major drawbacks in antidepressant (AD) therapy are still the high rate of non-responders (about 50-70%) and the delayed onset of amelioration of symptoms (4-12 weeks [15]).

1.2. Neuronal circuits involved in depression

Several limbic and cortical brain regions have been shown to play crucial roles in depression (see **Fig.1,** adapted from [2, 3]). These highly interconnected circuits involve brain structures that are important for interpreting and responding to stress and reward as well as cognitive functions [3, 16]. In the simplified scheme, one can see dopaminergic

neurons (blue arrows) projecting from the ventral tegmental area (VTA) to the nucleus accumbens (NAc) and hippocampus (HIPPO), among other areas. The NAc receives glutamatergic inputs (red arrows) from the prefrontal cortex (PFC), the HIPPO and amygdala (AMY) [2, 3, 16]. These interaction between the PFC and NAc are primarily part of the reward system and are implied in MDD [17]. Degeneration or lesions in these areas were found to increase the risk of patients to develop depressive episodes [18], while deep brain stimulation in the NAc and Cg25 (subcallosal cingulate gyrus) of treatment resistant patients successfully reduced depressive symptoms [19, 20]. With regard to these connections, it has been postulated that the PFC can exert regulatory effects on the NAc. Reciprocal connections between the PFC, especially the medial (m)PFC and AMY, via the uncinate fasciculus (black arrow, a long-range white matter association fiber-tract in the human brain, connecting the orbitofrontal cortex to the anterior temporal lobes through a direct, bidirectional monosynaptic pathway [21]) have been shown to exist in rats and non-human primates [22]. A reduction in the PFC-AMY connectivity has been suggested to play a role in MDD and it normalizes after drug treatment [23]. Another important area is the dorsal raphe nucleus (DR), which is the main site of serotonin (5-HT) synthesis in the brain. It receives glutamatergic inputs from the PFC [24], among which most of the projections terminate onto local GABAergic (γ-Aminobutyric acid) interneurons that inhibit 5-HT neurons, impacting neuronal excitability. Antidepressant treatment with, for example, selective-serotonin-reuptake inhibitors (SSRIs) might interact with these connections. Dysfunctional HIPPO-PFC interactions are known to play a central role in MDD, which is not surprising, considering the central role of the HIPPO in regulation of the hypothalamic-pituitary-adrenal (HPA) axis [25]. The HIPPO is also highly interconnected via glutamatergic projections to the NAc and AMY, which both play important roles in the formation of emotional memory [26]. So far, most studies focused on the HIPPO and NAc, but the PFC represents an emerging target in the pathophysiology of depression, whose implications still need to be explored thoroughly.

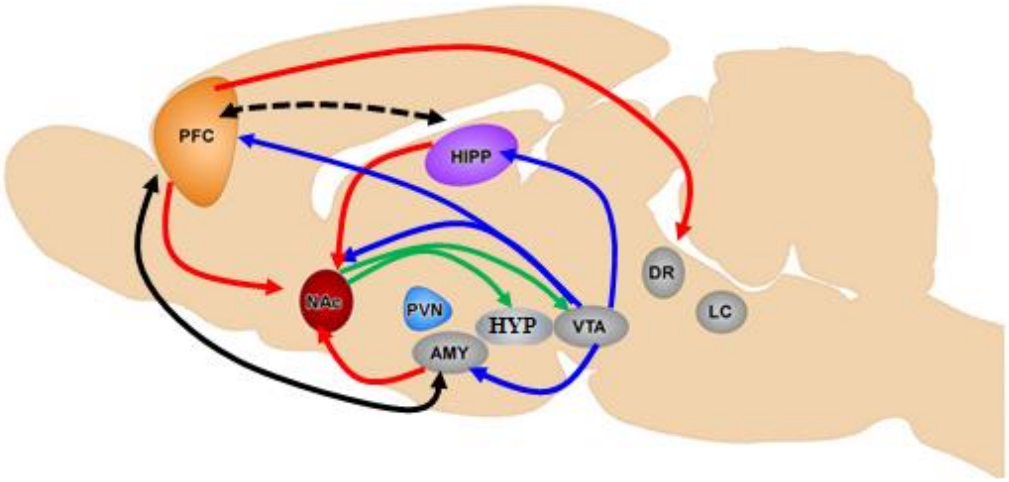

Fig. 1: Neuronal circuitries involved in depression (adapted from [2, 3])

Abbreviations: PFC = prefrontal cortex, AMY = amygdala, HIPP = hippocampus, NAc= Nucleus accumbens, PVN = paraventricular nucleus of hypothalamus, VTA = ventral tegmental area, HYP = Hypothalamus, DR= dorsal raphe nucleus, LC = locus coereleus. Blue arrows = dopaminergic neurons projecting from VTA, red arrows = glutamatergic projections to NAc, black arrows = grey matter connections, green arrows = GABAergic connections

1.3. Theories on the etiopathogenesis of depression

Since the discovery of the first ADs [27], many hypotheses have been developed to explain the pathophysiology of depression and the action of ADs. With the emerging of new research fields and advances in the understanding of this multifaceted disorder, the theories were refined and new perspectives were added. Nevertheless, to date, none of them is able to fully explain the development of MDD and how ADs work. Therefore, I will introduce the main hypotheses that developed over the past 60 years, specifically focusing on the most promising ones.

1.3.1. Monoamine hypothesis

The ´monoamine hypothesis´ of depression was the first one to be postulated [28], stating that depression is caused by a decrease in monoaminergic signaling in the brain. This assumption is based on clinical findings of the late 1950s. Back then, two structurally unrelated compounds originally developed for non-psychiatric diseases, namely ipronazid (for tuberculosis) and imipramine (IMI, for schizophrenia) were found to “enhance the mood” in patients treated with these drugs [29]. Both drugs were later proven to affect the monoaminergic system by enhancing the availability of 5-HT and noradrenalin (NA) transmission. Since then, several antidepressants have been developed, but most of them are still designed to intervene with the monoaminergic system, either by inhibiting neuronal re-uptake of 5-HT or NA (e.g. fluoxetine (FLX), a SSRI; reboxetine, a selective noradrenalin reuptake inhibitors (NRI); venlafaxine, a serotonin and noradrenalin reuptake

inhibitor (SNRI)) or by inhibiting their degradation (e.g. phenelzine, a monoamine oxidase A inhibitors (MAOI)) [11]. Although these compounds have been proven to be potent antidepressants, the simplified view that a sole monoamine deficiency is causing depression has been disproven. First of all, such substances increase the availably of monoamines on an acute basis, whereas behavioral amelioration requires several weeks. Moreover, a depletion of monoamines in animal models is not sufficient to elicit depressive symptoms [30]. Furthermore, illegal drugs like cocaine and amphetamines, which enhance the availability of serotonin, dopamine or norepinephrine do not seem to possess antidepressant effects. These data suggest that a dysregulation of the monoamine system is far from being the only factor which contributes to MDD.

1.3.2. Neurotrophic hypothesis

To target the question why antidepressants require several weeks of treatment before an amelioration of symptoms takes place, it was thought that an enhancement of monoamines in the synaptic cleft might lead to subsequent changes in neuroplasticity. As far as these changes are dependent on transcriptional and translational adaptations they might probably require a longer time scale, thereby explaining the delayed onset of ADs´ action. Together with data from post-mortem tissue and imaging studies, which showed structural alterations in several brain areas (e.g. PFC and HIPPO [31, 32]), this hypothesis proposes that depression might result from a decreased neurotrophic support, which in turn leads to neuronal atrophy (i.e. decreased dendritic arborization and synaptic contacts), a decreased hippocampal neurogenesis and glia cell loss, and that antidepressants are capable to block and/or reverse these deficits [33-35]. Among other neurotrophic factors (e.g. vascular endothelial growth factor, VEGF; insulin-like growth factor -2, IGF-2; fibroblast growth factor-1, FGF-1; glia-cell derived neurotrophic factor, GDNF), the most prominent and best-studied is brain-derived neurotrophic factor (BDNF) [34, 36-40]. Decreased levels of BDNF were found in post-mortem brain tissue as well as in the serum of depressed patients [34, 41]. Decreased levels of BDNF in specific brain areas are found in several animal models of stress-induced depression, thereby substantiating the human results [26, 34, 38]. Infusions of BDNF in relevant brain areas are sufficient to elicit AD-like effects, but these effects seem to be dependent on the respective brain area. While BDNF displays antidepressant properties in the HIPPO [42], it exerts pro-depressive effects in the NAc [43]. Additionally, depletion of BDNF is not sufficient to cause depressive symptoms in male knockout mice [44]. Pinning down the cause of depression to a single neurotrophic factor, like BDNF, might as well be too simplistic. However this theory raises awareness to

incorporate the fact that neurotrophic factors are involved in neuroplastic responses to stress and antidepressant treatment. Numerous studies have shown that stress and antidepressants evoke opposite effects on neurogenesis and neuronal complexity. This might be a possible explanation for the delayed onset of symptomatic improvement. Neurogenesis occurs in specific brain areas of the adult brain, the subventricular zone (SVZ) that gives rise to neurons of the olfactory bulb and the subgranular zone (SGZ) that generates granular cells of the dentate gyrus [45]. Different types of acute and chronic stress, both psychological and physiological, decrease neurogenesis [46], while several classes of antidepressants, including SSRIs (e.g. FLX) and SNRIs induce it [45, 47]. Nonetheless, inhibiting neurogenesis, via irradiation [47] or genetic manipulations is not sufficient to induce depressive-like behavior in rodents. Although this theory sheds light on some important mechanisms that need to be considered, it can neither explain why antidepressant efficacy varies greatly among patients (high rate of non-responder) nor does it consider differences in pathways between stress-induced depression and genetically determined ("endogenous") depression.

1.3.3. Glia cell hypothesis

Pioneering work by Rajkowska and colleagues extended the complex topic of depression even further [12, 31, 48]. Their work revealed tremendous glia cell impairment, with regard to both number and size, in post-mortem tissue of MDD patients [31, 49-51], thereby attracting notice to astrocytic abnormalities as a cause and/or consequence of depression. Additionally, several studies observed neuronal atrophy, displayed by smaller cell body sizes and reduced branching [31, 32, 50, 52], rather than complete loss of neurons. These results were substantiated by a study examining the serum of MDD patients for the amount of enolase 2 (a neuron-specific protein). The authors could not detect any difference in its expression, whereas the levels of S100β, an astrocyte specific marker, were elevated [53]. Furthermore, injecting a neuron-specific toxin (ibotenic acid) into the PFC of rodents did not cause any behavioral changes, while ablation of astrocytes (via L-alpha-aminoadipic acid (L-AAA)) was sufficient to induce a depressive-like behavior [54]. These data led to the suggestion that MDD might not primarily be caused by neuronal deficiencies but in first instance by alterations in astrocytes. In fact, astrocytes have been shown to play a pivotal role in synaptic transmission by physically stabilizing synapses and also by actively participating in the exchange of signaling molecules, such as diverse neurotrophic factors and glutamate, between the pre- and post-synaptic terminals. On the one hand, astrocytes enwrapping synapses can clear the synaptic cleft from excess of those

signaling molecules, on the other hand, they supply neurons with diverse neurotransmitters and nutrients, such as glucose [55-57]. In particular, astrocytes play an important role in regulating the release and reuptake of glutamate, which in high concentrations is detrimental for neuronal survival. Dysfunctional astrocytes may contribute to the development of MDD, as their buffering capacities on the glutamate system seem to be compromised, thereby leading to a consequential (not causal) loss of neurons [11, 58]. This hypothesis further suggests that antidepressants may act on the remaining astrocytes by increasing their number and reinstate a proper glia-neuron proportion via enhancing their proliferation through the release of glia-derived trophic factors [59]. Such neurotrophic factors released from astrocytes (e.g. BDNF and GDNF) can signal back to neurons, which in turn are capable to control presynaptic activity through regulation of factors responsible for neuronal survival and maturation [11]. Indeed, those neurotrophic factors play an important role in the neurogenic response to antidepressants. They have been shown to be beneficial in restoring the physiological state of neuronal branching that is reduced under pathological conditions [60, 61]. Antidepressants can also directly act on astrocytes. Several classes of antidepressants activate specifically the ERK/MAPK (extracellular signal–regulated kinases/mitogen-activated protein kinase) pathway, whose downstream effectors are, among others, GDNF and BDNF [57, 62, 63].

Further supporting the role of glia cells in response to antidepressants is the involvement of the blood brain barrier (BBB) in the uptake of clinically efficient dosages of drugs.

The BBB is most tightly regulated by astrocytic endfeet, which surround and interact with blood vessels, thus controlling the passage of exogenous substances in and out of the brain. Very recently it has been shown that in MDD patients, blood vessels of the prefrontal cortex (PFC) lack the coverage with Aqp-4 (aquaporin-4)-positive endfeet of astrocytes [12]. A finding that was reproduced by our group in an animal model of depressive-like behavior (see below **1.11**) [51]. Furthermore, we could show that Aqp-4 is necessary to mediate antidepressant effects on restoring a basal amount of astrocytic processes in astrocytes derived from the PFC of an animal model for depression. Considering these facts about astrocytes as cause and/or consequence of MDD and their responses to antidepressant treatment, it makes them a highly interesting target to study in order to elucidate molecular underpinnings of depression.

1.3.4. Epigenetic hypothesis

Over the past decade several epigenetic mechanisms have been identified as important effectors of psychiatric diseases [3, 16, 64, 65]. It is known that depression can, at least partially, be inherited (heritability around 40% in familial cases [66]), nevertheless so far only very few genetic variants could be robustly correlated with depression. Additionally, the high discordance rate in monozygotic twins cannot be explained by pure genetic underpinnings. Therefore, the combination of genes with environment came into the spotlight of research. Indeed, epigenetic mechanisms are ideal candidates to study mental diseases that are caused by interaction of genetic factors (predisposition) and environmental exposure. Several lines of evidence have linked alterations in PTMs, DNA methylation and non-coding RNAs to psychiatric diseases. It is proposed that misbalances in such a delicate system of epigenetic modifications can severely impact brain functions. Various animal models of stress-induced depression and early life experiences demonstrated aberrant histonemodification, leading to changes in gene expression. The glucocorticoid receptor (GR) is one of these candidates, whose expression is altered in offspring derived from low maternal care mothers [67], regulated by DNA methylation. This effect could be reversed by application of histone-deacetylase inhibitors (HDACi), suggesting a crosstalk between epigenetic mechanisms. HDACi can also exert antidepressant-like effects dependent on the brain area. Besides acetylation, several other PTMs occur to play a role in MDD, foremost methylation of different histones (see below). For example elevate levels of a specific activating PTM (histone 3-lysine 4-trimethylation, H3K4me3), were found at the synapsin promoter in the PFC of depressed patients [68], whereas histone 3-lysine 27-trimethylation (H3K27me3, repressive) levels are increased at certain BDNF promoters in the PFC and both can be reversed by AD treatment. Research has only begun to understand how epigenetic modifications influence the outcome of MDD and how to target inter-individuals differences. Understanding the interplay of a potential predisposition interacting with environmental circumstances on the development of psychiatric diseases needs more detailed analysis to identify how epigenetic regulation impacts specific genes or gene networks related to depression. Keeping these hypotheses in mind, it seems valid to take a closer look at the different levels and at their functions under physiological and pathological conditions.

1.4. Astrocytes

In the 1850s the term “Nervenkitt” (i.e. “brain glue”) was first introduced by the pathologist Rudolf Virchow. He defined neuroglia cells as small round-shaped cells that fill up the extracellular space as parts of the connective tissue. Although the term neuroglia still persists, to date especially the definition of astrocytes has changed drastically [69]. With the rise of more elaborate techniques than a simple Nissl staining, it is now well accepted that astrocytes are a highly heterogeneous cell population with numerous functions in the brain [70].

Glia cells are considered to be the most abundant cell-type in the mammalian CNS (central nervous system) [71]. A comprehensive study by Pelvig and colleagues [72] quantified the number of neurons and glia cells in the neocortex of adult humans. Their results show that the total number of glia cells ranges between 27.9 billion (females) and 38.9 billion (males), while the total number of neurons only ranks between 21.4 billion (females) to 26.3 billion (males), providing a 1.3-1.5 glia/neuron ratio. With about an average of 75%, oligodendrocytes account for the majority of glia cells, followed by astrocytes (20%) and microglia cell (5%).

1.5. Lineage of astrocytes

Gliogenesis is the generation of astrocytes and oligodendrocytes, which starts in the late embryonic development and continues during the neonatal and postnatal period. The cerebral cortex is one of best documented brain regions for gliogenesis. Astrocytes derive from three different sources. As depicted in **Fig. 2,** they derive from (1) radial glia cells in the embryonic ventricular zone (VZ), (2) progenitors in the postnatal SVZ and (3) probably another lineage determined by glia-restricted precursors.

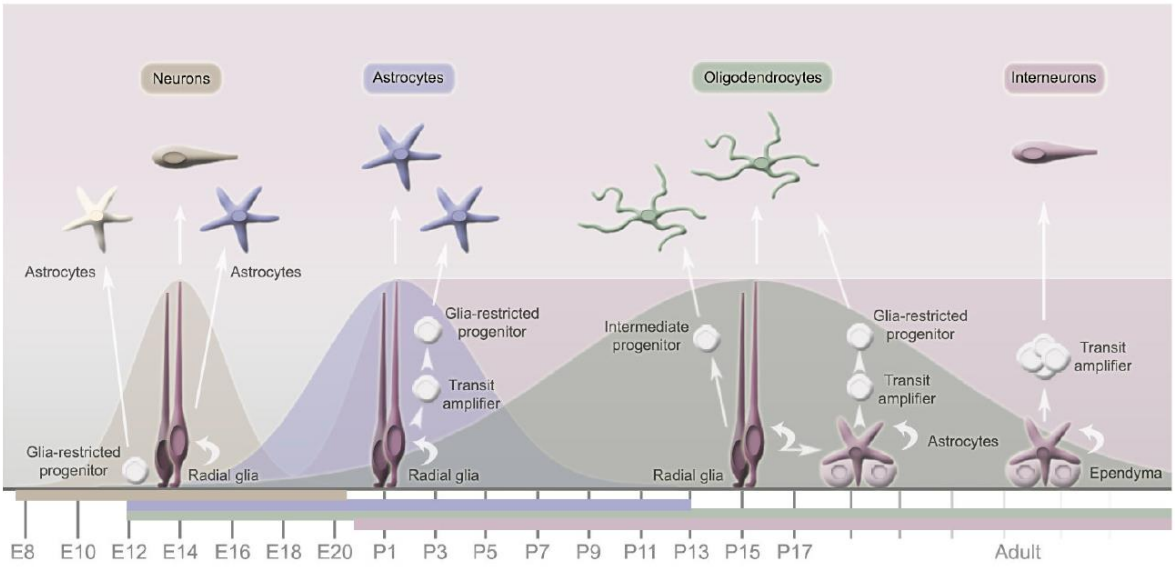

Fig. 2: Diagram summarizing different lineages of neuron glia development [69]

Radial glia cells originate from the early transformation of neuroepithelial cells in the VZ. They have the potential to generate both neurons and astrocytes [73]. After a period of neuronal migration along radial fibers, these cells retract their processes and transform into star-shaped astrocytes during the perinatal period [74]. They can further develop into specialized astrocytes, e.g. Bergmann glia in the cerebellum.

In the early neonatal period radial progenitor cells can generate intermediate progenitors before transforming into astrocytes of the SVZ. These intermediate progenitors migrate into the cortex and differentiate into mature astrocytes or oligodendrocytes [69].

Recent studies suggest the existence of multipotent, bi-potential progenitor [75] cells and possibly glia-restricted progenitors in the neonatal SVZ [76], though these multipotent progenitors need to be further investigated.

1.5.1. Characterization

Astrocytes, originally named after their star-shaped appearance, are defined as process-bearing cells that lack axons and dendrites and are distributed throughout the CNS [69]. But the different astrocytic lineages already indicate that these cells are highly heterogeneous and that it is not easy to distinguish all sub-populations by a single criterion. For this reason, I will elucidate the most important criteria how astrocytes can be characterized.

a. Morphology

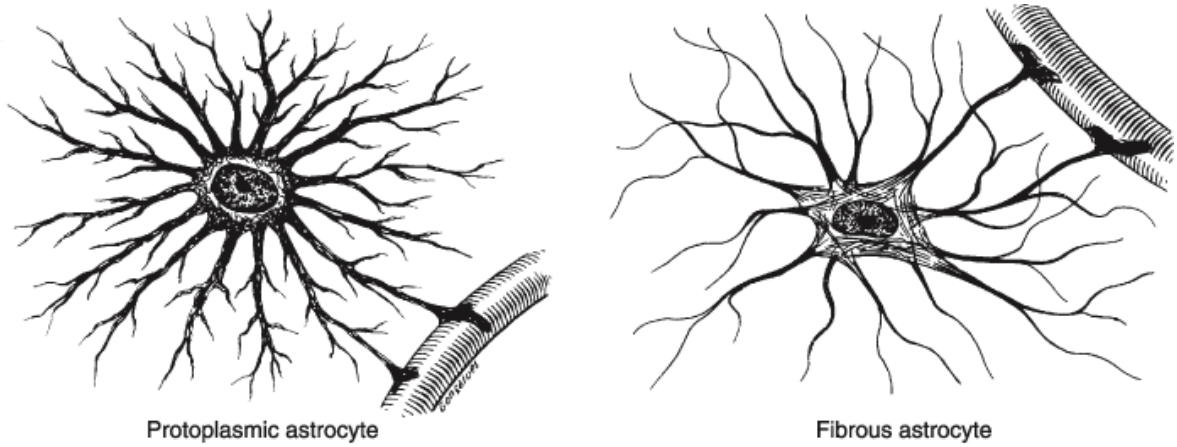

Fig. 3: schematic illustration of protoplasmic and fibrous astrocytes [77]

In general astrocytes can be distinguished by their particular location and morphology. **Protoplasmic astrocytes** (**Fig. 3**) are found in the grey matter and mainly derive from embryonic radial glia cell (to a lesser extent also from intermediate progenitors). These astrocytes are characterized by their numerous, highly branched processes (~50µm length) that envelop synapses. They can also contact blood vessels via their so-called ´perivascular endfeet´.

Fibrous astrocytes (Fig. 3), on the other hand, are mostly found in the white matter. They are predominantly derived from SVZ progenitors. Their characteristic morphology encompasses long (up to 300µm), thin and widely unbranched processes, with endfeet enveloping the nodes of Ranvier [78]. With their processes, astrocytes are capable to infiltrate neuronal networks including synaptic terminals, dendrites and dendritic spines, though the degree of synaptic ensheathment varies greatly among brain areas. In the HIPPO only 57% of synapses have astrocytic processes opposing them, and among those only half surround the synaptic interface [79]. Such an arrangement might allow a certain degree of neurotransmitter spillover between synapses. Whereas in the cerebellum the degree of ensheathment can be as high as 94% in climbing fibers, which are sending excitatory inputs to Purkinje cells [69]. Recent studies have elucidated the organization within mature astrocytes, suggesting that they may consist of hundreds of independent compartments, each capable to interact autonomously with the ensheathed synapse. This high degree of compartmentalization allows them to communicate with synapses in a one-to-one manner which may be necessary hence a single astrocytes can contact over 100,000 synapses at once [80]. This work also led to a reevaluation of astrocytic morphology away

from the star-shaped appearance to a more spongiform one, with dense ramifications of fine processes extending 2-10 µm from the main branches.

b. Antigenic properties

Another commonly used approach to identify astrocytes is via their expression of diverse markers. The major component of their cytoskeletal intermediate filaments is the glial fibrillary acidic protein (GFAP), which is strongly expressed in mature and reactive astrocytes [81]. To date, eight different isoforms of GFAP have been identified to distinguish specific subpopulations of astrocytes during development, aging and disease. But GFAP is not exclusively expressed in astrocytes. Cells derived from radial glia progenitor cells, like ependymal cells, which do not belong to the astrocytic family, also express GFAP [82]. Consequently, it seems necessary to include other markers in the characterization of astrocytes. S100β is another commonly used marker, which belongs to the family of calcium binding proteins and is predominantly expressed in astrocytes of the grey matter [83]. Other markers which are considered to be exclusively expressed in astrocytes are glutamate transporters, such as the glutamate aspartate transporter-1 (GLAST-1) and the glutamate transporter (GLT-1) (equivalent to human EAAT1 and EAAT2) [84], glycogen granules and glutamine synthase (GS), an enzyme that catalyzes the conversion of ammonia and glutamate into glutamine [85]. In addition some channels, including Kir 4.1, an inwardly rectifying K^+ channels and Aqp-4 (water channel) and the most recently identified aldehyde dehydrogenase family, member 1 (AldhL1), represent possible candidates to identify specific astrocytic populations.

c. Receptors

Furthermore, astrocytes express virtually all receptors of the major neurotransmitter systems, including the glutamatergic, GABAergic, serotonergic, dopaminergic, acetylcolinergic and purinergic ones [86]. Astrocytes also express receptors for growth factors, chemokines, steroids and receptors involved in the innate immune response [69]. It is also important to take into account that astrocytes can modify their receptor expression according to the environmental surrounding, e.g. after brain injury astrocytes express EGF (ependymal growth factor) receptors, which can trigger resting astrocytes to become reactive [87]. This high degree of adaptability is very interesting to study the roles of astrocytes in a variety of psychiatric disorders.

1.6. Astrocyte activity

Astrocytes were long considered as non-excitable cells, because their activity cannot be measured by electrophysiological recordings. However, astrocytes exhibit regulated increases in intracellular calcium concentrations that represents a form of excitability [88]. By now, a large body of evidence suggests, that these intracellular oscillations are of functional significance in astrocyte-astrocyte and astrocyte-neuron communication. Astrocytes respond to synaptic activity with increases in cytosolic Ca^{2+}. These Ca^{2+} elevations occur as intrinsic oscillations resulting from calcium release of internal stores triggered by glutamate, which is released during neuronal activity and might reach astrocytic receptors through synaptic spillover or ectopic release [89]. Thereby, astrocytes can trigger receptor mediated currents of neighboring cells [71]. This mode of excitability has been implicated in direct roles on synaptic transmission and in the functions at the vasculature [90] as well as in response to antidepressant treatment [91].

1.7. Functions of astrocytes

In the CNS astrocytes display a great variety of functions, which, next to metabolic support, include promoting neuronal maturation and survival, synapse formation, regulating angiogenesis and maintenance of a viable microenvironment for neurons.

1.7.1. Metabolic support

The most accepted functions of astrocytes include the maintenance and support of neuronal development. Astrocytes represent the major source of adhesion molecules and proteins of the extracellular matrix (ECM). Cultured astrocytes can act bi-directionally depending on the surrounding environment and constitution of the ECM, either promoting or inhibiting neurite outgrowth. Growth-promoting factors include laminin, N-cadherin, fibronectin and NCAM (neural cell adhesion molecule). Moreover, they also express inhibitory proteoglycans and synthesize/secrete proteolytic enzymes, like MMPs (matrix metalloproteases) that play important roles in degradation and remodeling of the ECM [92]. *In vitro* studies have well characterized the growth factors released from astrocytes, including BDNF, FGF, nerve growth factor (NGF), neurotrophin-3 (NT-3) and GDNF. All of them control neuronal maturation, survival and differentiation, some via Ca^{2+} - dependent pathways.

Due to their close proximity to blood vessels, neuronal axons, perikarya and synapses, astrocytes are in a superior position to take up metabolites (e.g. glucose) and provide them to different neuronal elements in the brain. Compelling evidence demonstrates that

astrocytic glycogen utilization can sustain neuronal activity during hypoglycemia and periods of high neuronal activity [93].

Furthermore, astrocytes can buffer extracellular K^+ ions that are released during neuronal activity, but can elicit detrimental effects when present in too high concentrations. Astrocytes can take up the excessed K^+, distribute them through the gap junction-coupled astrocyte syncytium and extrude the ions at sites with lower K^+. To exert these regulatory mechanisms astrocytes possess channels and co-transporters (for a passive uptake) as well as Na^+/K^+ - ATPases for active transport. Passive uptake is mainly mediated by K^+ channels (Kir) expressed at their endfeet. Blockade of Kir channels (e.g. Kir4.1) results in depolarization of astrocytes. This in turn leads to impaired K^+ buffering, glutamate uptake and thereby possibly to behavioral abnormalities [94, 95].

1.7.2. The blood-brain barrier

The BBB is a specialized system that regulates the penetration of molecules in and out of the brain parenchyma. The major constituents of the BBB are cerebral capillary endothelial cells that form tight junctions and are surrounded by a basal lamina, perivascular pericytes and astrocytic endfeet. Together they form close connections with capillaries, thus making astrocytes the primary target of any molecule entering the brain [96]. During development, astrocytes contribute to the tightening of the BBB and the up-regulation of different transporter mechanisms. Several astrocytic signals that regulate various aspects of BBB properties have been identified, including transforming growth factor-β (TGF-β), GDNF, FGF, interleukin- 6 (IL-6) and Aqp-4 [12, 51]. The release of these molecules opens the paracellular pathway by increasing the permeability of tight junction, indicating that astrocytes are involved in regulating the BBB by cross-talk with endothelial cells, possibly upon Ca^{2+} and ATP receptor mediated signaling. Interestingly, components of the BBB have been implicated to play a role in depression and in response to antidepressants (see below).

1.7.3. GABA and Glutamate

Astrocytes express a high density of high affinity GABA transporters, which are located near the synaptic cleft, most likely controlling GABA spillover from the cleft either alone or together with neuronal transporters. Just recently, astrocytes were also indicated as GABA-releasing cells. This release is proposed to occur through different pathways: (1) vesicular release, (2) reversal of GABA transporters and (3) non-vesicular channel mediated release [97]. But the identification of the true mechanism still needs to be determined.

Astrocytes also express glutamate transporters, including GLAST (in human EAAT1) and GLT-1 (in human EAAT-2) suggesting active participation in the uptake, metabolism and recycling of glutamate. Glutamate is internalized and subsequently converted within the astrocytes to glutamine via the GS [85]. The newly synthesized glutamine is released by astrocytes, taken up by neurons and can be converted to glutamate or GABA.

The regulation of extracellular levels of these transmitters by astrocytes has raised an avalanche of new studies investigating its function in health and disease.

1.7.4. Neurotransmission and synapses

It is well established that astrocytes sense neuronal activity through activation of ion channels, transporters and receptors, resulting in fast depolarization and/or intracellular calcium increases [98]. Calcium transients can be induced following the activation of different metabotropic receptors. It was shown that astrocytic depolarizations following neuronal stimulation is involved in short-term plasticity [90]. These findings indicate that astrocytes have the capability to process and integrate information in response to neuronal activity.

In fact, with the postulation of the tripartite synapse [90], it became clearer that astrocytes actively participate in the regulation of synapses. Using-time lapse confocal microscopy Haber and colleagues demonstrated that astrocytes can rapidly extend or retract fine processes to and from postsynaptic dendritic spines [99], suggesting a possible involvement in synaptic plasticity [100]. At the synaptic level, astrocytes contribute to the regulation of synaptic and extrasynaptic transmission [101]. In particular they control the level of activation of presynaptic metabotropic glutamate receptors on glutamatergic terminals, thereby regulating the strength of excitatory synapses. Astrocytes seem to be directly involved in dendritic spine formation, shown by a study using astrocyte-conditioned medium, which promotes proliferation of spines [102]. Furthermore, Nishida and Okabe could show that astrocytic motility is essential to stabilize individual dendritic protrusions and their subsequent maturation into spines [103]. Additionally, they could show that manipulations of the ephrin/Eph dependent neuron-astrocytes signaling suggest the involvement of this pathway in astrocyte-dependent stabilization of newly dendritic protrusion.

1.8. Astrocytes in depression

Considering the multiple functions of astrocytes under physiological conditions, a fruitful research field opened, examining possible functions in various neuropathological diseases.

A major branch of these studies is dedicated to the involvement of astrocytes in psychiatric disorders like MDD. In the following section I will focus on the findings implicating astrocytes as a cause and/or consequence in the development of MDD, based on aberrancies from the physiological state.

1.8.1. Morphometric evidence

Groundbreaking work in 1999 by Rajkowska and independently also by Öngür revealed that the observed volumetric changes in post-mortem tissue of MDD patients are most likely not caused by neuronal cell loss, but rather occur due to the loss of glia cells [31, 104]. 3D cell counting approaches identified that neurons are indeed affected in depression, but it is rather a shrinkage or morphological atrophy than a complete loss, as observed in neurodegenerative diseases, like Huntington´s disease. A reduction of glia cell density in the PFC is accompanied by enlargement of glia cell bodies, making this combination a unique patter for MDD, hence typically enlargement of glia cell bodies occurs together with increased glia cell density [31, 104]. The significantly reduced cortical thickness in MDD is possibly related to decreased metabolic support in response to neuronal activity, implying an extremely important function of astrocytes in MDD. These studies were the first to implicate glia cells in the histopathology of depression, opening new insights into the underlying neurobiological mechanisms. Since then, the knowledge about morphological aberrancies in depression greatly enhanced. Using animal models, it became possible to investigate underlying mechanism of neuronal atrophy and glia cell loss. Chronic stress paradigms or application of glucocorticoids decreased the number and length of apical dendrites in hippocampal CA3 pyramidal neurons of tree shrews and reduced neurogenesis [105]. Moreover, adult rats subjected to chronic unpredictable stress (CUS) exhibit a reduction in glia cells in the prelimbic cortex and selective ablation of glia cells, by using astrocyte specific L-AAA, but not neuronal toxins is sufficient to induce depression-like behavior [54]. Together these findings indicate that stress paradigms might provide a cellular basis for the astrocytic impairments seen in MDD patients [106].

In 2011 a post-mortem study investigated further the exact morphological alterations in cortical astrocytes, comparing healthy subjects to depressed suicide completers [52].

Fibrous astrocytes of the Brodmann area 24 in suicide completers were found to be larger and to extend longer and more ramified processes than in matched controls, shedding light on selective cellular changes occurring in the white matter in depression, independently from adjacent protoplasmic astrocytes of the grey matter. These hypertrophic fibrous astrocytes might reflect local inflammatory processes on the white matter, suggesting

neuroinflammatory processes among additional causes of depression [107]. It has been documented that MDD patients have significantly higher levels of circulating pro-inflammatory cytokines and that these cytokines are implicated in stress-induced depressive symptoms [108]. Previous studies demonstrated a significant reduction in the number of astrocytes (in HIPPO) after chronic social stress. This loss of glia cells could be reversed by chronic FLX treatment [109]. Data suggest that antidepressants might enhance gliogenesis. Pronounced gliogenesis has been observed after electroconvulsive therapy in the HIPPO and PFC, as well as after FLX treatment in animals [59, 110].

1.8.2. Antidepressants act on astrocytes

Knowing about the drawbacks of current antidepressant treatment options, several groups independently analyzed transcriptional and translational changes with unbiased approaches to reveal common molecular targets of different antidepressants [111, 112]. Interestingly, they found pronounced up- or down-regulation of astrocyte associated genes like GFAP, Aqp-4 and vimentin, whereas others reported upregulation of connexin 43 (a major component of astrocytic gap junctions) in the PFC upon chronic FLX or clozapine treatment, whereas non-antidepressants (lithium, haloperidol) showed opposite effects [113]. Furthermore, astrocytes release several trophic factors and cytokines which have been hypothesized to be misregulated in depression. For example, stress-induced reduction of GFAP and GDNF expression in the HIPPO could be reversed by clomipramine (a tricyclic antidepressant) in a rodent model of depressive-like behavior [114]. Additionally, other trophic factors are affected by antidepressants. In primary cortical astrocytes, treatment with the SSRIs FLX and paroxetine caused a pronounced up-regulation of BDNF, VEGF and VGF mRNA expression [115], although tricyclic antidepressants (IMI, desipramine) did not affect these factors.

We and other groups have identified the ERK/MAPK pathway as a common target in glial cells for most antidepressants [57, 62, 63]. FLX and several other classes of antidepressants applied to primary rat astrocytes or C6 glioma cells (a model cell line for astrocytes) *in vitro* targeted the MAPK signaling pathway and induced specific downstream effects on BDNF, GDNF and their respective receptors TrkB and GFRα. Furthermore, in our lab we could show that reboxetine and norquetiapine (the major metabolite of a recently approved antidepressant) activate simultaneously ERK1 and ERK2, with a subsequent increased release of GDNF [116]. A recent study demonstrated a differential epigenetic status of the GDNF gene that is responsible for susceptibility vs. resilience to chronic stress [117]; the authors demonstrated that IMI could reverse these

effects, indicating a possible underlying mechanism of an increased GDNF expression after antidepressant treatment. These data led to the suggestion that interfering with the MAPK pathway specifically in astrocytes may allow a faster response to antidepressants.

Given the plethora of divergent receptors expressed on astrocyte, many of which have already been implicated in depression, it became very interesting to investigate their contribution in response to antidepressants. FLX and nortriptyline were shown to block Kir4.1, an astrocytic inwardly rectifying K^+ channel, responsible for potassium buffering in astrocytes [94, 118], a highly interesting finding since potassium channels have been implicated in the pathophysiology of mood disorders in human and animal models [119].

Among the receptors expressed on astrocytes, also glutamate and GABA receptors have been implicated in the pathophysiology of mood disorders. Post-mortem microarray studies in the locus coereleus and cortical areas of depressed patients revealed significant changes in the expression of proteins involved in glutamate homeostasis, some of which are highly associated with astrocytes [120]. Central or region-specific injections of dihydrokainic acid, an inhibitor of GLT-1, cause anhedonia and cognitive impairments similar to depressive symptoms [121]. In a stress paradigm the observed depressive-like phenotype, accompanied by impaired glia cell metabolism in the PFC, could be restored by riluzole, a glutamate-modulating drug [122], enhancing the glutamate uptake from the extracellular space (ECS) by astrocytes. Compelling evidence demonstrated that the glutamatergic and GABAergic systems are involved in MDD and in response to antidepressants presumably via activation and/or inhibition of astrocytes.

Astrocytes are excitable by Ca^{2+} oscillations resulting in the release of glutamate into the ECS, thereby triggering receptor mediated currents in neurons [90]. Two SSRIs (FLX and citalopram) have been shown to elicit calcium signals in the PFC of acute mouse brain slices, even if neuronal signal propagation is inhibited. The intracellular calcium signaling is involved in the regulation of numerous essential functions, therefore it seem highly important to investigate the calcium signaling propagation in astrocytes under pathological conditions.

Astrocytic processes, as part of the tripartite synapse, actively participate in the modulation of synaptic transmission, in response to environmental cues [90, 100]. Synaptic plasticity is one of the most fundamental functions in the CNS, playing a key role in memory processing, specifically short- and long-term memory, and the disruption of underlying mechanisms has been implicated in depression. Post-mortem studies found reduced numbers of synapses in the PFC of depressed patients [123]. Chronic administration of

MAOIs increase the levels of monoamines in the synaptic cleft and can thereby interfere with neurotransmission on different levels, including neurogenesis, neurotrophic factor expression and synapse formation. Chronic FLX treatment has been shown to ´rejuvenile´ the adult brain via the re-opening of the so-called critical period of postnatal development. In the ocular dominance paradigm, Maya Vetencourt and colleagues demonstrated that FLX is able to induce recovery of visual functions of the deprived eye through reactivation of the neuroplastic program [124]. Similar observations were made in the amygdala, where it has been shown that FLX can change the fate of neuronal circuits, important for fear conditioning. In both studies BDNF was implicated in the effects of FLX [125]. Moreover, there is evidence that chronic FLX treatment can increase spine density and block the effects of chronic stress [126, 127].

Further implications of effects of ADs on astrocytes come from the aforementioned work by Rajkowska and colleagues [12, 128], which demonstrated that the coverage of blood vessels by astrocytic endfeet is significantly reduced in MDD patients. But this reduction was only observed in astrocytic processes immunoreactive for Aqp-4 in the grey matter. Just recently our group could substantiate these finding in high anxiety-related behavior (HAB) animals, further validating HAB rats as a good model for depression [51].

Aqp-4, as mentioned above is the predominant water channel in the adult CNS and is primarily expressed on the endfeet of astrocytes [129]. It balances K^+ -buffering in astrocytes [130] and has been in implicated as a mediator of antidepressant efficacy and as protective factor against corticosterone-induced depressive-like behavior, which is accompanied by an astrocyte pathology [105, 131]. Furthermore, Aqp-4 plays a role in regulating adult neurogenesis [132] and is necessary for FLX induced neurogenesis, thus making Aqp-4 in astrocytes a new target for the mechanism of action of antidepressants. The decrease in Aqp-4^+ -positive astrocytic endfeet might have many consequences. The decreased number might reduce the effective surface for exchanges with the blood circulation, thereby putatively regulating the uptake of antidepressants from the blood stream. Thus, possibly explaining the slow onset of AD efficacy, as far as first the BBB needs to recover a proper coverage with astrocytic processes before clinically effective dosages of ADs can be transported into the brain parenchyma. Therefore we examined further if FLX causes morphological alterations in our animal model.

Our data [51], together with the observation in humans [31], support the link between cerebrovascular pathology and MDD, providing the first links at the cellular level.

Taken together, the findings that antidepressants can directly target several astrocytic functions as the regulation and availability of neurotransmitters (GABA, glutamate), the regulation of metabolic homeostasis and are involved in regulation at the level of the BBB and synapses, make them promising target to study mechanisms underlying the effects of ADs.

1.9. Epigenetic mechanism

Originally, the term epigenetics was defined by Conrad Waddington [133] as "the interaction of genes with their environment which brings the phenotype into being", stating further "the importance of epigenetic modifications as being a mechanism for an adaptive response that can be fixed without waiting for a mutation to occur".

More recent definitions describe epigenetic modifications as an "ensemble of alterations in gene functions that are heritable through both mitosis and meiosis, but cannot be explained by changes in the DNA sequence itself" [134]. On the molecular level, epigenetic mechanisms represent biochemical modifications of the DNA and histone proteins which are the major constituents of chromatin. Histones (**Fig. 4**) consist of a basic protein core octamer encompassing two copies of each histone (H2A, H2B, H3 and H4), and an N-terminal histone tail composed of loosely-structured sequences of amino acids. 147bp of DNA are wrapped around the core, typically linked to the next nucleosome via an H1-linker histone.

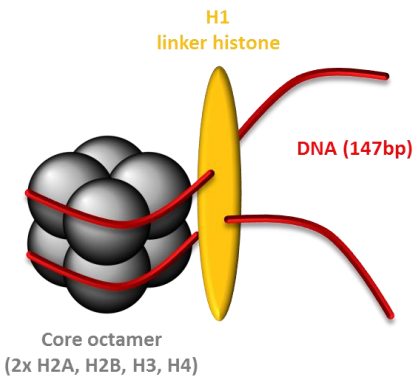

Fig. 4: The nucleosome is the major constituent of chromatin

The nucleosome core consists of 147bp of DNA wrapped around a core octamer consisting of two copies of each histone H2A, H2B, H3 and H4. The nucleosomes are linked via a H1-linker histone.

Posttranslational modifications occur on virtually all amino acids of the N-terminus, controlling the spacing between nucleosomes and degree of condensation, thereby determining access of the transcriptional machinery to the DNA, and ultimately

determining the degree of gene activity. Generally spoken, chromatin consists of a continuum between inactivated, highly condensed heterochromatin, and open, easily accessible, euchromatin (**Fig. 5**).

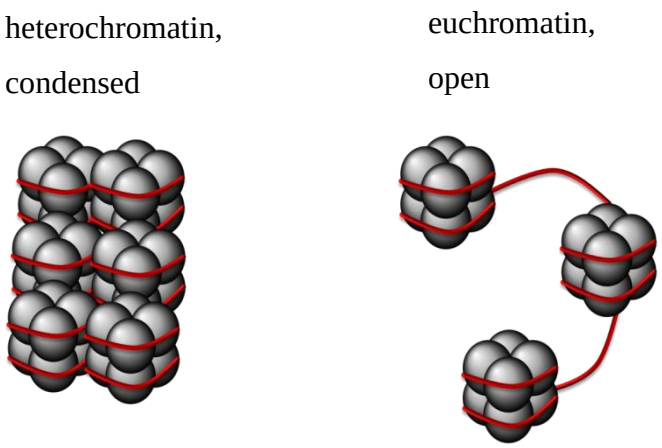

Fig. 5: Highly condensed heterochromatin and easily accessible euchromatin

These chromatin states determine gene activity in a highly regulated manner by complex biochemical processes. In general, there are three major epigenetic mechanisms that can be clearly distinguished: 1. DNA methylation, 2. non-coding RNA and 3. posttranslational histonemodifications. Only very little is known about non-coding RNAs in psychiatric diseases, therefore I will focus mainly on PTMs with a short overview about DNA methylation.

1.9.1. DNA methylation

DNA methylation occurs throughout the genome, but predominantly at so-called CpG islands (i.e. cytosine-guanine dyads [5]), often found at promoter regions. Due to the covalent binding of methyl-groups at the C_5 carbon in cytosine projecting into the major groove of DNA, DNA methylation is thought to be the most stable epigenetic mark [135] which can persist throughout the lifetime. In the human genome approximately 3% of all cytosines are methylated and this methylation is highly involved in cell differentiation, genetic imprinting, suppression of repetitive elements and X-chromosomal inactivation. DNA methylation is catalyzed by DNA-methyltransferases (DNMTs) including DNMT1 DNMT2, DNMT3a, and DNMT3b [136], which play very distinct roles. DNMT1 is also known as the ´maintenance methyltransferase´ that perpetuates DNA methylation during replication, whereas DNMT3a and 3b catalyze ´*de novo*´ methylation at the unmehtylated

DNA double-strand. Although generally considered to be gene silencing, DNA methylation has been shown to exert also gene activating effects, depending on the recruitment of other transcription factors. Nearly 80 different transcription factors are known to interact with DNMTs [137]. For example, interaction with methyl-CpG-binding proteins (MeCP) can further recruit modifying enzymes to compact nucleosomes and inhibit gene expression. Moreover, additional studies identified more forms of DNA methylation such as 5-hmC (5-hydroxymehtylcytosine), 5-formylcytosine and 5-carboxylcytosine. These chemical variant of 5-mC are thought to derive through oxidation steps catalyzed by TET (ten-eleven-translocation) enzymes, representing a mechanism of active demethylation. Together these findings indicate that DNA methylation is rather a highly dynamic, especially in the brain, than a permanent modification.

1.9.2. Posttranslational histonemodification

More than 100-amino acid residue-specific PTMs are known in vertebrae cells [138, 139]. These modifications include mono-, di- and tri- methylation, acetylation, phosphorylation, ubiquitination, sumoylation and several recently found additional types, like crotonylation and succinylation [138, 139]. The best studied modifications are the ones occurring on histone tails, but several new modifications were identified also on the globular domains of histones, which are not yet functionally characterized. Here, I will focus on acetylation and methylation, with only briefly mentioning phosphorylation and ubiquitination.

a. Acetylation

Acetylation occurs mainly on lysine (K) residues and is associated with active gene transcription (permissive mark), by neutralizing the positive charge of the ε-amino group. This event causes a decrease in the affinity to the DNA (negatively charged) and leads to less condensed, more easily accessible chromatin. Histones are acetylated by HAT (histone-acetyltransferases) using acetyl coenzyme A as a co-substrate and can be deacetylated by HDAC (histone-deacetylases). HDACs are divided into four classes, class Ⅰ (HDAC 1-3, 8) located in the nucleus and mainly involved in epigenetic regulation. Class Ⅱ (HDAC 4, 7, 9, 10) can be shuttled between the nucleus and cytoplasm and function to deacetylate histones and cytoplasmic proteins. ClassⅢ, also known as sirtuins are dependent on the NAD^+ (nicotinamide adenine dinucleotide) and are important regulators of metabolisms and transcription through the deacetylation of numerous histones and non-histone substrates. ClassⅣ (HDAC 11) is largely unknown.

b. Methylation

Methylation on the other hand is associated with both actively transcribed and silenced genes, depending on the residues (lysine (K), arginine (R) and histidine (H)) and valence state (mono-, di-, or tri-methylated) [140]. Combinations on different lysine residues play a crucial role in gene expression, whereas methylation on arginine residues is poorly understood. By now more than 20 methyl-marks have been described [141]. Most studies so far focused on six specific sites, namely histone 3-lysine 4 (H3K4), histone 3-lysine 9 (H3K9), histone 3-lysine 27 (H3K27), histone 3-lysine 36 (H3K36), histone 3-lysine 79 (H3K79) and histone 4-lysine 29 (H4K29).

Several examples exist indicating the complexity of lysine methylation. H3K4me1 is highly involved in neuronal activity-induced transcription at enhancer sequences, but di- and trimethylated forms are mainly found at the 5´-end of genes. H3K4me3 is mostly arranged as distinct sharp peaks within 1-2 Kb of the transcription start site, providing a docking station for remodeling complexes either inducing transcription or silencing [141]. The enzymes involved are histone-methyltransferases (HMT) transferring methyl groups from the donor S-adenosyl-methionine (SAM) to the lysine residues and histone-demethylases (HDM).

c. Phosphorylation

Phosphorylation is most commonly associated with active gene transcription, by creating a repulsive force between the negative charges of the phosphorylated histones and DNA. This repulsion leads to decondensation of chromatin and hence increases the accessibility of the transcriptional machinery to the DNA. This modification provides a functional link between chromatin remodeling and intracellular signaling pathways, which both depend on kinases and phosphatases.

d. Ubiquitination

Attachment of the 76 amino acid ubiquitin peptide to residues on the histone tail is associated with transcriptional activation and nucleosomal loosening and has been identified as prerequisite for subsequent methylation.

1.9.3. Histone code hypothesis

An essential feature of PTMs is their ability to crosstalk. Such modifications can act in concert involving multiple feed-forward and feed-back mechanisms on the same nucleosome or histone or even on distinct histones [142]. This led to the formulation of the "histone code hypothesis" by Jenuwein and Allis [143] stating that the sum of modifications at a particular gene defines a specific state of gene activation or silencing.

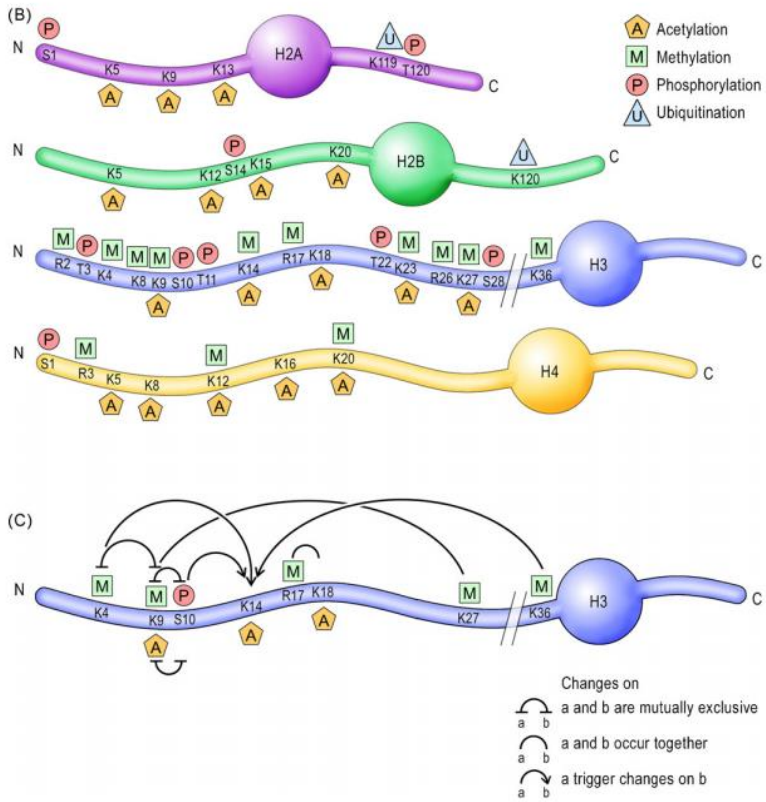

Fig. 6: Epigenetic marks on histone tails [5]

Schematic representation of the N- and C- termini of histones and their residue specific epigenetic modifications. Depicted is the crosstalk between different modifications of the H3- N-terminus tail.

The crosstalk between different modifications can either enhance chromatin condensation or chromatin opening depending on whether gene activity or silencing is required. The enzymes described above, which are responsible to establish and remove these modifications, operate independently and in synergy to establish the histone code, which determines the patter of gene expression in response to external stimuli [5, 143] (**Fig. 6**). Combinations of different epigenetic modifications have been identified in depression on the *Bdnf* promoter in stressed mice. Stress induces an increase in the demethylation of H3K27, a repressive modification. Although treatment with ADs is sufficient to reverse the behavioral phenotype, the specific H3K27me2 is not targeted by them. Instead, ADs rather

increase acetylation of other PTMs of the *Bdnf* promoter, leading to an increased gene expression [144]. Therefore, investigation of the interplay between different kinds of modifications, acting either in combination or excluding each other, represents a highly interesting endeavor to investigate gene specific alterations in depression and might be predictive for individual treatment responses to ADs.

1.10. Epigenetic mechanisms in depression

Epigenetic modifications have been suggested as a potential underlying mechanism in the pathophysiology of mood disorders. The first line of evidence that linked histonemodifications to antidepressant effects was the observation that HDACi exert AD-like effects in an adult rodent stress model [144-146]. Administration of HDACi (e.g. sodium butyrate) was shown to ameliorate depressive symptoms in socially defeated mice. More specifically, the selective HDACi MS275 could reverse the stress induced changes in gene expression, in a very similar way as FLX, although both compounds also target very unique subsets of genes [147].

Furthermore, the effects of HDACs were revealed to be brain region specific. In the NAc the overexpression of HDAC2 exerts AD-like effects and HDAC5 exerts resilient-like effects [148], whereas in the HIPPO HDAC5 seems to have pro-depressive roles. In the HIPPO HDAC5 expression is decreased after imipramine treatment in stressed mice and overexpression seems to block the AD effects [144].

Possible explanations for the opposite effects are that HDAC5 is part of diverse complexes depending on the brain regions where it is activated, thereby targeting a subset of genes which differentially contribute to vulnerability. Alternatively, HDAC5 may regulate the same genes, but these genes elicit different effects in different brain regions. In the cortex of inbred mice, high levels of HDAC5 are associated with reduced depressive-like behavior [149]. However, further work needs to focus on the precise mechanisms to understand how histone acetylation impacts depression and response to ADs.

Histone methylations and their responsible enzymes are also implicated in psychiatric diseases. The first HMT identified in the nervous system was lysine-methyltransferase 2a (KMT2a)/*Mll1* a member of the mixed lineage leukemia family. In heterozygous mice with a loss-of-function mutation in *Mll1* distinct abnormalities in hippocampal plasticity and related molecular signaling pathways were found to be associated with defects in learning and memory [150]. Recently, this HMT was shown to be essential prefrontal synaptic plasticity and working memory [151]. Disruption of certain transcription factors such as

DLX2 has shown their role as key regulators for the differentiation of forebrain GABAergic neurons, possibly contributing to cognitive deficits in *Mll1* mutant mice. An observation that might be important for the pathophysiology of schizophrenia, as far as some patients show deficits in H3K4me3 and gene expression of *Gad1*, a GABA synthesizing enzyme [152]. Additional evidence suggests that epigenetic fine-tuning of H3K4-methylation is critical for proper neurodevelopment [141], hence loss-of-function mutations in demethylases such as lysine demethylase 5C (KMD5C) have been linked to neurodevelopmental disorders such as mental retardation and autism spectrum disorder. This demethylase operates in a chromatin remodeling complex together with HDAC1/2 and the transcriptional repressor REST, thereby poising neuron-restrictive silencer elements for H3K4 demethylation and decreasing the expression of target genes, among which synaptic proteins and sodium channels [153].

KMT6a, a specific H3K27 methyltransferase is associated with the Polycomb Repressive Chromatin remodeling complex 2 (PRC2) and is essential for self-renewal of cortical progenitor cells and neuron production. Loss of KMT6a function is therefore associated with severe thinning of the cerebral cortex and a disproportionate loss of neurons [154]. JMJD3, the H3K27-specific demethylase, is important for neurogenesis and neuronal lineage commitment [155]. Methylation of this mark is dynamically regulated in the mature brain and involved in the neurobiology of psychiatric diseases, as it was shown to induce opposite changes in the expression of *Bdnf* in the HIPPO of mice subjected to either enriched environment or chronic stress [144, 156]. Furthermore, alteration in H3K27 methylation were described at the *TRKB* gene in the orbitofrontal cortex of suicide completers [157].

Chronic social defeat has been found to decrease several HMTs, such as G9a, GLP and SUV39H1 and a co-repressor, Co-REST, which are involved in transcriptional repressive complexes in the NAc of susceptible mice, whereas these factors are upregulated in resilient animals. Overexpression of G9a (H3K9-specific) leads to antidepressant effects in the NAc and its dampening exerts pro-depressive effects. This implicated that stress-induced loss of repressive methylation might be maladaptive in this context and that ADs might act, at least in part, by reinstating these marks at specific loci.

Very few genes have been identified so far as being implicated in depression and regulated by PTMs. One of them is BNDF. For this gene it was shown that electroconvulsive stimulation induces H3 and H4 acetylation at the promoter region in the HIPPO, which reflects the observed gene expression changes [158]. Follow up studies demonstrated that

chronic social defeat decreases total *Bdnf* mRNA in HIPPO, which was reversed by chronic IMI treatment [144], and was correlated with an increase in H3K27me3 (repressive) at the *Bdnf* promoter, also persistent after IMI treatment. IMI caused induction of acetylation in H3 on *Bndf* promoter that correlated with reversal of BDNF expression. Interestingly, a study examining the effects of postnatal FLX exposure on BDNF expression in normal mice did not reveal any differences in H3 acetylation or methylation, indicating the necessity of a preexisting stress state for epigenetic changes associated with AD treatment [159]. Furthermore, in post-mortem studies, elevated levels of H3K4me3 were reported for the synapsin gene in the PFC of depressed patients [68].

Another gene, *TrkB.T1*, the truncated version of *TrkB* receptor, also has been found to be decreased in the orbitofrontal cortex of suicide completers and this decrease correlated with increased H3K27me3 [157]. In the NAc of susceptible vs resilient mice, Uchida and colleagues found that GDNF is pro-adaptive to stress. In susceptible mice, GDNF expression is decreased in NAc after chronic variable stress and reversed by IMI treatment, associated with decreased H3 acetylation, decreased H3K4me3 and increased HDAC2/MeCP2 recruitment at the G*dnf* promoter. In the resilient animals, GDNF was increased in the NAc by chronic stress and this was associated with increased H3 acetylation and decreased H3K27me3. H3K4me3 was paradoxically decreased after stress [117]. A landmark series of experiments was carried out by Meaney and colleagues in which they compared the offspring of low grooming (LG) mothers to high grooming (HG) mothers. LG offspring show increased anxiety levels and stress reactivity, accompanied by decreased GR receptor mRNA in the HIPPO corresponding to decreased H3K9 acetylation at the gene promoter compared to HG offspring [67]. They also show lower levels of GAD-1 and corresponding decrease in H3K9 binding at the promoter [160]. Although much information is available about global epigenetic changes, the evidence on misregulated PTMs specifically in astrocytes is very sparse. One epigenome-wide association study by Nagy and colleagues identified two candidate genes which are affected in the PFC of suicide completers, namely the glutamate receptor, ionotropic kainate 2 (GRIK2) and the brain-enriched guanylate kinase-associated protein (BEGAIN) [161]. GRIK2 is found in astrocytes and polymorphisms of this gene have been implicated in mood disorders [162]. Moreover, mood stabilizers were found to lower GRIK2 levels in mouse astrocytes [163]. GRIK2 is hypomethylated in suicide completers, which probably influences its splicing. On the other hand BEGAIN is hypermethylated in suicide completers. The differentially methylated region of BEGAIN has both gene promoter and

enhancer functionalities and *in vitro* reporter-based assays indicate that DNA methylation of this region almost completely abolishes these activities [161]. These data suggest that these markers may be specific to depression in the presence of an astrocytic dysfunction.
However, to date no study is available that directly links PTMs in astrocytes of the PFC to MDD.

1.11. Animal model

To investigate the neurobiological mechanisms of MDD and to understand the underlying molecular factors, it is necessary to have proper animal models.
The difficulty in designing suitable animal models mainly comprises the high complexity of mood disorders that need to be mimicked. There are several possibilities on how to generate such an animal model, including genetic, environmental or physical as well as pharmacological manipulations or a combination of them [164]. A proper animal model must fulfill the following criteria to be validated: face validity (i.e. its phenotype is similar to the human syndrome), predictive validity (i.e. it has comparable treatment modalities) and construct validity (i.e. it shows common pathological substrates).
In this study, I am using rats derived from a selective breeding approach, either bred for high (HAB) or for low (LAB) anxiety- and depression-related behavior [165]. This selective breeding approach started in 1990s, by selecting from a cohort of naïve outbred Wistar rats, the animals that showed bidirectional performance on the elevated plus-maze (EPM, [166]). This test is a well-established, unconditioned test for anxiety that creates a conflict between an animal´s exploratory curiosity and avoidance of open brightly-lit spaces [167, 168]. To establish the two extreme breeding lines, animals were chosen which spent less than 5% (HAB) or more than 40-45% (LAB) time on the open arm [165, 167]. Since 2003 these lines are being bred exclusively at the University of Regensburg. Over the past decades, exhaustive behavioral, neuroendocrinological and pharmacological characterization of these lines was carried out. Due to the fact that in this study I am focusing on the depressive-like phenotype of the HAB breeding line, I am summarizing briefly the available information.

1.11.1. Anxiety-related behavior

In addition to the performance of HAB rats (both genders) on the EPM, these animal were also tested in a broad variety of other test for anxiety-related behavior, like the open field, modified hole board [169, 170] and the light-dark box, as well as tests for fear conditioning, all of which are confirming the highly anxious phenotype. These

observations have been shown to be independent from age (overly ultrasonic vocalization on post-natal day (PND) 11, behavioral testing between 9 weeks and 19 months of age) and gender and have been validated in different European laboratories [171].

1.11.2. Depressive-like behavior

One of the most comprehensive preclinical tests for depressive-like behavior is the forced swim test (FST). It is based on observing the coping mechanism of rodents subjected to an inescapable situation, i.e. placing the animal in water-filled cylinder. After an initial period of active, escape-directed behavior (swimming, struggling) the animals adopt an immobile posture, which is indicative of behavioral despair [172-174]. HAB rats display a more passive coping style, with a higher immobility (floating) time and less struggling behavior [173, 175] in the FST, resembling a depressive-like phenotype.

1.11.3. Hypothalamic-pituitary-adrenal (HPA) axis and pharmacological intervention

The HPA axis is one of the major stress systems; it is regulated by the release of corticotrophin-releasing hormone (CRH) and arginine vasopressin (AVP) from the PVN into the pituitary, which stimulates the secretion of adrenocorticotropic hormone (ACTH) into the bloodstream. ACTH in turn triggers the release of corticosterone in rodents, which facilitates physiological and behavioral adaptations to a stressor. Dysregulation in the HPA axis has been linked to several psychopathologies including anxiety and depression [164].

HAB rats respond much stronger to a mild, non-social stressor (e.g. open arm exposure), by secreting more ACTH and corticosterone, which indicates a hyper-reactive HPA axis [176], although under baseline conditions no differences can be measured. HAB also show an aberrant response to the dexamethasone-suppression/CRH challenge test [174].

The DEX/CRH test characterizes neuroendocrine aberrations in depressed patients, who typically show signs of non-suppression of ACTH upon DEX exposure and, despite DEX, respond to synthetic CRH with an increase in ACTH secretion [177]. This hyper-reactivity in HAB animals resembles the clinical situation in patients, whereas persistent abnormalities correlate with therapeutic resistance or relapse in patients [178].

This aberrant DEX/CRH response normalized upon treatment with an acute intravenous administration of an AVP V1a receptor antagonist as well as chronic administration of paroxetine, a SSRI, by blunting the overexpression of vasopressin in the PVN [165, 173, 174] In patients, this normalization is indicative of a favorable response to antidepressant treatment. Furthermore, the observed depression-like phenotype in HABs is reversible after chronic administration (8 weeks) of paroxetine [174]. In comparison to untreated HAB

rats, paroxetine-treated animals show a decreased time floating and a higher percentage of time engaged in active coping behavior (i.e. struggling) in the FST [165, 174].

In conclusion, extensive characterization proves HAB rats to be an established and proper model to study underlying etiology and mechanism of psychiatric disorders, specifically depression.

1.12. Microarray – candidate genes

Recently, we identified gene expression changes in primary astrocytes and C6 glioma cells, a model to study astrocytes, elicited by antidepressant treatment in an unbiased microarray screening approach. Several genes were specifically upregulated after treatment with the two ADs desipramine and FLX but not with non-ADs (haloperidol, diazepam). Among the identified candidate genes, we further investigated the growth differentiation factor 15 (GDF15) and ephrinA1, a ligand of the EphA2 receptor, which turned out to be upregulated in the screening.

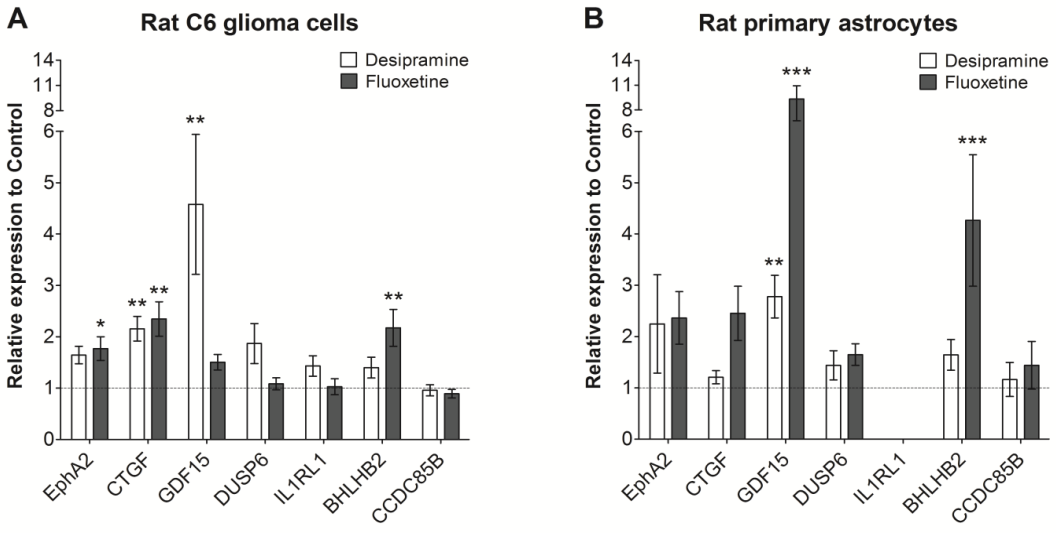

Fig. 7: Microarray screening and validation via qPCR of candidate genes

A, Microarray screening on C6 glioma cells revealed that several candidate genes show induced expression after 2 h of AD treatment (FLX and desipramine)

B, Validation in primary rat astrocytes by means of qPCR, showed a significant induction of GDF15 after treatment with both ADs (n=3, Kruskal-Wallis-test, *p<0.05, **p<0.01, ***p<0.001, data are represented as means ± SEM).

1.12.1. Growth differentiation factor 15 (GDF15)

Dysfunctions at the BBB might be indicative for the recently found high degree of comorbidity in patients diagnosed with either a primary cerebrovascular pathology or a mood disorder [179]. Interestingly, the unbiased microarray screening revealed, GDF15 as a factor highly induced by antidepressants in C6 glioma cells and primary astrocytes.

GDF15 (also known as MIC-1, PTGFB, NAG-1), is a member of the TGF-β superfamily, which shows the lowest sequence conservation of all members of this family. GDF15 is synthesized as a 62kDa intracellular protein, that is cleaved by a furin-like protease and it is secreted as a 25kDa - 35kDa disulfide-linked dimer [180, 181]. *Gdf15* mRNA is predominantly expressed in prostate, intestinal mucosa, kidney, lung (bronchi and bronchioli), exocrine glands, placenta, macrophages and the in the CNS in the choroid plexus [182]. Recent studies indicate that GDF15 is secreted in both processed and unprocessed forms, at different speeds and via alternate secretory pathway [183], which might modulate the amounts of stored and circulating levels. The signaling pathway of GDF15 is not fully understood, although there are suggestions that it signals through the TGF-β receptors and its downstream signaling pathways, but also that inhibition of the PI3K-kinase and ERK block the response to GDF15. Data from the group of Unsicker (2003) indicate that GDF15 promotes survival of dopaminergic neurons through a cytokine receptor and that phosphorylated Akt and ERK are downstream effectors of GDF15 mediated signaling on cerebral granule neurons [181]. GDF15 has been greatly implicated as a biomarker and predictor for cardiometabolic risk and heart failure [184, 185]. GDF15 is widely expressed in the central and peripheral nervous system. Its mRNA and protein are found in virtually all regions of the rat and mouse CNS, in peripheral nerves and in isolated astrocytes. However, the highest levels are found in the choroid plexus, where the protein is secreted into the cerebrospinal fluid (CSF) [186]. GDF15 has been shown to be a potent neurotropic factor for dopaminergic neurons, as unilateral injections in the medial forebrain bundle or the left ventricle significantly reduced the loss of neurons elicited by 6-hydroxydopamine injections [186]. However, in the unlesioned brain GDF15 expression levels are below detection level in glia and neuronal cells [187], indicating that this factor might be a specific marker for changes occurring after lesion/inflammation or other aberrant changes in the CNS. Knowledge about GDF15 expression and functions in glia cells are still very limited. In the CNS GDF15 is synthesized by microglia cells, whereas astrocytes in the CNS seem to be devoid of GDF15, which is different from cultured cells, where it can be detected [187].Very recently, GDF15 has been implicated as a potential

biomarker for bipolar disorder, as it was found to be significantly upregulated in the serum of patients suffering from bipolar disorder [188]. Another study found that GDF15 levels are 22% higher in the serum of patients suffering from MDD [189], but these findings seem to be at least in part dependent on lifestyle factors, such as smoking, alcohol use and physical activity. Investigation of the functions and underlying pathways of GDF15, especially in the CNS, represents a highly interesting route to be considered in the treatment of neurodegenerative and psychiatric diseases. In this study we further elucidate implications of GDF15 in the HAB rat model of depression, with a major focus on the effects of FLX on its expression in astrocytes.

1.12.2. Ephrin

Eph (**e**rythropoietin-**p**roducing-**h**eptaocellular carcinoma) receptors (EphR) are the largest family of receptor tyrosine kinases (RTK) that transduce extracellular to intracellular signals through ligand-induced activation of their kinase domain. EphR mediate contact-dependent cell-cell communication by interacting with surface-associated ligands – the ephrins (**Eph r**eceptor-**in**teracting-signals) – located on neighboring cells. [190]. They elicit bidirectional signals that affect both- the EphR and ephrins- co-expressed in the same cell. Furthermore EphRs can modulate cell behavior independently of ephrin binding and kinase activity. This system regulates many developmental processes and adult tissues homeostasis and abnormalities in its functionality have been implicated in various diseases.

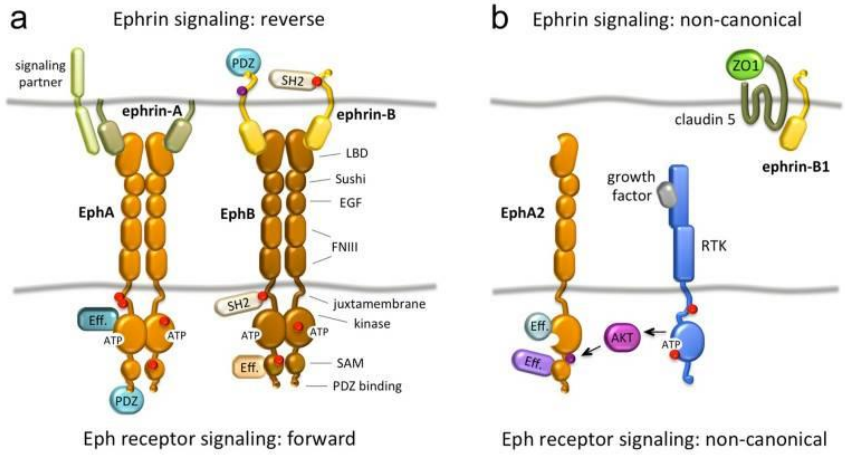

Fig. 8: signaling mechanism in the EphR/Ephrin system [1]

a. General features

EphRs consist of a multidomain extracellular region, including the ephrin ligand-binding domain, a single transmembrane segment and a cytoplasmic region that contains the kinase domain (**Fig. 8**). In humans 14 EphRs are described, which can be subdivided into two classes (EphA and EphB). Nine EphA-R bind five ephrin-A ligands and five EphB-R bind three ephrin-B ligands [1]. Both classes include a conserved Eph-R-binding domain, which is connected to the plasma membrane by a linker segment. EphrinAs are attached to the cell surface by a GPI anchor, but they can also be released to activate distant receptors. EphrinBs contain a transmembrane segment and a short cytoplasmic region. [190]. Combinations of these receptors and ligands are present in most cell-types, including the brain.

EphRs bind ephrins on neighboring cells mediating a contact-dependent, bidirectional communication that regulate cell shape, movement, survival and proliferation [191]. During development this system plays a role in the spatial organization of different cell populations, axon guidance, formation of synaptic connections and remodeling of blood vessels. In the adult brain, among others it regulates remodeling of synapses, epithelial differentiation and integrity [192]. In the EphR/ephrin system three form of signaling are described, namely forward, reverse and bidirectional signaling (**Fig. 8**). Forward signaling depends on ephrin binding, which induces EphR clustering, autophosphorylation and kinase activity and can lead to endocytosis or proteolytic cleavage, thereby generating intracellular fragments with distinctive signaling abilities.

Reverse signaling is stimulated by EphR binding in the ephrin-expressing cell via interaction with signaling partners. EphrinB signaling involves phosphorylation by the Sarcoma kinase (SRC) creating binding domains for other signaling proteins, e.g. non-catalytic region of tyrosine kinase adaptor protein 2 (NCK2), which controls axon pruning, synapse formation and dendritic spine morphogenesis in the developing mouse HIPPO [193].

Bidirectional signaling transduction can be further regulated. EphrinAs can be released from the cell surface by metalloprotease cleavage and activate EphA receptors in a paracrine manner. Interaction between receptor and ligand co-expressed in the same cell can attenuate the cell contact-dependent signals induced by *trans* interaction EphRs can also function through non-canonical signaling modalities, including intracellular proteins. After binding of the ligand, the EphRs are internalized by endocytosis into either EphR or ephrin expressing cell through the formation of vesicles containing plasma membrane

fragments derived from both cells in an Ras-related C3 botulinum toxin substrate 1 (RAC-1) dependent process, termed trans-endocytosis [190]. Besides trans-endocytosis, the complexes can activate metalloproteases like ADAM10 which can associate with ephrinA2 in the same cell surface and cleave it following EphAR binding in *trans* to enable repulsive axon guidance [194]. Ephrin binding and other stimuli can also induce cleavage of EphR extracellular domain, followed by further transmembrane proteolytic processing via γ-secretase to generate cytoplasmic fragments capable of signaling [190].

b. Implications in CNS pathologies

Many receptors and ligands are expressed after injury and negatively affect axon sprouting and other repair processes [192]. Several studies established a connection between pharmacological inhibition of EphA4-ephrin binding and EphA4 gene inactivation with improved functional recovery in rodent spinal cord injuries [195]. In Alzheimer's disease the cytotoxic β amyloid peptides can activate EphA4 forward signaling, which has been shown to participate in the synaptotoxicity and can be blocked by EphA4 antagonists [196]. Intracellular fragments of EphA4 are decreased in Alzheimer´s disease, but can promote dendritic spine formation independently of kinase activity [190]. A soluble form of ephrinA1 (ephrinA1-Fc) promotes regeneration of brain dopaminergic neurons in a rat model of Parkinson's disease [197]. The Eph/ephrin system controls blood vessel sprouting, assembly, remodeling and stabilization by regulating endothelial cells and pericytes. EphA2 regulated vascular permeability, mainly in concert with ephrinA1 through the interplay with VEGF, indicating that this system represents a promising target for therapeutic intervention of vascular pathologies. In glioblastoma, downregulation of EphA2 or EphA3 expression either by RNAi or administration of high doses of ephrinA1-Fc drastically reduces tumorigenicity [198]. In a very recent study, levels of EphB2 and its downstream molecules were found to be decreased in the medial PFC in mice that were susceptible to chronic social defeat and activation of EphB2 by ephrinB1-Fc produced stress-resistant and antidepressant-like behavioral effects in susceptible mice, whereas knockdown (k/d) using shRNA (short hairpin RNA) increased susceptibility and induced depressive-like behavior. These changes were associated with α-amino-3-hydroxy-5-methyl-4-isoxazolepropionic acid receptor (AMPAR) trafficking and the expression of synaptic protein in the PFC. It also regulated stress-induced spine remodeling in the PFC. [199]

Already in 2003 EphA receptors were shown to be important regulators of spine morphology in the HIPPO [200]. However, the role of ephrinAs is less understood.

EphrinA5 is linked to spine density and synapse function in the cortex and HIPPO. EphrinA5 knockout (k/o) mice have increased numbers of filipodia-like protrusions in the cortex during early development [201], but after completion of synaptogenesis these cells display significantly fewer dendritic spines. In the HIPPO ephrinA5 regulates synaptic development and function by modulating the PI3K/Akt pathway. Presynaptically, ephrinA5 promotes BDNF-induced synapse formation, whereas synapse formation is significantly reduced in cultured neurons form k/o mice. In contrast, binding of postsynaptic EphA receptors to presynaptic ephrinA5 leads to suppression of BDNF-induced synaptogenesis [202]. As described before, neuron-glia communication is an important regulator of synapse development and function [100]. EphR and ephrins are especially located at synaptic terminals of hippocampal and cortical neurons and some are also localized at the perisynaptic astrocytic processes, allowing them to participate in synaptic transmission [203]. Hippocampal astrocytes express high levels of ephrinA3 and regulate spine morphogenesis, glutamate transport and long-term potentiation at CA3-CA1 synapses by interacting with EphA4 on dendrites of CA1 pyramidal neurons [204, 205]. K/o animals for either of these factors have abnormally shaped dendritic spines and reduced long-term potentiation, as well as impaired contextual fear memory. These deficits are most likely due to an upregulation of GLAST and GLT-1 receptors in the k/o animals, causing an exaggerated removal of glutamate form the synaptic cleft, which in turn leads to reduced LTP. Dysfunction in glutamate metabolism and aberrant dendritic and glia cell morphologies have already been implicated in MDD, thus studying these interactions at the synaptic level in our animal model might depict a very exciting possibility to shed light on the pathophysiology of depression.

1.13. Scope of study

Major depressive disorder has become the leading cause of disability worldwide [7]. Although several treatment options exist, the major drawbacks, like late onset of beneficial effects and a high rate of non-responders still represent a huge burden for patients. To date the molecular underpinnings of MDD are still very poorly understood, making the most reliable criterion to diagnose MDD dependent on a subjective perception of symptoms. Additionally, suitable animal models mimicking depression are sparse. Therefore, it is highly important to identify the underlying molecular mechanisms of depression. In this study I specifically focused on posttranslational histonemodifications that might account for gene expression changes, which in turn could contribute to the depressive phenotype observed in HAB animals.

Therefore, I first investigated whether under basal conditions HAB animals showed different expression patterns of several PTMs in comparison to "healthy" NAB rats and if these differences were specific to cortical astrocytes or neurons (*ex vivo* and *in vitro*). Both cell-types have been implicated in depression, with striking evidence that aberrancies in astrocytes, rather than in neurons, might be the cause of depression. Furthermore, I investigated if these PTMs were targeted by antidepressant treatment and if the misregulation in HAB could be reversed. Moreover, I investigated if the observed differences in PTMs could be linked to the expression of specific candidate genes that were previously identified to belong to pathways modulated by AD treatment in our lab.

With regard to our recently published paper, stating astrocytes to be misregulated at the level of the blood-brain-barrier, I further investigated if one of the identified candidate genes might be involved in the formation of astrocytic processes and whether a putative imbalance in its expression could be rescued by antidepressant treatment *in vitro* and *ex vivo*. On the one hand, I hypothesized that HAB animals display aberrant gene expression caused by misregulation of PTMs and that this misregulation could be rescued by AD treatment. Moreover, investigation of specific genes might provide a possibility to identify new pharmacological targets in the pathophysiology of MDD. On the other hand, I investigated how structural aberrancies at the glia-vasculature interface can be targeted by antidepressant treatment, focusing on the actions of ADs on astrocytic processes.

2. Material and MethodsAnimals

All animal experiments were approved by the government of the Oberpfalz (Germany) and carried out in accordance to the European communities Council Directive of 24 November 1986 (86/609/EEC).

For this study, adult male rats (10-12 weeks old, 280-350 gram) selectively bred for high anxiety-related behavior (HAB) and weight-matched non-selectively bred Wistar rats (NAB), serving as controls, were used. Animals were bred in the in-house animal facility at the University of Regensburg (HAB) or purchased from Charles River Laboratories (NAB; Charles River, Sulzfeld, Germany; strain code 003). Animals were kept under standard housing conditions (room temperature (RT) 22-24°C, humidity 55 %, 12 hours (h) light/dark cycle with lights on at 6:00 a.m.). Water and pelleted food were provided *ad libitum*. For preparation of primary cortical astrocytes, HAB and NAB pups on post-natal day (PND) 0-4 were used, for cortical neurons NAB embryos on embryonic day 18 (E18) were used.

2.2. Drugs

Fluoxetine hydrochloride (FLX) and escitalopram oxalate (ESC) were purchased from Abcam®, Cambridge, UK (#ab12077 and #ab145177, respectively). For experiments in brain slices (*ex vivo*) FLX was diluted on the day of the experiment in phosphate buffered saline (PBS) and injected intraperitoneal (i.p.), twice daily, at a concentration of 10 mg/kg, on two consecutive days.

For *in vitro* experiments both drugs were prepared in water at a stock concentration of 10 mM and diluted to a final working concentration of 5 µM and 10 µM (for more details, see respective experiments).

2.3. Preparation of astrocytes

Primary cortical astrocytes were isolated on PND 0-4 from cerebral cortices of HAB and NAB rat brains. Rat pups were decapitated, the skull was opened using small scissors, and meninges were removed carefully. Brains were isolated and cortices dissected in ice-cold HBSS (Hanks´ balanced salt solution, Gibco, #14025-092). After fragmentation of the cortices into small pieces, the pieces were pooled, transferred to a sterile 15 ml falcon containing 5 ml ice-cold HBSS and shortly centrifuged. Supernatants (SN) were removed and an appropriate amount of 0.25 % trypsin containing 1 mM EDTA (Sigma, #T4049) was added for digestion (20 minutes (min) at 37°C), while gently shaking. Remaining brain tissue was homogenized using fire-polished Pasteur-pipettes, with decreasing tips´s

diameters, to obtain dissociated cells. Cell homogenates were centrifuged at 90x g for 5 min, supernatants were aspirated and cells were resuspended in warm astrocyte-growth medium DMEM (Dulbecco´s modified eagle medium, Gibco, #41965-062) supplemented with 10 % fetal calf serum (FCS, Sigma, #F7524), 1 % antibiotic-antimycotic (100x, Sigma, #A5955), 1 % sodium pyruvate (Sigma, #S8636), 1 % HEPES 1M (Gibco, #15630-056), 1 % MEM non-essential amino acids (Gibco, #11140-035). Cells homogenates were plated on poly-D-lysine (PDL, Sigma, Taufkirchen, Germany, #P7886) coated T75 cm^2 flasks (Sarstedt, #83.3911.002) [206, 207].

2.3.1. Cell culture passaging

Freshly isolated astrocytes were allowed to grow for approximately 7-10 days *in vitro* (D*IV*) (37°C, 5 % CO_2/ 95 % air) in astrocyte-growth medium that allows the growth of astrocytes, but does not favor the growth of other cell-types (e.g. neurons or microglia). To remove remaining cell-types (neurons/microglia/oligodendrocytes) flasks were shaken for 4 h at RT, causing a detachment of these cells which can then be eliminated by washes with PBS. This procedure helps to reach a nearly pure astrocytic cell culture. As soon as astrocytes reached a confluency of 90-100 % medium was removed, cells were trypsinized, resuspended in freezing medium (DMEM supplemented with 20 % FCS and 10 % (v/v) dimethylsulfoxide (DMSO, Sigma, #D-2650), aliquoted (approx. $1x10^6$ cells/vial) and gradually frozen at -20°C (24 h) followed by -80°C for 24 h until permanent storage in liquid nitrogen (-196°C).

2.3.2. Cultivation

For cultivation, deep frozen (-196°C, liquid nitrogen) cell aliquots containing approximately $1x10^6$ cells were thawed quickly and seeded in a PDL coated T75-flask with astrocyte-growth medium. Cells were maintained in growth medium until they reached confluency (~14 D*IV*), with medium change every 3d. Confluent cells were trypsinized and seeded into corresponding experimental plates. Primary rat astrocytes were used until passage 4 (P4), every trypsinization step was considered as an additional passage.

2.4. Preparation of neurons

Primary cortical neurons of NAB rats were isolated on E18. In brief, the dam was sacrificed using CO_2, the peritoneum was opened and the embryos were carefully removed. The embryos were decapitated and the skull was opened. The meninges were removed carefully, the brains isolated and the cortices dissected. Cortices were centrifuged, debris was removed and the pieces were homogenized using fire-polished Pasteur-pipettes. Cells

were then seeded in on laminin-coated (Sigma, # L-2020) cover glasses or 24-well plates in neuron-specific medium (Neurobasal-A-medium Invitrogen, #10888022, supplemented with B27 #17504-044 and Glutamine #25030024). Pure neuronal cultures were allowed to grow for 21 D*IV*. Half of medium per well was changed every 3d.

2.5. Preparation of co-cultures

For the preparation of co-cultures, primary cortical astrocytes derived from HAB and NAB rats were used. Cells were seeded on PDL -coated cover glasses in astrocyte-growth medium. Astrocytes were allowed to grow for approximately 3-5 D*IV*, and then medium was changed to neuron-specific medium shortly before freshly isolated neurons were plated onto the feeder layer of astrocytes. The resulting co-cultures were allowed to grow approximately 14 D*IV*. Half of the neuron-specific medium was changed every 3d, to allow the co-cultures to remain in their established environment.

2.6. Antidepressant treatment

After astrocytes reached confluency (90-100 %, approximately 7-14 D*IV*), medium was changed to serum free medium 24 h prior to the treatment with ADs. Cells were treated with FLX or ESC for 48 h (once, 10 µM) or 120 h (two times, 5 µM each). According to the following scheme:

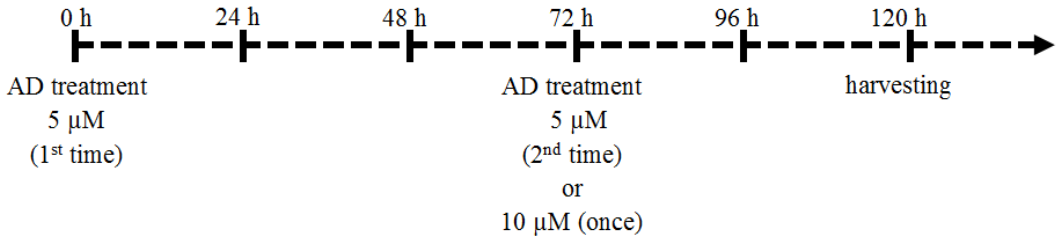

Neuronal cultures and co-cultures were treated only once at the beginning of the experiment with 10 µM FLX or ESC without changing the medium 24 h before. Treatment was terminated either after 48 h or 120 h. Eventual variations on AD treatment are specified for the single experiments.

2.7. Harvesting

To terminate the treatment, medium containing ADs was discarded; single cultures were washed with ice-cold PBS, scraped off the surface in PBS, transferred to Eppendorf tubes and immediately put on ice. Cells were centrifuged for 10 min (12.000 rpm (rounds per minute)) using a pre-cooled (4°C) microfuge (Eppendorf AG, Wesseling-Berzdorf,

Germany), supernatants were discarded and cell pellets were stored at -80°C until further processing.

2.8. Immunofluorescence (IF) analysis

2.8.1. Drug treatment and perfusion

For immunofluorescent-immunohistochemical (IF-IHC) analysis, animals were either naïve or injected with saline or FLX (i.p., twice daily, 0 or 10 mg/kg FLX for 2d). 12 h after the last injection animals were deeply anesthetized using CO_2 and perfused transcardially with cold PBS, followed by fixation with 4 % paraformaldehyde (PFA, Roth, #0335.2) in PBS.

Brains were removed and post-fixed in 4 % PFA overnight (O.N.) at 4°C. Then, brains were washed 3 times with PBS and cryoprotected in 25 % sucrose in PBS or at -80°C until they were cut in 40 µm coronal sections on a cryostat (Leica CM1950, Leica Microsystems, Nussloch, Germany). Sections were preserved in 25 % ethylene glycol/ 25 % glycerol in PBS and stored at -20°C until further processed.

2.8.2. Immunofluorescent-Immunohistochemistry

Free-floating sections from the PFC were selected and washed thoroughly in PBS (3x 20 min), followed by permeabilization and blocking in 2 % normal goat serum (NGS, Linaris, #S1000), supplemented with 0.1 % Triton-X-100 in PBS, for 1 h at RT.

After washing, staining was performed by incubating the slices with different combinations of primary antibodies, O.N. at 4°C (**see Table 1**), diluted in the aforementioned solution with gentle shaking.

Combination	Protein	Specificity	Concentration	Company	Experiment
H3K4me3 global	rabbit-anti-H3K4me3	histone 3 -lysine 4-trimethylation	1: 1000	Millipore. #07473	3.1.1 3.2.1 3.2.3
H3K4me3 in neurons	mouse-anti-NeuN	neuron specific marker	1: 500	Millipore, #MAB377	3.1.2 3.2.2 3.2.4
	rabbit-anti-H3K4me3	histone 3 -lysine 4-trimethylation	1: 1000	Millipore. #07473	
H3K27me3 global	rabbit-anti-H3K27me3	histone 3 -lysine 27-trimethylation	1: 1000	Millipore, #07449	3.4.
H3K27me3 in neurons	mouse-anti-NeuN	neuron specific marker	1: 500	Millipore, #MAB377	3.4.1
	rabbit-anti-H3K27me3	histone 3 -lysine 27-trimethylation	1: 1000	Millipore, #07449	
H3K4me3 in astrocytes	mouse-anti-GFAP	glia specific marker	1: 400	Sigma. #G3839	3.1.2 3.2.2 3.2.4
	mouse-anti-S100β	glia specific marker	1: 1000	Sigma, #S2532	
	rabbit-anti-H3K4me3	histone 3 -lysine 4-trimethylation	1: 1000	Millipore. #07473	
H3K27me3 in astrocytes	mouse-anti-GFAP	glia specific marker	1: 400	Sigma. #G3839	3.4.1

	mouse-anti-S100β	glia specific marker	1: 1000	Sigma, #S2532	
	rabbit-anti-H3K27me3	histone 3 -lysine 27-trimethylation	1: 1000	Millipore, #07449	
ephrinA1	rabbit-anti-ephrinA1	ephrinA1	1: 100	Invitrogen #34-3300	3.6
EphA4	mouse-anti-EphA4	EphA4	1: 500	Invitrogen #37-1600	

Table 1: Primary antibody combinations in IF-IHC

On the second day brain slices were washed (3x 10 min in PBS) to get rid of unbound primary antibody and incubated for 2 h with the corresponding secondary antibodies. As secondary antibodies for neuronal (NeuN) and astrocytic markers (GFAP/S100β) Cy3-labeled anti-mouse (Sigma, # C2181), at a concentration of 1:250, was used.

For both histone markers (H3K4me3 and H3K27me3) the biotin-avidin enhancer system was applied. First, slices were incubated with biotin-coupled goat anti-rabbit 1: 300 (Dianova, #111-065-003) followed by the incubation with tertiary fluorescent antibody Alexa Fluor 488-labeled avidin anti-biotin 1: 1000 (Invitrogen, # A21370).

Secondary antibodies for ephrinA1 and EphA4 were goat-anti rabbit-Alexa Fluor 488 (1:250, Invitrogen, # A-11008) and Cy3-labeled-anti-mouse (1:250), respectively.

To label nuclei in all IF- experiments DAPI (1: 1000, Sigma, # 32670) was used.

Secondary and tertiary antibodies were diluted in 2 % NGS in PBS and incubated for 1 h at RT, each. At the end of the procedure slices were washed (3x 10 min in PBS) and mounted on specimen slides using aqueous mounting medium (Abcam, #ab128982) for confocal analysis.

2.8.3. Immunofluorescent-Immunocytochemistry (IF-ICC)

For IF-ICC primary cortical rat astrocytes (NAB and HAB) were seeded on glass coverslips (Ø 12 mm, Roth, #P231.1), coated with PDL, at a density of $1x10^5$ cells/well. Cells were allowed to grow until they reached 80 % confluency. For co-cultures: 24 h before neurons were seeded onto the layer of astrocytes, the medium was changed to

neuron-specific medium. Then neurons, derived from NAB animals, were seeded on the feeder layer of astrocytes. The co-cultures were allowed to grow approximately 14 D*IV*.

For functional experiments on ephrinA1/EphA4, the co-cultures were treated according to the following scheme:

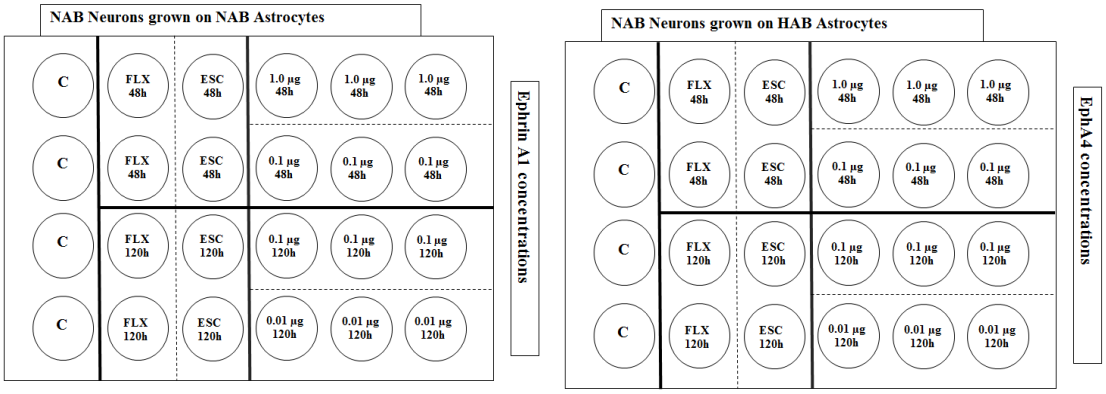

Fig. 9:Layout of Co-Cultures neurons growing on astrocytes derived from either NAB or HAB rats.

NAB-NAB co-cultures were treated with FLX, ESC and recombinant ephrinA1-Fc, at different concentrations and time points. HAB-NAB co-cultures were treated with the same way using FLX, ESC, but with recombinant EphA4-Fc.

Ephrin A1-Fc (recombinant human chimera protein, R&D Systems, #6417-A1-050) and EphA4-Fc (recombinant human chimera protein, R&D Systems, #6827-A4-050) were used at three different concentrations: 1.0 µg/ml 48h, 0.1 µg/ml 48 h and 120 h and 0.01 µg/ml 120 h.

ESC and FLX were administered once to the co-cultures at a concentration of 10 µM for 48 h or 120 h.

After termination of the treatment, cells were washed with cold PBS and fixed in 4 % PFA for 20 min. PFA was removed, cells were washed 3x 10 min in PBS and stored in PBS at 4°C until further processing.

For IF-ICC, cells were permeabilized and blocked in 0.1 % Triton-X-100/2 % NGS in PBS for 15 min at RT. Subsequently cells were incubated O.N. at 4°C with primary antibodies, while gently shaking **(Table 2):**

Combination	Protein	Specificity	Concentration	Company	Experiment
Synaptic compartments	mouse-anti-PDS 95	Postsynaptic protein	1: 300	NeuroMAB, #75-028	3.7
	rabbit-anti-Synaptophysin	Presynaptic protein	1: 500	Abcam, #ab52636	
	chicken-anti-MAP 2	Cytoskeletal protein	1: 1000	Acris, #CH22103	

Table 2: primary antibody combination for IF-ICC functional experiments

On the next day cells were washed (3x 10 min in PBS) and incubated for 2 h with the corresponding secondary antibodies. For PSD95, Cy3-labelled-anti mouse (1: 500), for MAP2 anti-chicken Alexa Fluor488 (1: 1000) and for synaptophysin the avidin-enhancer system was used, with biotinylated-anti-rabbit (1:500) and avidin-anti-biotin Alexa Fluor 647 (1: 1000). For all stainings DAPI (1: 1000) was used to label the nuclei.

Secondary and tertiary antibodies were diluted in 2 % NGS/PBS and incubated for 2 h at RT, each. Finally coverslips were washed (3x 10 min in PBS) and coverslips were mounted on specimen slides using aqueous mounting medium for confocal analysis.

2.8.4. Confocal microscopy

To analyze IF-IHC and IF-ICC, microphotographs were taken using a Leica SP8 confocal microscope (Leica, Wetzlar, Germany) or a Olympus (at the Max Planck Institute of Psychiatry, Munich, inverted type IX81, (see below; Olympus Europe holding GmbH, Hamburg, Germany). In brief, appropriate lasers for detection of fluorochromes were selected and settings were adjusted based on the highest fluorescent signal. The following settings were adjusted at the beginning of each experiment and kept constant throughout.

- objective and digital zoom
- exact range of wavelengths
- pinhole
- gain/offset
- line average
- number of pixels per picture (512x512)

To ensure an appropriate recoding of entire sections (thickness: brain slices 30-40 µm, coverslips with cells 8-9 µm and co-cultures 3-4 µm), Z-stack acquisition was used. The focal plane was set, and the beginning and end point were defined, as well as the step size (1.23 µm and 1 µm of co-cultures). To avoid bleed-through between the different channels, a sequential acquisition mode was used.

IF-IHC: For each animal 2-3 cortical slices were stained and microphotographs were taken. For each slice 8-12 randomly selected, non-overlapping Z-stacks were acquired and included for further analysis.

IF-ICC: 15-20 randomly selected cells (Z-stack) of each treatment condition were taken for analysis.

IF-ICC in co-cultures: only qualitative analysis of single pictures

2.9. Quantitative analysis

2.9.1. Histone marks

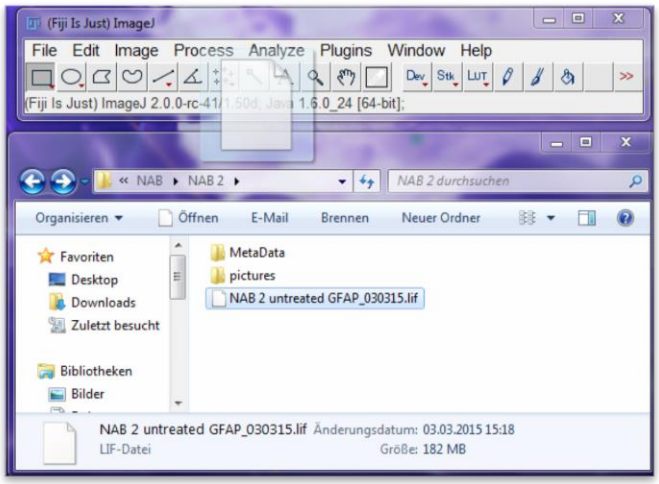

Acquired images were saved by the confocal microscope as .lif files, which contained all the relevant metadata. A .lif file was opened (via drag´n´drop, **Fig. 10**) by the Bio-Formats-Importer plugin [4] in Fiji (ImageJ 1.50d [6]).

Fig. 10: Open .lif files in Fiji via drag ´n´drop

Fiji allows opening the acquired Z-stacks individually or all at once.

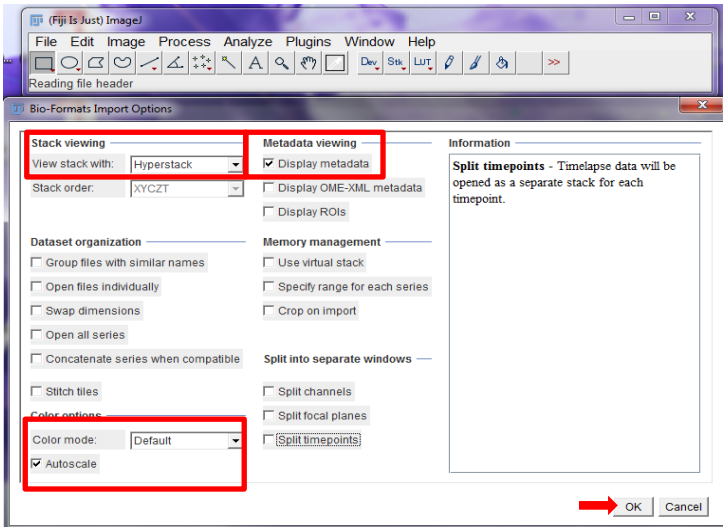

Fig. 11: Import options Bio-Formats Importer Fiji

To open images, the appropriate import options in the Bio-Formats Importer were chosen (**Fig.11,** Stack viewing: Hyperstack, Display metadata, color mode: default, Autoscale).

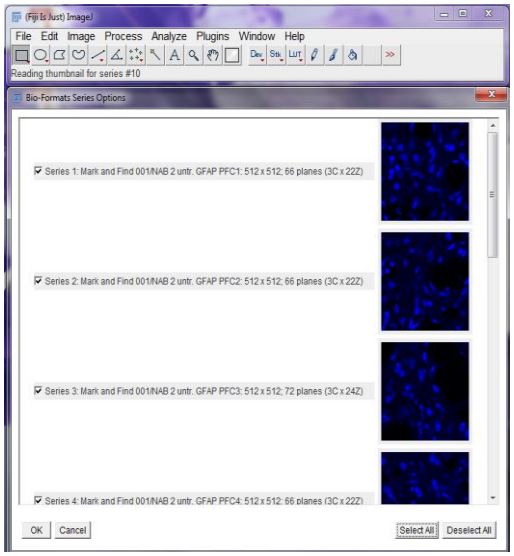

Fig. 13: Bio-Formats Series Options

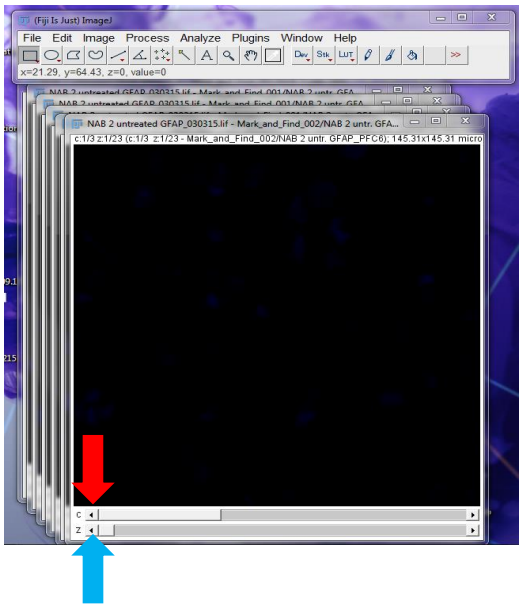

Fig. 13: Slider bars can be used to scroll through single channels and picture

By choosing to open all series of one .lif file at once, the single stacks are opened individually, with the respective default data included by the microscope (**Fig.13**). Single channels were displayed and could be selected by using the slider "C" (red arrow, **Fig.13**). To scroll through the single pictures of the acquired series, the slider "Z" was used (blue arrow, **Fig.13**).

For analysis single channels were converted into a composite, displaying all channels in the same picture. Image→Color→ Channel tools→ Composite (**Fig.14**)

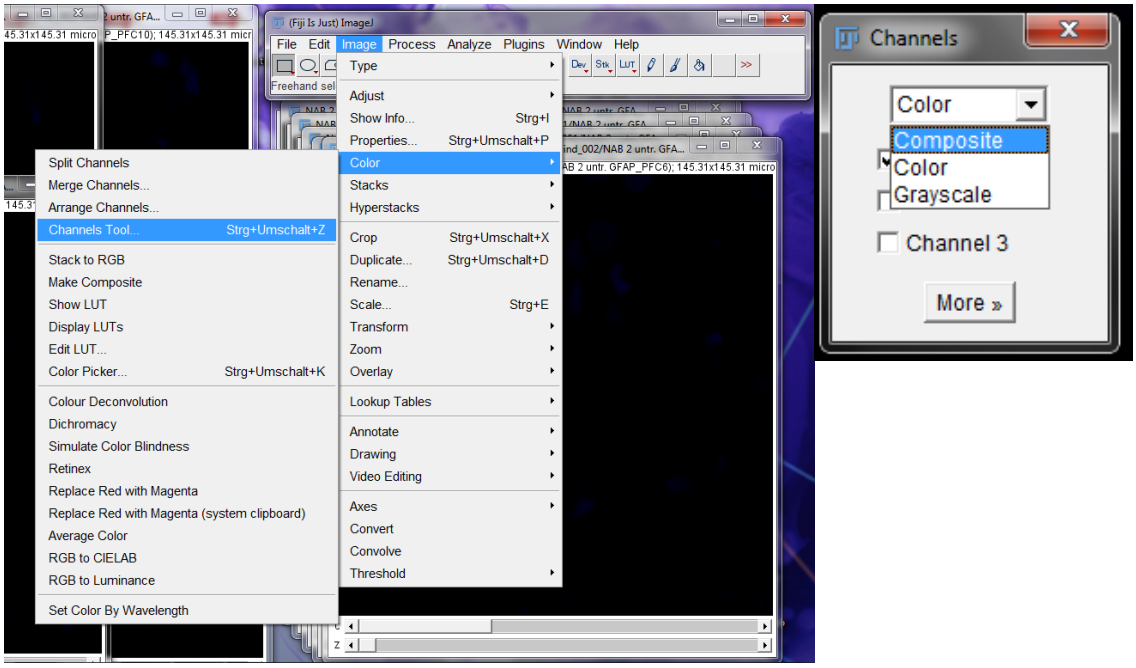

Fig. 14: Conversion of acquired series into a composite

The final image shows the overlay of all channels and acquired images in one window, still giving the possibility to turn on and off the single channels, exemplarily displayed in **Fig.15**.

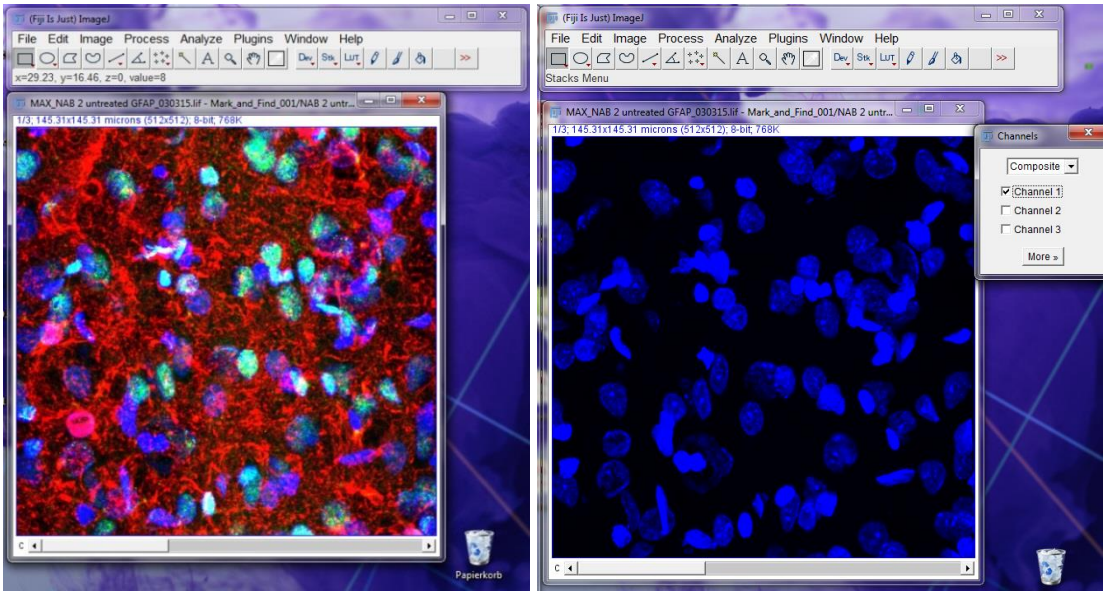

Fig. 15: Overlay of channels with the possibility to enable single channels

For the analysis of the single channels, one channel at a time was enabled and all cells, labeled with the different fluorescent antibodies, were counted using the Cell Counter (Plugins → Cell Counter → Cell Counter, **Fig.17)**

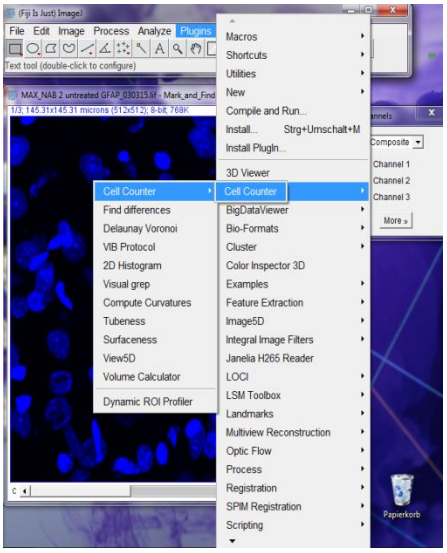

Fig. 17: Cell Counter plugin

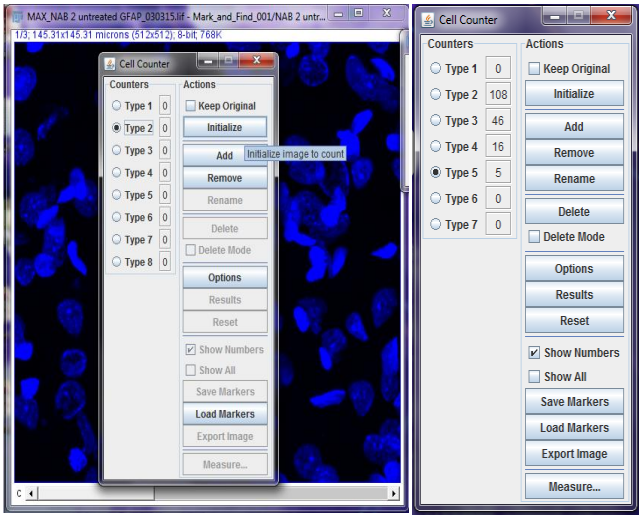

Fig. 17: Fiji Analysis of single channels using the built-in plugin Cell Counter

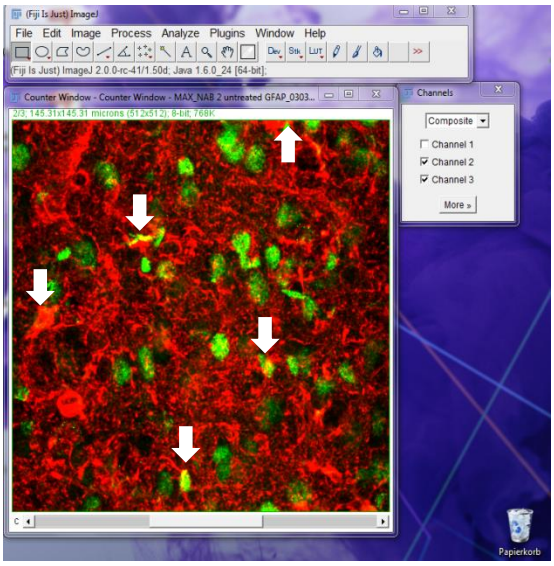

Fig. 18: Colocalization analysis of double-labeled cells

After initializing the Z-stack for analysis by the plugin, I choose different counter types to analyse every single channel individually (**Fig.17**).

First, I counted all nuclei in each single field (DAPI staining), which served as a normalizer later on. Then, the two other channels were analyzed in the same way (histone staining, astrocytes or neurons). To be able to analyze a possible colocalization between the histone marks and astrocytes or neurons, both channels were enabled at the same time and I counted cells that were labeled with both fluorescent antibodies (**Fig.18**).

For statistical analysis, the following parameters were calculated, first for each randomly selected field individually:

global expression histone marks: total number of cells labeled with histone mark/ total cell number

Cell-type specific expression: total number of cells colocalizing/total number of specific cell-type (astrocytes or neurons)

Then the mean for each single animal was calculated and the means were used for statistical analysis.

2.9.2. Statistical analysis

To choose the appropriate statistical test for each data set, the D´Agostino and Pearson omnibus normality test was used. Data IF-IHC (histone marks) are depicted as mean of single animals (dots and triangles) and mean over all animals (columns) + standard error of means (SEM). "n" indicates the number of independent experiments.

The two-tailed Students t-test was used for the IF-IHC experiments examining H3K4me3, when comparison between two groups was suitable. A one-tailed Student´s t test was applied for the IF-IHC experiments analyzing H3K27me3, when comparing two groups.

The one-way ANOVA, followed by Dunnett´s multiple comparison *post hoc test*, was used for the analysis of the western blot experiments, when comparing more than two groups.

Differences were considered significant, when the level of significance (p-value) was equal or less than 5 % ($p<0.05$, indicated with "*"), very significant, when equal or less than 1 % ($p<0.01$, "**") or extremely significant, when equal or less than 0.1 % ($p<0.001$, "***"). All graphical data were obtained by GraphPad Prism version 5.00 for Windows, GraphPad Software, San Diego California USA.

2.10. Western blot experiments

For western blot experiments HAB and NAB astrocytes were seeded in 6-well plates (Corning, #3506) at a concentration of 3x 10^5 cells/well and maintained (medium change every 3d) until they reached confluency. After treatment with ADs (FLX or ESC for 48 h (10 µM and 120 h (2x 5 µM)) cells were harvested, as stated above (**see 2.7**).

Western blot experiments were performed according to the following protocol. Cell pellets were resuspended in 40-80 µl homogenization buffer (1 M Tris at pH 7.5 (Sigma, #1503), protease inhibitor cocktail in H_2O (Roche Diagnostics, #04693116001) and manually homogenized for 30 s, using a pistil. RIPA buffer was added (1: 5 ratio, pH 7.6, containing 1M sodium dihydrogen phosphate (Roth, # T878.1), 10 mM disodium hydrogen phosphate (Roth, #P030.1), 154 mM sodium chloride (VWR, #27810295), 4 mM sodium deoxycholate (Sigma, #D6750), 1 % Triton-X-100 (Sigma, #X100), 20 % SDS (sodium duodecyl-sulfate, Roth, #4360.1) in H_2O). Cell homogenates were lysed O.N. at 4°C, on a shaker.

On the next day, 5x Laemmli buffer (ratio 1:5, 0.3 M Tris, 5 M Glycerin (Sigma, #2289), 25 mM EDTA (Roth, # 3053.1), 0.5 M DTT (Sigma, # D0632), 0.5 mM Bromphenolblue (Fisher Scientific, # 10187220), 10 % SDS in H_2O was added, cell lysates were denatured at 99°C for 10 min, quickly spun down and 28 µl lysate were loaded on a SDS-acrylamide gel (12 % SDS for histone marks, 10 % SDS for ephrinA1). Additionally, 5 µl of PageRuler^{TM} prestained protein ladder (Thermo Scientific, #26616) were loaded to ascertain an appropriate separation. Gel run was performed for 1.5 h, 90 V at RT in running buffer (25 mM Tris, 190 mM Glycine (Sigma, # G8898), and 0.1 % SDS in aqua dest. pH 8.3). After full separation of all the proteins, the gel was transferred to a blotting chamber.

To guarantee the complete protein transfer onto a polyvinylidene fluoride (PVDF) membrane (Zefa Laborservice, #79090), proteins were blotted for 2 h, 90 V at 4°C. To maintain a stable temperature environment the transfer buffer (20 mM Tris, 140 mM Glycine, 20 % Methanol (Merck, #M6009) in aqua dest, pH 8.3) was pre-cooled (4°C) and a cooling aggregate was inserted into the blotting chamber. For ephrinA1 the blotting was carried out at RT for 2 h at 100 V. After verification of the protein transfer via Ponceau S (Applichem, #A29350.500) staining, the membrane was blocked either O.N. in 5 % bovine serum albumin (BSA, Roth, #8076.4) at 4°C for histone marks or for 2 h at RT for ephrinA1. Afterward, membranes were incubated with primary antibodies for 24 h. All ABs were diluted in 5 % BSA in 1x PBS unless stated otherwise.

The following antibodies were used (**Table 3**):

Protein	Concentration	Company	Experiment
anti-β-actin (42 kDa, mouse)	1: 2000-4000	Sigma, #A-5441	Housekeeper in all experiments
anti-H3K4me3 (15.5 kDa, rabbit)	1: 1500	Millipore, #07-473	3.3.1
anti-H3K27me3 (15.5 kDa, rabbit)	1: 1500	Millipore, #07-449	3.3.2
anti H3K27ac (14 kDa, rabbit)	1: 1000	Abcam, # ab4729	3.3.3
anti-ephrinA1 (26 kDa, goat)	1: 500	Acris, # AP22424PU-N	3.5.2 3.5.3

Table 3: primary antibodies for western blot analysis

To enable chemiluminescent analysis, corresponding secondary antibodies coupled with horseradish peroxidase (HRP) were used:
rabbit anti-mouse HRP 1: 5000-10000 (Jackson ImmunoResearch, #315-035-003)
goat anti-rabbit HRP 1: 2000 (Jackson ImmunoResearch, # 111-035-003)
rabbit anti-goat HRP 1: 2000-2500 (Jackson ImmunoResearch, #305-035-003)
Membranes were incubated with the secondary antibodies diluted in 2 %NGS/PBS at RT for 2 h, on a rotating shaker.
Membranes were washed 3x 10 min in PBS and incubated with Pierce™ ECL Western blotting substrate (ThermoFisher Scientific, #32106) for 3-5 min. Chemiluminescent reaction was visualized with the ImageQuant LAS4000 (GE Healthcare Life Sciences, Freiburg, Germany).
Further analysis was carried out using Fiji (version 1.50d, National Institutes of health, USA, http://imagej.nih.gov/ij [6, 208]).

2.10.1. Protein expression quantification

Analysis of western blot experiments was carried out using Fiji. In brief, .gel files were imported in ImageJ via drag´n´drop, picture contrast was adjusted with the tool "Brightness & Contrast" to guarantee a proper analysis. The "gels tool" was used to define

the bands of interest and a plot profile was generated by Fiji. The raw data (area and percent) were used to calculate the results.

All lanes were normalized to the corresponding total amount of housekeeper protein (β-actin) (protein of interest/ actin = normalized results). First the mean of all controls was calculated in % (results normalized * 100/ mean of all controls). Then the mean of the different treatments (48 h and 120 h) was calculated accordingly. To analyze baseline differences in the proteins of interest between NAB and HAB astrocytes, normalized results of HAB were expressed as difference with respect to normalized results of NAB controls.

2.11. Short interfering RNAs (siRNA) fot the downregulation of ephrinA1

2.11.1. Transfection

HAB and NAB astrocytes were seeded in growth medium on PDL-coated 6-well plates at a concentration of $3x10^5$ cell/well for western blot experiments or glass cover slips at $5x10^4$. Cells were allowed to grow until reaching 30-50 % confluency.

I designed siRNAs complementary to the mRNA sequence of ephrin A1 (NCBI Reference Sequence: NM_053599.2) using the siDesign Center (Dharmacon Research, Lafayette, Co, USA). Four different siRNAs were selected and synthesized:

si1: 5´- GGA GAA GCU GUC UGA GAA A -3´
si2: 5´- GGG CAA GGA GUU CAA GGA A -3´
si3: 5´- CCG GAG AAG CUG UCU GAG AUU- 3´
si4: 5´- GAA GAG ACU CCA AGC AGA UUU -3

A non-targeting scrambled sequence (5´- CCUAAGGUUAAGUCGCCCUUU-3´) served as a negative control. All sequences were submitted to a BLAST search in order to verify the specific targeting of the siRNAs (si1-4) to ephrinA1, or the lack of targeting of any sequence for scrRNA. [209].

Transfection of primary rat astrocytes was performed using Lipofectamin™ 2000 (Invitrogen, # 11668-027) according to the manufacturer's instructions. In brief, 24 h prior to transfection the medium was changed to growth medium without antibiotics. The appropriate amount of each siRNA was diluted in Opti-MEM I Reduced Serum Medium (Invitrogen, # 31985-070) to reach a final working concentration of 50 nM or 100 nM. Lipofectamin™ 2000 was diluted at a ratio of 1: 50 in Opti-MEM I Reduced Serum Medium and incubated at RT for 5 min. Both dilution were combined and incubated for 20

min at RT. Finally the mixture was added onto the cells. Cells were allowed to grow for three additional days, before depriving the cells of FCS, 24 h prior to AD treatment. FLX was administered for 48 h and 120 h at a working concentration of 10 µM and 2x 5 µM. To terminate the treatment, cells were washed with cold PBS and harvested in Eppendorf tubes or fixed in 4 % PFA for 20 min at RT. PFA was removed and the fixed cells were washed with PBS and stored in PBS at 4°C until further processed with IF-ICC/Western blot

2.12. Native chromatin-Immunoprecipitation (ChIP) [151, 210]

To investigate, if the previously chosen genes of interest (**1.12**) were regulated by histone modifications (H3K4me3), I performed in cooperation with Dr. Mira Jakovcevski (Max Planck Institute of Psychiatry, Munich, Germany) a native ChIP on astrocytes derived from HAB and NAB rats under baseline conditions.

2.12.1. Cell culture

Cells were seeded in growth medium, on PDL-coated 150 mm cell culture dishes (Faust Lab Science, Klettau, Germany) at a concentration of $1x10^6$ cells and maintained under constant conditions in an incubator with 5 % CO_2 at 37°C. Medium was changed every 2-3d until cells reached 90-100 % confluency (approx. 20 D*IV*). 24 h before the treatment started, astrocyte-growth medium was exchanged to serum free medium. Cells were treated for 48 h and 120 h with FLX concentrations according **2.6**. Cells were then harvested in cold PBS, centrifuged (12.000 rpm, 10 min, 4°C), cell pellets were stored in -80°C and sent to Munich on dry-ice, guaranteeing a proper delivery.

2.12.2. Preparation of native chromatin

Native ChIP was performed by Dr. Jakovcevski at the Max Planck Institute of Psychiatry, as previously published [151, 211]. In brief, samples were directly homogenized in 400 µl MNase digestion/nuclei permeabilisation buffer (10 mMTris, pH 7.5, 4 mM $MgCl_2$ and 1 mM Ca^{2+}) and prewarmed to 37°C for 2 min. Afterwards 5 µl of MNase (0.4 U/µl) were added and homogenized cells were incubated for 5 min at 37°C for enzymatic sharing of chromatin. The reaction was then stopped by adding 40 µl 0.5 M EDTA. 900 µl hypotonization buffer (0.2 mM EDTA, supplemented with 0.1 mM Benzamidin, 0.1 mM PMSF and 1 mM DTT) were added for 1 h with intermittent vortexing to swell nuclei and release chromatin. Cell debris was removed by centrifugation (3000 rpm, at 4°C for 5 min.). 1000 µl of the supernatants were transferred into a fresh tube and the ChIP was carried out by adding ChIP dilution buffer (containing 50 mM EDTA, 200 mM Tris and

500 mM NaCl) and anti-H3K4me3 antibody (5 µl, Millipore, #07-473). Samples were incubated at 4°C for 16 h. In order to recover the immunoprecipitated chromatin, sample were incubated with magnetic Protein G beads for 2 h, beads were washed for 3 min each in low salt buffer (150 mM NaCL, 20 mM Tris pH 8.0, 2 mM EDTA, 1 % Triton X-100, 0.1 % SDS), high salt buffer (500 mM NaCL, 20 mM Tris pH 8.0, 2 mM EDTA, 1 % Triton X-100, 0.1 % SDS), followed by lithium chloride buffer (250 mM LiCL, 10 mM Tris pH 8.0, 1 mM EDTA, 1 % Deoxycholic acid, 1 % IGEPAL), and finally with TE buffer (10 mM Tris pH 8.0, 1 mM EDTA). Bound chromatin was eluted form the beads with 0.1 M NaHCO3 and 1 % SDS by vortexing 30 min at 65°C. The eluates, containing chromatin, were incubated with 40 mM Tris pH 6.5, 10 mM EDTA and 250 µg/ml ProteinaseK for 3- 4 h at 52°C.

Afterwards, DNA was purified using a QIAqick PCR purification kit (Quiagen, # 28104) according to the manufactures instructions. DNA from 200 µl of each input sample was extracted in parallel. Input DNA was used to check the efficacy of the enzymatic shearing with MNase on a 2 % Agarose gel. For quantification by qPCR, the ChIP DNA was diluted 1:5 in elution buffer (Quiagen). PCRs (10 µl final volume) were performed using QuantiFast SYBR Green PCR Master Mix (Quiagen, # 204054), specific primers (see **Table 5**) at a final concentration of 1:5 µM, and 2 µl of ChIP DNA or input DNA per reaction on a LightCycler 2.0 or a LightCycler 96 System (Roche Diagnostics). PCRs were run in duplicates. Ct values for the target H3K4me3 enriched sequences of ephrinA1 were normalized by the housekeeping gene B2m and by the input Ct value. Expression levels are represented relative to NAB control levels set to 1.

Gene	**Forward**	**reverse**
B2m (normalizer)	CGTCTCTCGGGAAAGGAGTG	ACTGTCCGCATACTCGCAAA
ephrinA1	GGTCCACCATACCTCCCTCT	GCCCTTTGTTCTTGCCCTTG

Table 4: Primer sequences ChIP- qPCR

2.13. GDF15

Primary astrocytes were derived from HAB and NAB rats (see **2.3**). For Western blot experiments, cells were seeded in PDL-coated 6-well plates, and for IF-ICC/siRNA experiments on glass cover slips and maintained in astrocyte-growth medium (changed

every 3d) until reaching 90-100 % confluency (Western blot) or 30-50 % confluency (ICC and siRNA).

2.13.1. Treatment

For Western blot experiments cells, were treated with FLX at a final concentration of 10 µm for 48 h and 96 h. Untreated cells served as a control.

For ICC experiments, cells were treated with exogenous GDF15 (R&D Systems, # Q99988) for 48 h and 96 h using the following concentrations:

- 1.0 ng/ml
- 0.1 ng/ml
- 1.0 ng/ml

Untreated cells served as a negative control and FLX treated cells (10 µM, 48 h and 96 h) as treatment control.

2.13.2. Western blot

Western blot experiments were carried out as stated above (**2.10**), with the following modifications. Cells were resuspended in 40 µl homogenization buffer and manually homogenized using a fire-sealed pipette tip. 10 µl RIPA was added, and cells were allowed to lyse O.N. at 4°C. Cells were denatured for 5 min at 99°C. Proteins were separated on a 10 % SDS-acrylamide gel. Transfer onto PVDF membraned was carried out at 70 V for 1 h at RT. Followed by blocking in 5 % BSA for 2 h at RT. Membranes were incubated with the following primary antibodies, O.N. 4°C, on a rotating shaker (**Table 5**):

Protein	Concentration	Company	Experiment
anti-β-actin (42 kDa, mouse)	1: 4000	Sigma, #A-5441	Housekeeper
anti-GDF15 (35 kDa, goat)	1: 250	Abcam, #ab39999	3.10.4

Table 5: primary antibodies western blot GDF15

Membranes were washed 3x 10 min in PBS + 0.1 % Tween (PBST) and incubated for 2 h at RT with secondary antibodies:

rabbit anti-mouse lgG (H+L) 1: 10000 (Jackson ImmunoResearch, # 315-035-033)

rabbit anti-goat IgG-HRP 1: 2500 (Santa Cruz, #sc-2020)

Protein bands were analyzed using Fiji. GDF15 band was normalized to the corresponding control (β-actin) (**see 2.10.1**).

2.14. Immunofluorescent analysis - GDF15

2.14.1. Fluorescent in situ hybridization (FISH) on CD1 mice, HAB and NAB

First, we generated a fluorescently labelled probe against Gdf15. For this aim, PCR oligonucleotides were designed complementary to bases 263–622 of the rat sequence of Gdf15 mRNA NM_019216.2 (5'- GGATACTCAGTCCAGAGGTGAGA-3' and 5'-CTGTCCTGTGCATAAGAACCAC-3'). PCR was performed on cDNA prepared from RNA extracted from rat primary astrocytes and cloning and preparation of the probe followed as previously described [212]. Sagittal hippocampal slices (350 µM) were prepared from CD1 mice that were deeply anesthetized using Isoflorane (Forene, Abbot, Wiesbaden, Germany) and quickly decapitated. Both hemispheres were cut on a vibratome (Microm HV 650V, Thermo Scientific, Walldorf, Germany). Slices were collected in artificial-CSF solution (1 mM magnesium chloride, 2 mM calcium chloride, 125 mM sodium chloride, 2.5 mM potassium chloride, 1.24 mM sodium dihydrogenphosphate, 25 mM D-Glucose, 25mM sodium hydrogencarbonate; D-Glucose, sodium hydrogencaronate, sodium chloride from Carl Roth; magnesium chloride, calcium chloride, potassium chloride from Merck) constantly bubbled with carbogen (95 % O_2/5 % CO_2, Linde, Munich, Germany). Following a 1 h recovery period, slices were treated for 2 h with 25 µM FLX. Subsequently slices were washed with 2x SSC (0.3 M sodium chloride, 30 mM sodium citrate, pH 7.0), fixed in 4 % PFA O.N. at 4°C and then washed in 2x SSC before proceeding to FISH as previously described [212].

For combined analysis of GDF15 $^{+}$/GFAP^{+} processes, brain slices derived from the PFC of HAB and NAB rats, were labelled at the end of the FISH with an antibody against GFAP, as described before (**See 2.8.2** GFAP staining). With the exception that the corresponding secondary antibody for GFAP^{+}-staining was coupled to Alexa Fluor 488 (green).

Images were acquired using an Olympus confocal microscope (2.8.4).

2.14.2. IF-ICC on primary astrocytes

For IF-ICC, astrocytes (HAB and NAB) grown on PDL-coated glass cover slips were treated with exogenous GDF15 according to the following scheme:

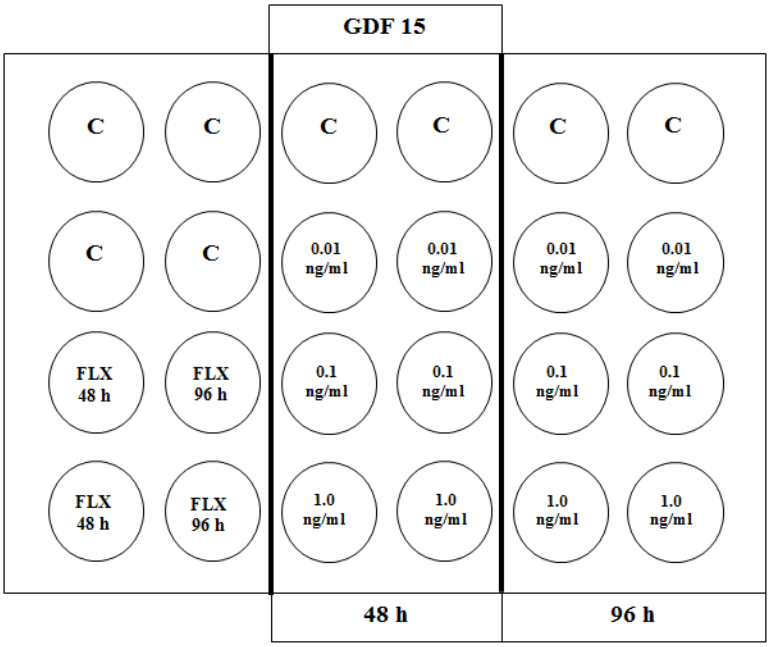

After terminating the treatment cells were fixed in 4 % PFA for 20 min, washed and stained with the following primary antibodies:

Combination	Protein	Specificity	Concentration	Company	Experiment
astrocytes	mouse-anti-S100β	glia specific marker	1: 1000	Sigma, #S2532	3.10.1
	mouse-anti-GFAP	glia specific marker	1: 400	Sigma. #G3839	3.10.2 3.10.3
GDF15	mouse-anti-GDF15	GDF15	1: 250	Abcam, #ab39999	3.10.4

Table 6: Antibody combination GDF15 IF-ICC experiments

Followed by fluorophore-labeled secondary antibodies:

donkey anti-goat IgG (H+L) AF488 1: 1000 (Invitrogen, # A-11055)

anti-mouse IgG F(ab')$_2$ fragment-Cy3 1: 400 (Sigma, # C2181)

In all IF-ICC DAPI (1:1000) was used to label nuclei. Microphotographs were acquired using a confocal microscope Leica SP8 as described **2.8.4.**

2.15. RNAi

siRNAs complementary to the mRNA sequence of GDF15 were designed.

si1: 5´- ACUCAACCCGGACGAGCUAUU-3´

si2: 5´- UGACCCAGCUGUCCGGAUAUU-3´

The same non targeting sequence as in **2.11** served as a negative control. siRNAs were subjected to a BLAST search to verify the specific targeting to GDF15 (si1&2).

Transfection was carried out as described in section **2.11.1** including the following alterations:

GDF15 siRNA oligonucleotides were diluted at a final working concentration of 100 nM in 50 µl Opti-MEM I Reduced Serum Medium and cells were treated according to the following scheme (**Fig.19)**:

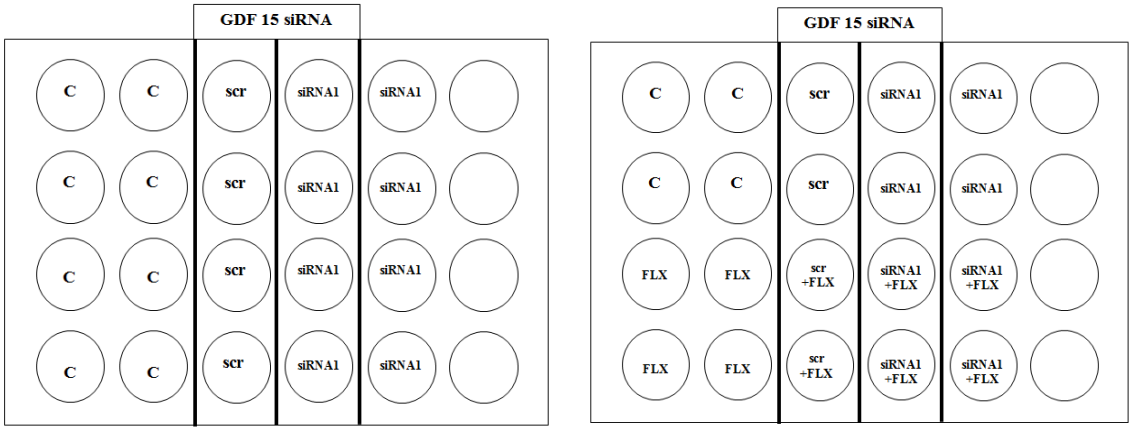

Fig. 19: treatment scheme for siRNA directed against GDF15

Cells were then incubated for 3d at 37°C (5% O_2/95% CO_2), cells were deprived of FCS and treated with FLX (10 µM) for 48 h, according to (**2.6**).

Cells fixed with 4 % PFA underwent IF-ICC staining as described 2.8.3**.** Microphotographs were acquired using a confocal microscope Leica SP8.

2.16. Fluorescent and morphological analysis of GDF15

To analyze astrocytes around blood vessels, microphotographs were taken using the Olympus IX81. As the Olympus software saves pictures and default data as .oib files, the files had to be transformed into .tiff files for further analysis in ImageJ, using the Fluoview FV1000 program (version 2.1 c, Olympus Fluoview Resource center).

For the analysis of the fluorescent intensity of *Gdf15*, the histogram function of Adobe Photshop CS3 (Version 10.0, Adobe Systems, San Jose, California, USA) was used. First the boundaries of the region of interest (ROI; choroid plexus or blood vessels) were marked using the "lasso" tool. The intensity of signal in the red channel, corresponding to *Gdf15* expression and the number of pixels in the ROI were recorded for each image. For

statistical analysis the values obtained were normalized to the pixels of the ROI and averaged per animal.

For the analysis of *Gdf15*$^+$ and GFAP$^+$ processes, Photoshop was used: in the green channel, which depicts GFAP$^+$ processes, the processes touching the previously defined ROI around blood vessels were counted manually. Additionally, *Gdf15*$^+$ (red channel) processes were quantified.

For the morphological analysis, a plugin of ImageJ, NeuronJ, was used [213, 214]. This tool provides the possibility to mark and analyze processes. Images need to be converted from the confocal format into 8 bit color pictures to be compatible with the plugin. Here NeuronJ was used to count the total number of processes per cell and to measure their lengths.

2.17. Statistical analysis

To choose the appropriate statistical test, the D´Agostino and Pearson omnibus normality test was used for each data set. The two-tailed Students t-test was used for the western blot experiments examining GDF15, as well as for ChIP experiments and for IF-IHC experiments, when comparing two groups. The One-way ANOVA, followed by Dunnett´s or Tukey´s multiple comparison *post hoc test*, was used for the analysis of the IF-ICC experiments, when comparing more than two groups as well as for western bot experiments. For experiments comparing dependent and independent variables a Two-way ANOVA with Dunnett´s or Bonferroni´s multiple comparison *post hoc test* was used. Differences were considered significant, when the level of significance (p-value) was equal or less than 5 % ($p < 0.05$, indicated with "*"), very significant, when equal or less than 1 % ($p < 0.01$, "**") or extremely significant, when equal or less than 0.1 % ($p<0.001$, "***"). All graphical data were obtained by GraphPad Prism version 5.00 for Windows, GraphPad Software, San Diego California USA.

3. Results

3.1. Histone 3 – Lysine 4 – trimethylation (H3K4me3)

3.1.1. Global expression of H3K4me3

In order to analyze the differences in the number of cells expressing H3K4me3 between HAB and NAB rats, I performed immunofluorescent- immunohistochemical stainings (IF-IHC) on brain slices derived from the prefrontal cortex (PFC) of both rat strains. As shown in **Fig. 20a) & b)**, under baseline conditions, no overall differences could be observed in the number of cells expressing H3K4me3 between NAB and HAB rats (NAB: n= 6, 52.32 ± 3.409 %; HAB: n= 5, 51.21 ± 4.049 %; Student´s t- test, $t_{(9)}$= 0.2114, p= 0.837, n.s.). The total number of cells (DAPI) did not differ between HAB and NAB (**see Suppl.1a)**).

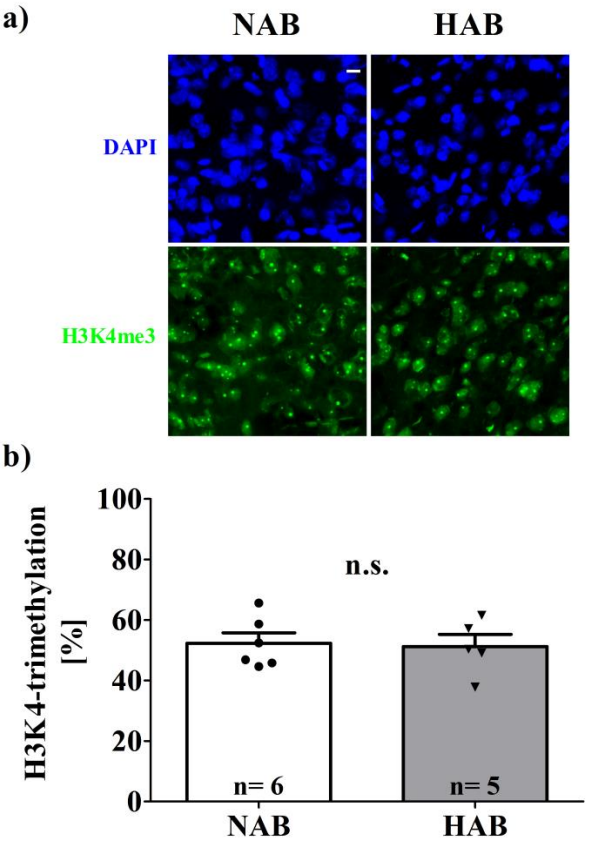

Fig. 20: Global expression of H3K4me3 in PFC does not differ between NAB and HAB rats, under baseline conditions

a) Representative microphotographs (Leica SP8, Z-stack series, 20-30 µm, step size 1.23 µm). $H3K4me3^+$ cells (green), nuclear staining DAPI (blue), scale bar 10 µm

b) Quantitative IF-IHC analysis in the PFC of NAB (n= 6 animals) and HAB (n= 5 animals) under baseline conditions, revealed no difference. The average H3K4-trimethylation [in %] is depicted as mean + SEM. Student´s t-test, p= 0.837, n.s.

3.1.2. Cell-type specific expression of H3K4me3

To investigate whether a specific cell-type might be affected, I performed a colocalization analysis of H3K4me3 with astrocytes and neurons. This analysis revealed that in the PFC of HAB rats significantly more astrocytes ($GFAP/S100\beta^+$, **Fig. 21 a)** colocalized with H3K4me3 than in NAB rats; white arrows indicate colocalizing cells; HAB: n= 4, 64.37 ± 4.194 %; NAB: n= 6, 47.31 ± 4.410 %; Student´s t-test, $t_{(6)}$= 2.802, p= 0.0311).

Whereas, the colocalization with neurons did not show any differences between the two strains ($NeuN^+$, **Fig. 21 b)**. In both strains about 75.0 % of all neurons were colocalizing with H3K4me3, (**Fig. 21 c)** (HAB: n= 4, 75.38 ± 8.334 %; NAB: n= 6, 75.01 ± 4.112 %). Additionally, I could observe that HAB rats had significantly less astrocytes in the PFC than NAB rats (**see Suppl. 1b)**), but the total number of neurons was equal (**see Suppl. 1c)**), as described for post-mortem brain tissue from depressive patients [31].

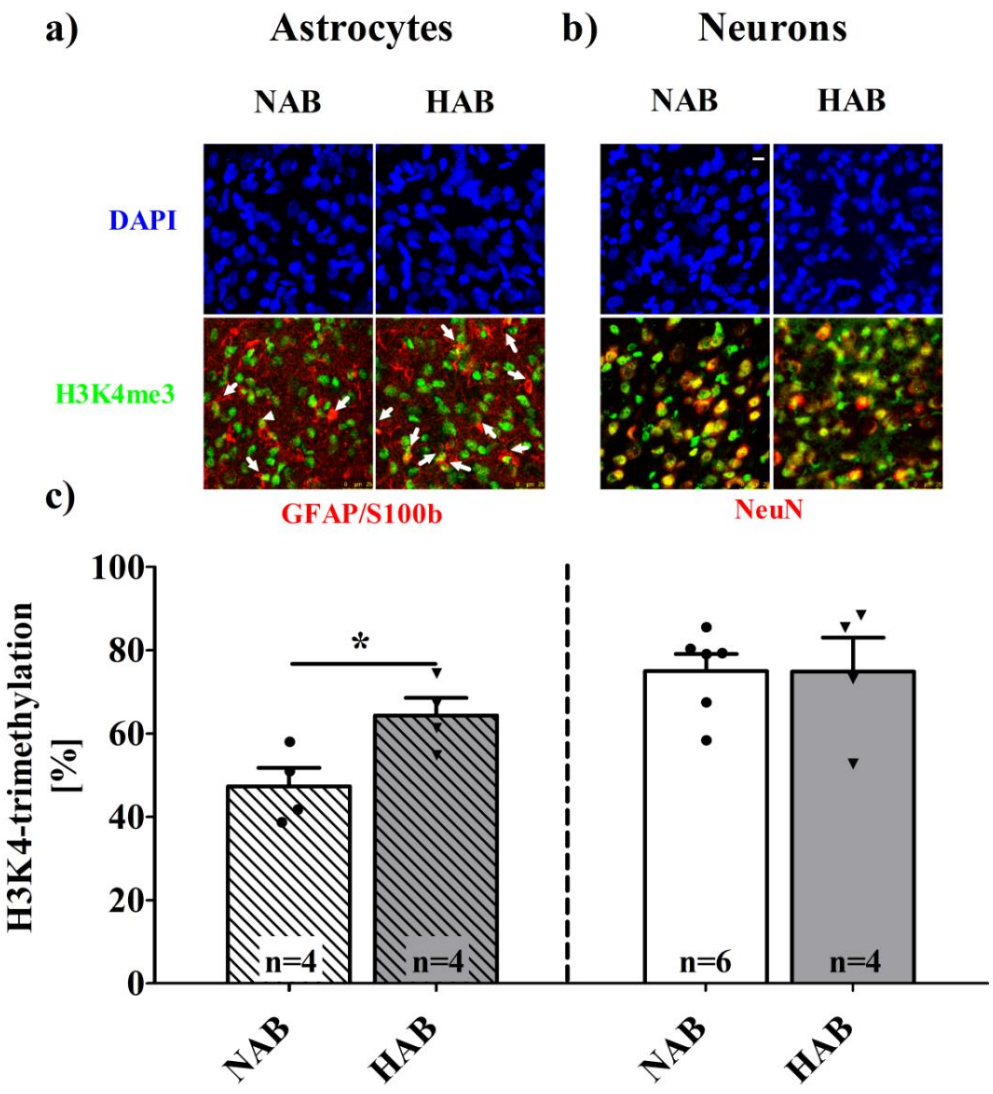

Fig. 21: Cell-type specific expression of H3K4me3 in PFC of NAB and HAB, under baseline conditions, shows a significantly higher amount of colocalization in HAB astrocytes

a) **+ b)** Representative microphotographs (Leica SP8, Z-stack series, 20-30 µm, step size 1.23 µm). $H3K4me3^+$ cells (green), nuclear staining DAPI (blue), $GFAP/S100b^+$ (a), red), $NeuN^+$ (b), red)); scale bar 10 µm

c) Cell type specific IF-IHC analysis in the PFC of NAB (n= 4/6) and HAB (n= 4), under baseline conditions, showed significantly higher colocalization with H3K4me3 in astrocytes in HAB rats. H3K4-trimethlyation [in %] is depicted as mean +SEM, Student´s t-test, * $p< 0.05$

3.2. H3K4me3 after fluoxetine treatment

3.2.1. Global expression of H3K4me3 after FLX injections in NAB

Subsequently, I investigated whether the differences observed under baseline conditions were affected by treatment with FLX. First, NAB rats were injected i.p. with either FLX (20 mg/ kg/ d) or saline (SAL). IF-IHC analysis of these animals revealed a significant increase in the overall expression of H3K4me3 in the PFC after treatment with FLX for 2 d (**Fig. 22 a)** and **b)**, SAL: n= 4, 40.07 ± 3.880 %; FLX: n= 4, 61.41 ± 3.192 %, Student´s t-test, $t_{(6)}$= 3.660, p= 0.0106). Besides that, when comparing basal (not injected) NAB to NAB that received a SAL injection, it was possible to rule out that the injection itself caused any changes in the overall expression of H3K4me3 (**see Suppl. 2**)

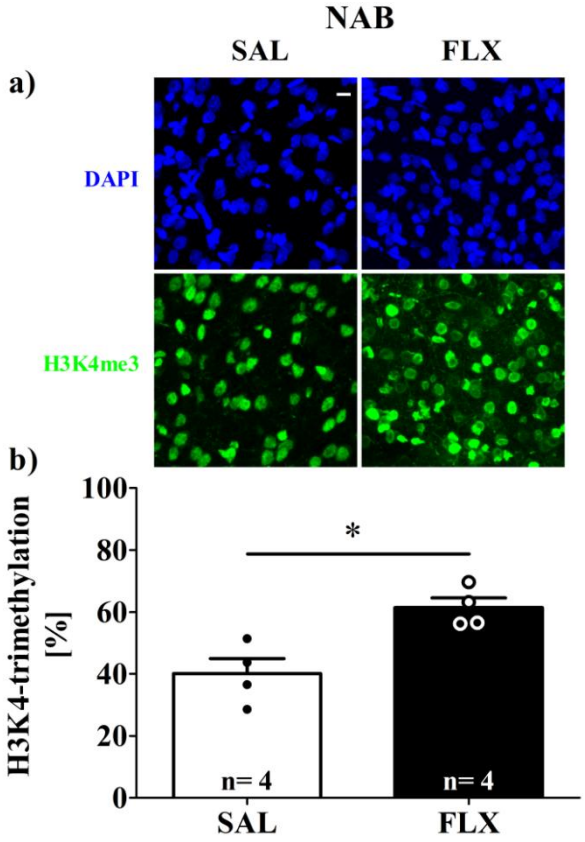

Fig. 22: Global expression of H3K4me3 in PFC of NAB after injection with FLX vs. control (SAL) is significantly increased

a) Representative microphotographs (Leica SP8, Z-stack series, 20-30 µm, step size 1.23 µm). $H3K4me3^+$ cells (green), nuclear staining DAPI (blue), scale bar 10 µm

b) Quantitative IF-IHC analysis in the PFC of NAB (n= 4), revealed a significant increase in overall H3K4me3 after FLX treatment. The average H3K4-trimethlyation [in %] is depicted as mean +SEM, Student´s t-test, * p<0.05.

3.2.2. Cell-type specific expression of H3K4me3 after FLX injection in NAB

To investigate which cell-type was targeted by FLX, I performed IF-IHC in the PFC of NAB animals, analyzing the colocalization of H3K4me3 with either astrocytes or neurons. I could show that in neurons, FLX injections did not change the amount of colocalization with H3K4me3 (**Fig. 23**), SAL neurons: n= 4, 62.48 ± 8.227 %, FLX neurons: n= 4, 75.59 ± 1.796 %, Student´s t-test, $t_{(6)}$= 1.556, p= 0.1707). Whereas in astrocytes, after FLX

treatment, a significant increase in the colocalization with H3K4me3 could be observed (**Fig. 23**); SAL astrocytes: n= 4, 32.28 ± 1.889 %, FLX astrocytes: n= 4, 49.59 ± 2.568 %, Student´s t-test, $t_{(6)}$= 5.422, p= 0.0016). Additionally, neither in astrocytes nor in neurons the injection itself changes H3K4me3 levels (**see Suppl. 3a)**).

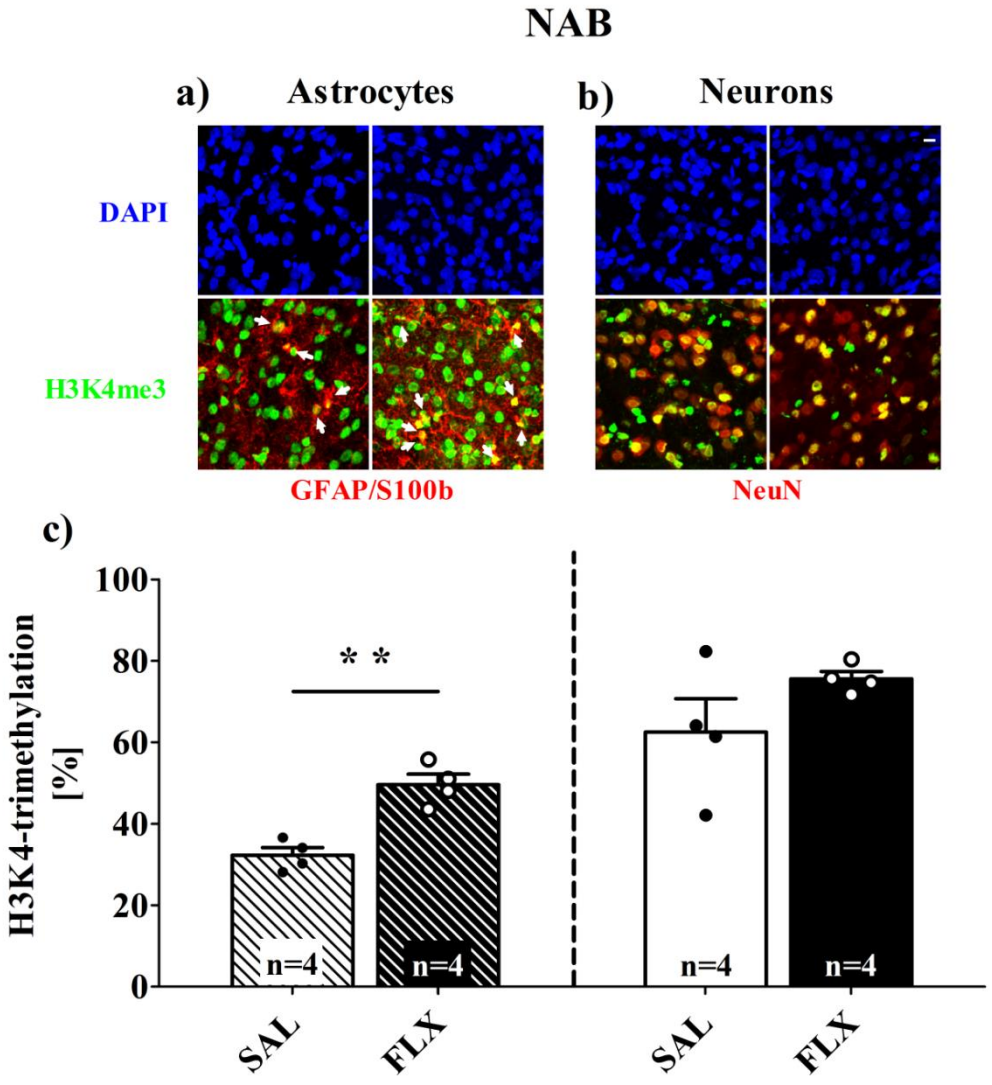

Fig. 23: Cell-type specific expression of H3K4me3 in PFC of NAB after injection with FLX shows a significantly increased colocalization in astrocytes

a) **+ b)** Representative microphotographs (Leica SP8, Z-stack, 20-30 µm, step size 1.23 µm). H3K4me3$^+$ cells (green), nuclear staining DAPI (blue), GFAP/S100b$^+$ (red), NeuN$^+$ (red); scale bar 10 µm

c) Cell type specific IF-IHC analysis in the PFC of NAB (n= 4), showed significantly higher colocalization with H3K4me3 in astrocytes after FLX injection. H3K4-trimethlyation [in %] is depicted as mean +SEM, Student´s t-test, ** p< 0.01

3.2.3. Global expression of H3K4me3 after FLX injection in HAB

Furthermore, I investigated if our animal model for depression-related behavior responds to pharmacological treatment with FLX. Therefore, HAB rats were injected either with FLX (20 mg/ kg/ d) or saline (SAL). IF-IHC analysis of the PFC of these animals revealed no significant differences in the global expression of H3K4me3 after treatment with FLX for 2d (**Fig. 24 a)** and **b)**, SAL: n= 3, 60.56 ± 5.480 %; FLX: n= 3, 52.17 ± 1.807 %, Student´s t-test, $t_{(4)}$= 1.454, p= 0.2196). Additionally, in HAB animals it was also possible to rule out an effect on H3K4me3 caused by the injection itself (**see Suppl. 2**).

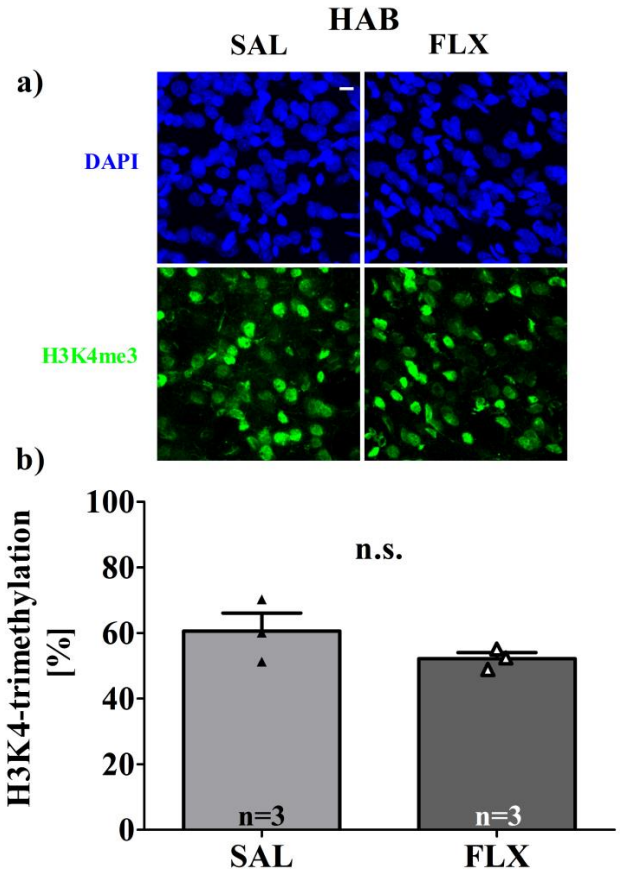

Fig. 24: Global expression of H3K4me3 in PFC of HAB after injection with FLX vs. control (SAL) does not show differences

a) Representative microphotographs (Leica SP8, Z-stack, 20-30 µm, step size 1.23 µm). $H3K4me3^{+}$ cells (green), nuclear staining DAPI (blue), scale bar 10µm

b) Quantitative IF-IHC analysis in the PFC of HAB (n= 3), showed no overall changes of H3K4me3 after FLX injection. The average H3K4-trimethylation [in %] is depicted as mean +SEM, Student´s t-test, p= 0.21, n.s.

3.2.4. Cell-type specific expression of H3K4me3 after FLX injection in HAB

Cell-type specific analysis of the PFC in HAB animals revealed no differences in the colocalization of H3K4me3 with astrocytes after FLX treatment (**Fig. 25 a)**, **b)** and **c)**, SAL astrocytes: n= 3, 70.03 % ± 3.533; FLX: n= 3, 62.53 ± 1.516 %, Student´s t-test, $t_{(4)}$= 1.1951, p= 0.1229. Whereas, in neurons after FLX treatment, a tendency towards a decrease could be observed (**Fig. 25**); SAL neurons: n= 3, 80.21 ± 1.008 %; FLX neurons: n= 3, 65.09 ± 5.707 %, Student´s t-test, $t_{(4)}$= 2.610, p= 0.0594). Also in this case, no cell-type specific effect of the injection itself could be observed in HAB animals (**see Suppl. 3b)**).

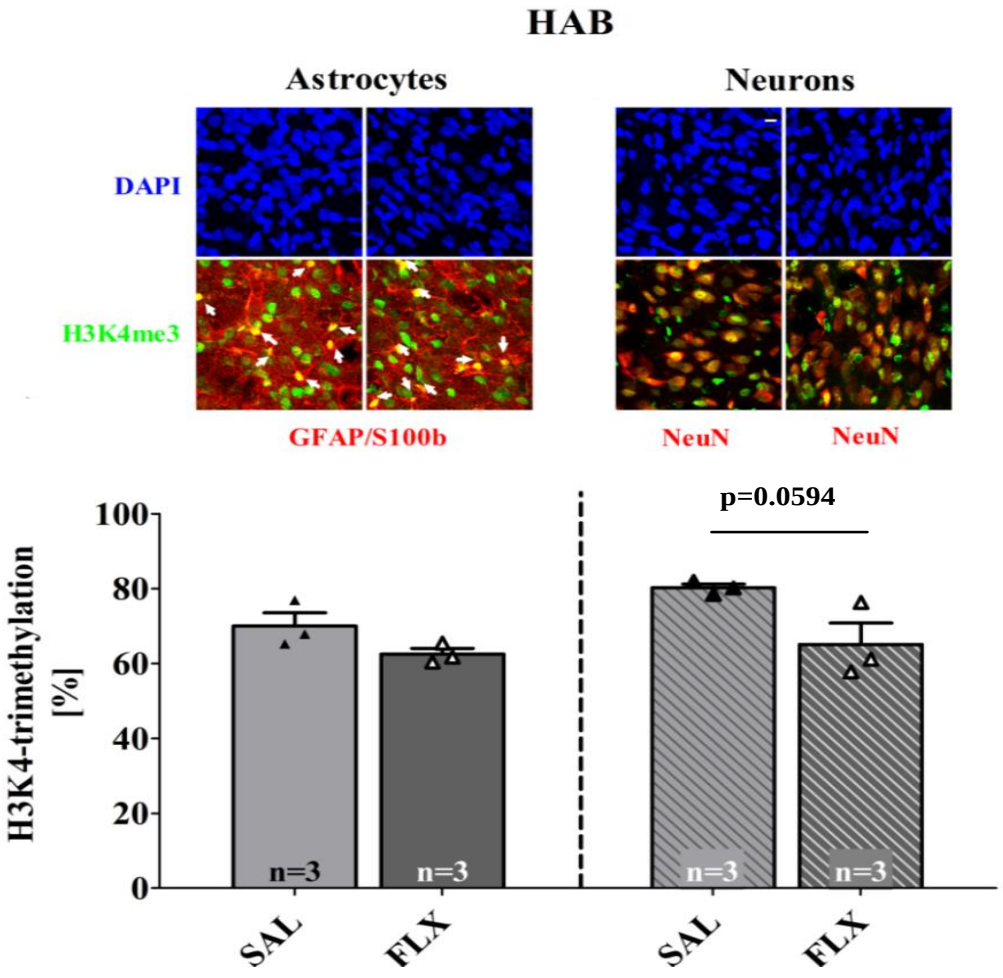

Fig. 25: Cell type specific expression of H3K4me3 in PFC of HAB after injection with FLX tends to decrease in neurons

a) **+b)** Representative microphotographs (Leica SP8, Z-stack, 20-30 µm, step size 1.23 µm). H3K4me3$^+$ cells (green), nuclear staining DAPI (blue), GFAP/S100b$^+$ (red), NeuN$^+$ (red,); scale bar 10 µm

c) Cell type specific IF-IHC analysis in the PFC of HAB (n= 3) revealed no differences in the in colocalization of H3K4me3 in astrocytes, but a tendency towards a decrease after FLX treatment in neurons. H3K4-trimethylation [in %] is depicted as mean +SEM, Student´s t-test, p= 0.0594.

3.3. Posttranslational histone modifications (PTM) – protein expression

3.3.1. H3K4me3

In order to analyze if our cell culture model was suitable to reflect the differences observed in animals, I used primary cortical astrocytes derived from HAB and NAB rats and treated the cells according to the scheme described in (**2.6**). After treatment of astrocytes with FLX or ESC for 48 h (10 µM, one time treatment) or 120 h (5 µM, two times treatment) and untreated controls (C), I performed western blot analysis using antibodies specific for H3K4me3 and β-actin, serving as the internal normalizer. Using this technique I could verify the baseline difference in HAB astrocytes compared to NAB astrocytes, with almost 2-fold higher expression of H3K4me3 in HAB cells (**Fig. 26** and **Fig. 27 a**; NAB C: n= 10, 100.00 % ± 13.32; HAB C: n= 6, 198.2 % ± 27.58, Student´s t-test, $t_{(25)}$= 3.609, p= 0.0013). After FLX treatment for 48 h and 120 h, no significant differences in the protein expression of H3K4me3 in NAB cells could be detected (**Fig. 26** and **27 b**; NAB 48: n= 10, 121.7 ± 19.73 %; NAB 120: n= 6, 150.7 ± 13.82 %; One-way ANOVA, with Dunnett´s multiple comparison *post hoc test*, $F_{(2, 42)}$= 0.6339, p= 0.5355).

However, although after 48 h FLX treatment no effect was visible, HAB astrocytes showed a significant decrease in H3K4me3 protein expression after 120 h FLX treatment, which dropped down to almost the same level observed in NAB C (**8c**; HAB 48: n= 6, 188.7 ± 19.73 %, HAB 120: n= 3, 80.32 ± 27.61 %; One-way ANOVA with Dunnett´s multiple comparison *post hoc test*, $F_{(2, 22)}$= 4.662, p= 0.0205). Comparison between the control in the ESC experiments revealed a difference similar to the one observed with FLX (**Fig. 27**, NAB C: n= 4, 100.00 ± 12.86 %; HAB C: n= 6, 344.9 ± 45.97 %, Student´s t-test with Welch´s correction, $t_{(9)}$= 5.131, p= 0.0006). After ESC treatment, no significant pharmacological effects were visible, although in both cell-types after 120 h, H3K4me3 expression seemed to increase (**Fig. 27 d-f**, NAB 48: n= 4, 157.6 ± 72.18 %, NAB 120: n= 5, 232.3 ± 69.45 %; HAB 48: n= 6, 301.5 ±97.66 %, HAB 120: n= 6, 458.1 ± 109.1 %, for both a One-way ANOVA with Dunnett´s multiple comparison *post hoc test* was used. NAB: $F_{(2,23)}$= 1.180, p= 0.3253; HAB: $F_{(2,25)}$= 0.8162, p= 0.4535).

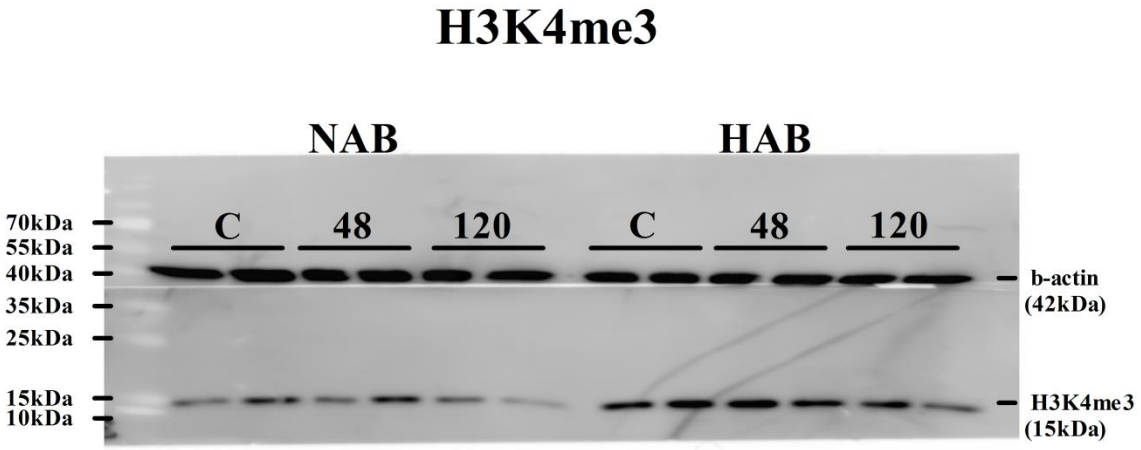

Fig. 26: Representative western blot for H3K4me3 on primary cortical astrocytes NAB vs. HAB

H3K4me3 [15.5 kDa] levels were measured in astrocytes derived from NAB and HAB rats under baseline conditions (C) *in vitro* and after FLX treatment for 48 h and 120 h. β-actin [42 kDa], serving as a normalizer

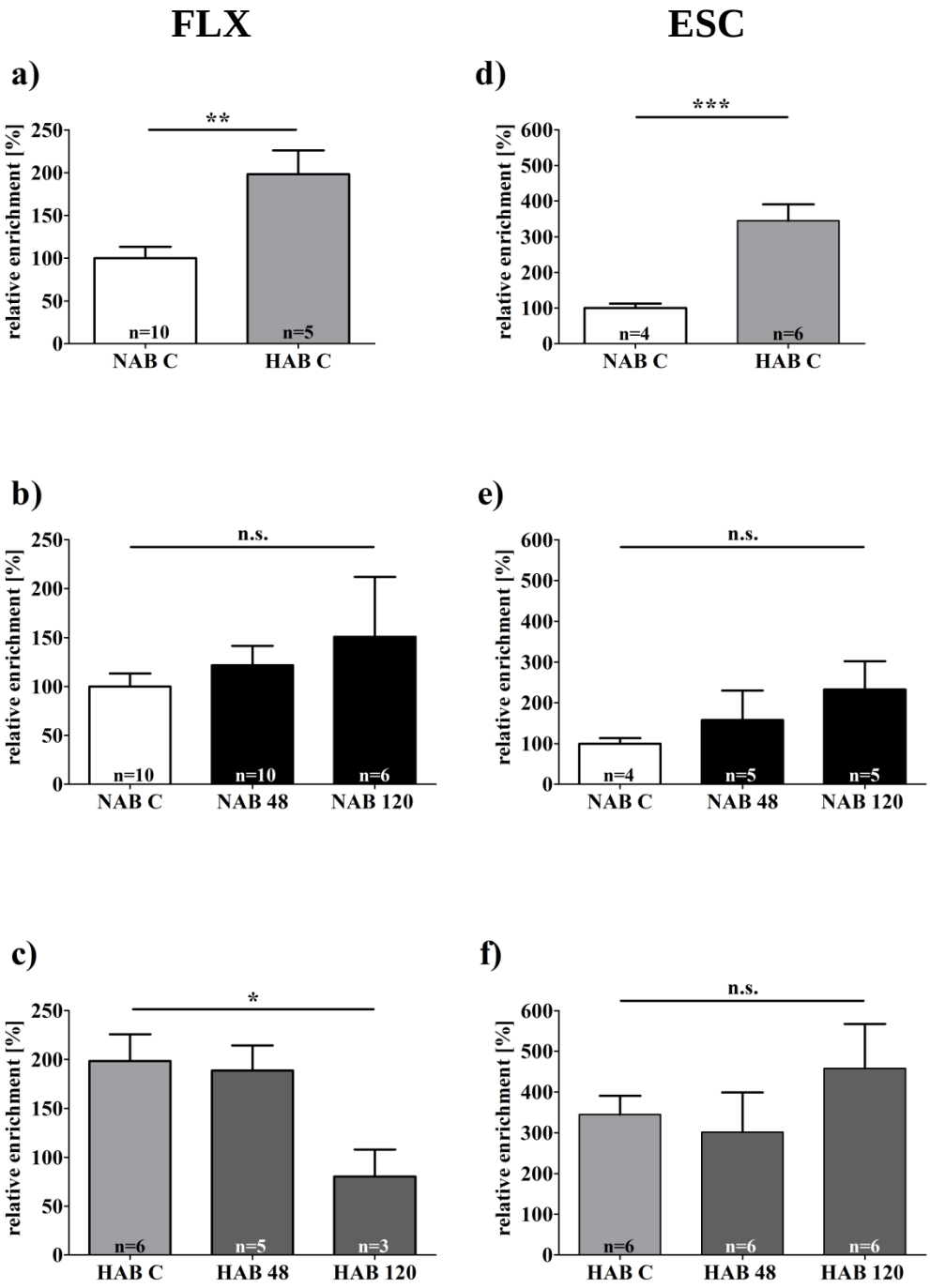

Fig. 27: Western blot analysis on primary cortical astrocytes under baseline conditions showed 2 - 3.5 fold higher expression of H3K4me3 in HAB astrocytes

H3K4me3 levels were measured in astrocytes derived from NAB and HAB rats under baseline conditions (C) *in vitro* normalized to β-actin before and after treatment with FLX (a-c) and ESC (d-f). Relative enrichment [in %] is calculated in respect to NAB C. All data are represented as mean +SEM. ***p<0.001, **p<0.01, *p<0.05 Student´s t-test (a), with Welch´s correction (d), or one way ANOVA with Dunnett´s multiple comparison *post hoc test* (b, c, e, f)

3.3.2. Histone 3-lysine 27-trimethylation

Along with the activating PTM, I analyzed H3K27me3 (repressive mark) in primary astrocytes derived from both HAB and NAB rats. The treatment was carried out in the same manner as described before. Astrocytes were treated with FLX or ESC for 48 h and 120 h. Analysis of H3K27me3 protein expression by means of western blot showed that, under baseline conditions, HAB astrocytes expressed 50 % less H3K27me3, as compared to NAB astrocytes (**Fig. 28** and **Fig. 29 a, FLX** NAB C**:** n= 10, 100.0 ± 21.53 %; HAB C: n= 5, 45.82 ± 4.933 %, Student´s t-test with Welch´s correction, $t_{(7)}$= 2.453, p= 0.0439; **ESC Fig. 29 d** NAB C: n= 4, 100.00 ± 4.567 %, HAB C: n= 6, 55.26 ± 7.398 %, Student´s t-test, $t_{(9)}$= 4.885, p= 0.0009). After FLX or ESC treatment in NAB astrocytes no significant differences could be observed, neither after 48 h nor after 120 h (**Fig. 28** and **Fig. 29 b, FLX** NAB 48: n= 10, 182.6 ± 59.02 %, NAB 120: n= 6, 185.7 ± 62.67 %, One-way ANOVA with Dunnett´s multiple comparison *post hoc test* $F_{(2, 24)}$= 0.7688, p= 0.4747; **ESC Fig. 29 e,** NAB 48: n= 4, 84.78 ± 21.10 %, NAB 120: n= 5, 113.5 ± 31.54 %, One-way ANOVA with Dunnett´s multiple comparison *post hoc test* $F_{(2, 18)}$= 0.3658, p= 0.6987). However, I should mention that after FLX treatment an increase (about 80 %) in NAB astrocytes could be observed, but it did not reach significance, probably due to the high heterogeneity of NAB cells. However, in HAB astrocytes H3K27me3 expression decreased even further to about 50 % after 120 h FLX treatment (**Fig. 28** and **Fig. 29 c;** HAB 120: n= 3, 26.70 ± 3.698 %), whereas after 48 h FLX treatment no differences were visible in HAB (**Fig. 28** and **Fig. 29 c,** HAB 48: n= 5, 49.06 ± 5.388 %, One-way ANOVA with Dunnett´s multiple comparison *post hoc test*, $F_{(2, 27)}$= 5.906, p= 0.0075). ESC treatment did not show the same effects in HAB, as seen after FLX treatment (**Fig. 29 f,** HAB 48: n= 6, 92.53 ± 17.27 %, HAB 120; n= 6, 78.43 ± 17.27 %, One-way ANOVA with Dunnett´s multiple comparison *post hoc test*, $F_{(2, 6)}$= 0.1953, p= 0.8276

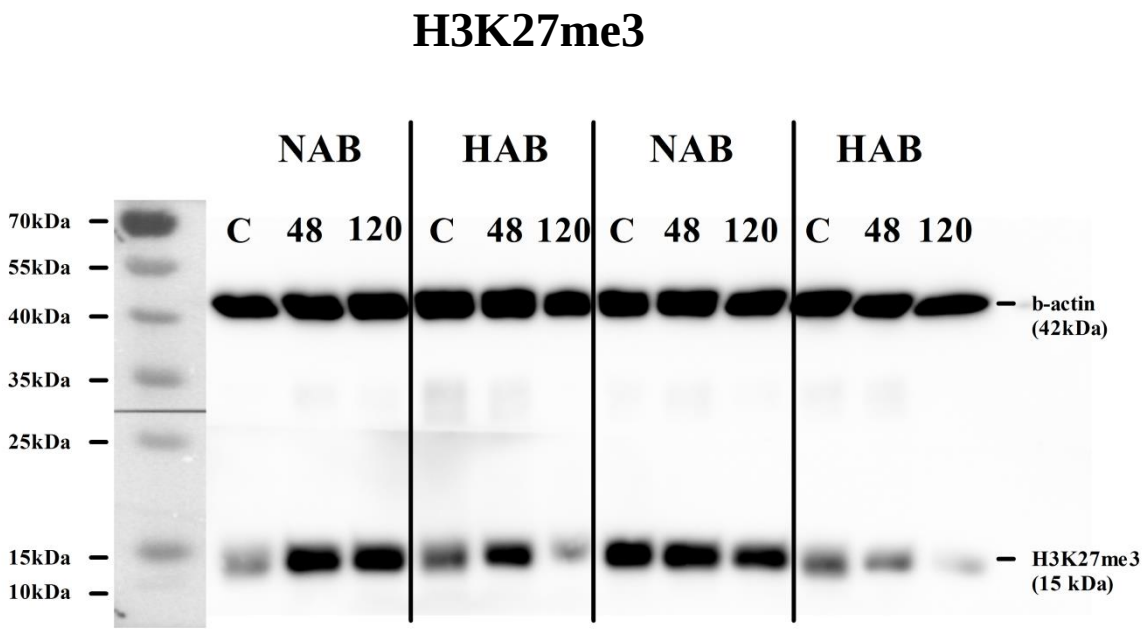

Fig. 28: Representative western blot of H3K27me3 on primary cortical astrocytes NAB vs. HAB
H3K27me3 [15.kDa] levels were measured in astrocytes derived from NAB and HAB rats under baseline conditions (C) *in vitro* and after FLX or ESC treatment for 48 h and 120 h. β-actin [42 kDa], serving as a normalizer

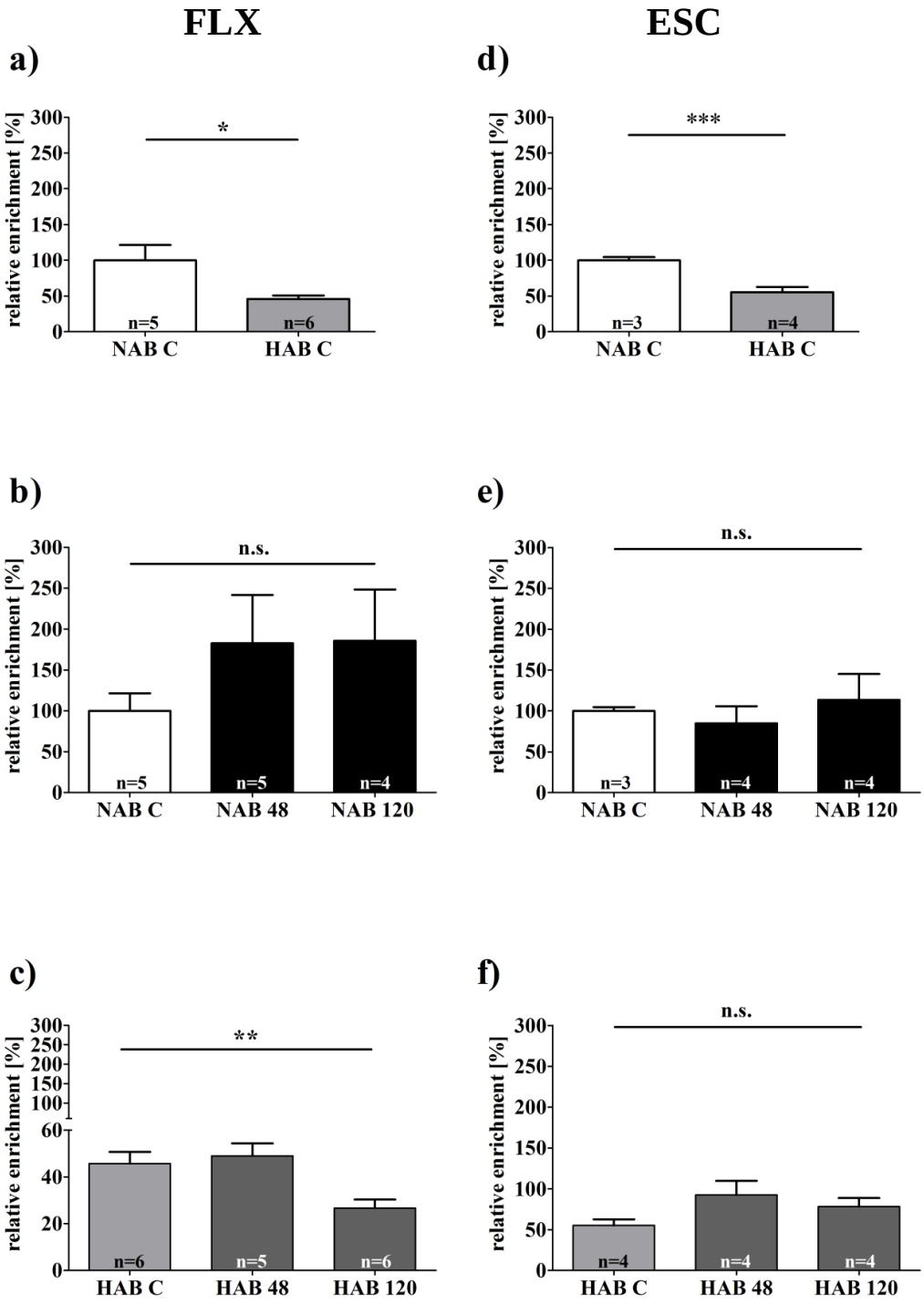

Fig. 29: Western blot analysis on primary cortical astrocytes under baseline conditions showed that HAB astrocytes express less than half of the amount of H3K27me3

H3K27me3 levels were measured in astrocytes derived from NAB and HAB rats under baseline conditions (C) *in vitro* normalized to β-actin before and after treatment with either FLX (a-c) or ESC (d-f). Relative enrichment (in %) is calculated in respect to NAB C. All data are represented as mean +SEM. ***p<0.001, **p<0.01,*p<0.05, Student´s t-test (d) with Welch´s correction (a) and one-way ANOVA with Dunnett´s multiple comparison *post hoc test* (b,c,e,f)

3.3.3. Histone 3-Lysine 27-acetylation (H3K27ac)

In addition to the methylation marks, I analyzed the acetylation on H3K27, another activating mark, known to interact with the two afore mentioned. Under baseline conditions in astrocytes derived from HAB and NAB rats, I observed that in HAB H3K27ac was almost 50 % less expressed compared to NAB**.** (**Fig. 30** and **Fig. 31 a,** FLX NAB C: n= 6, 100.00 ± 28.31 %, HAB C: n= 6, 51.84 ± 7.683 %**,** Student´s t-test with Welch´s correction, $t_{(10)}$= 1.642 p= 0.1317; ESC: **Fig. 31** d, NAB C: n= 5, 100.00 ± 51.11 %; HAB C: n= 6, 53.85 ± 18.42 %, Student´s t-test with Welch´s correction, $t_{(8)}$= 0.9421, p= 0.3737). After treatment with FLX for 48 h and 120 h in both cell-types, the analysis revealed a significant decrease of the mark in NAB to almost 60 % less, that was already visible after 48 h and persisted along the 120 h treatment (**Fig. 31 b;** NAB 48: n= 6, 46.33 ± 11.76 %; NAB 120: n= 6, 40.19 ± 9.716 %, One-way ANOVA with Dunnett´s multiple comparison *post hoc test*, $F_{(2,31)}$= 3.459, p= 0.0441). In HAB astrocytes, on the other hand, I observed a trend towards an increase after 120 h FLX treatment that was not yet present after 48 h. (**Fig. 31 c** HAB 48: n= 6, 46.58 ± 6.911 %; HAB 120: n= 6, 117.8 ± 38.36 %; One-way ANOVA with Dunnett´s multiple comparison *post hoc test*, $F_{(2,29)}$= 2.851, p= 0.0741). An almost identical treatment effect could be observed after ESC treatment (**Fig. 31 e**, NAB 48: n= 5, 53.85 ± 18.42 %, NAB 120: n= 5, 69.55 ± 19.96 %, One-way ANOVA with Dunnett´s multiple comparison *post hoc test*, $F_{(2,22)}$= 0.4281, p= 0.6570). In HAB astrocytes treated with ESC an increase of H3K27ac after 120 h was visible, but did not reach statistical significance (**Fig. 31 f**, HAB 48: n= 5, 49.47 ± 5.736 %, HAB 120: n= 5, 123.4 ± 42.10 %, One-way ANOVA with Dunnett´s multiple comparison *post hoc test* $F_{(2,20)}$= 3.079, p= 0.0683).

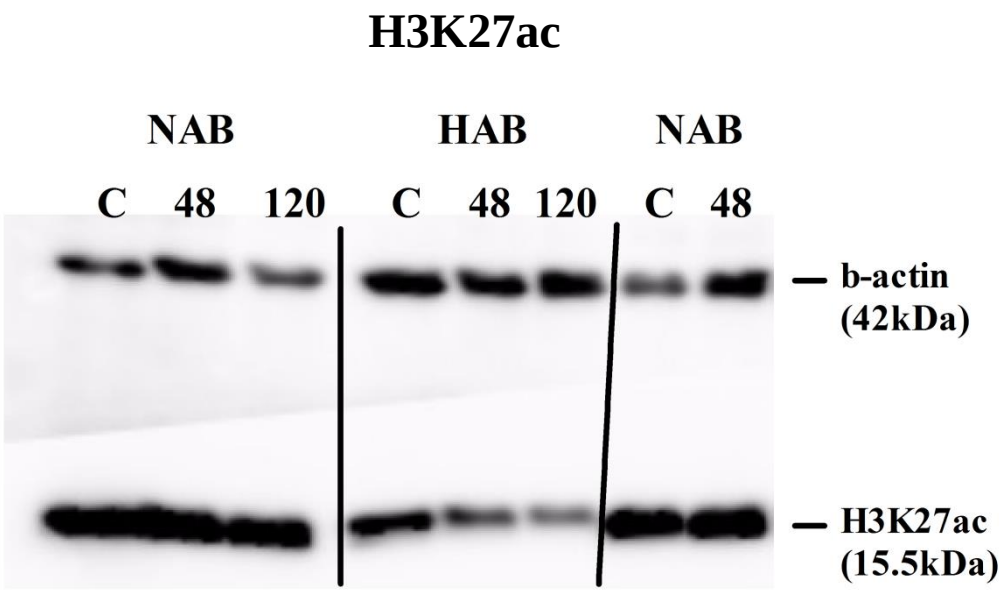

Fig. 30: Representative western blot on primary cortical astrocytes NAB vs. HAB

H3K27ac levels were measured in astrocytes derived from NAB and HAB rats under baseline conditions (C) *in vitro* and after FLX or ESC treatment for 48 h (10 µM, one time treatment) and 120 h (5 µM, two times treatment)

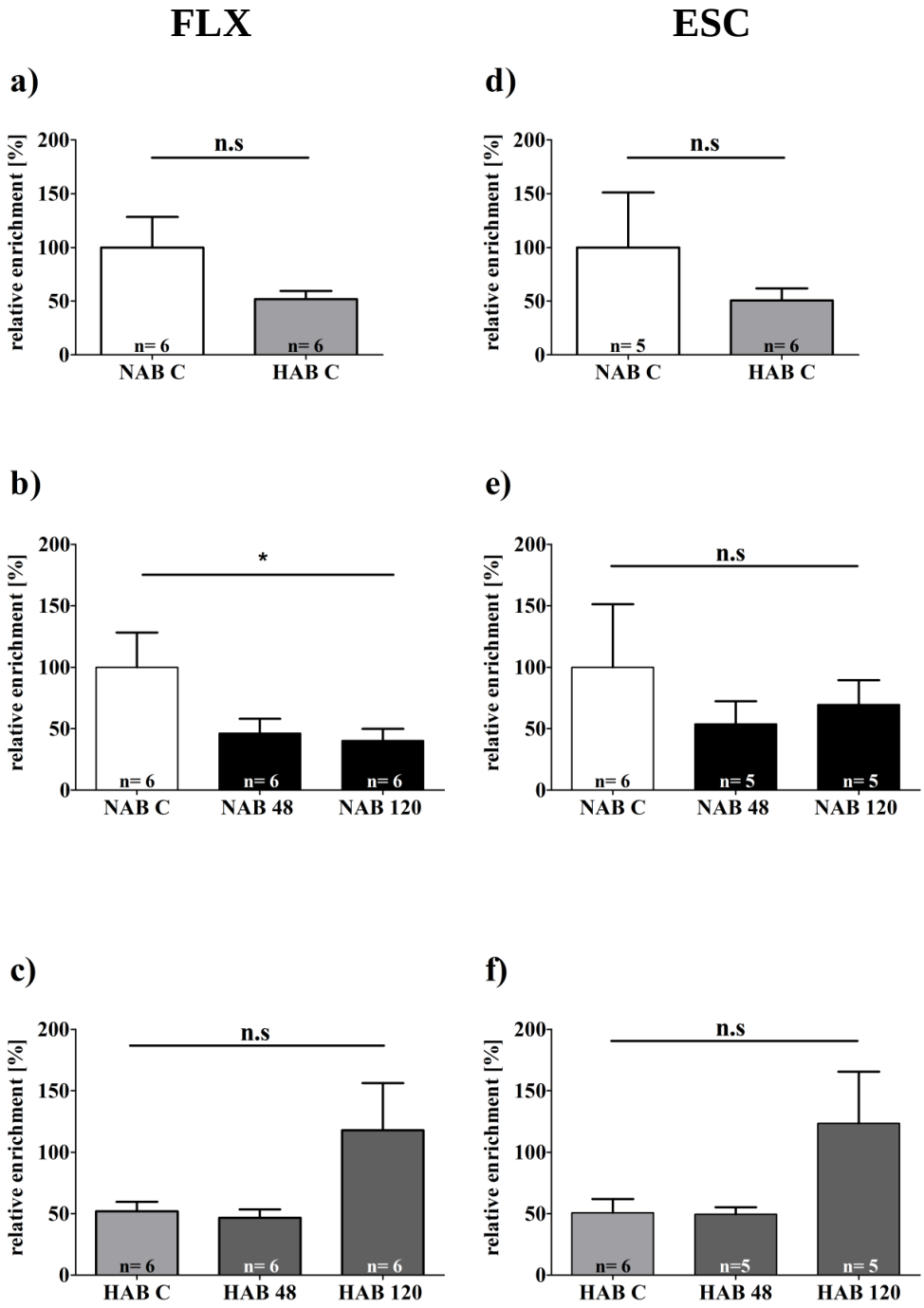

Fig. 31: Western blot analysis of primary cortical astrocytes NAB and HAB after FLX treatment

H3K27ac levels were measured in astrocytes derived from NAB and HAB under baseline conditions (C) and after treatment with FLX (a-c) or ESC (d-f) (10 µM total concentration) for 48 h and 120 h *in vitro*, normalized to β-actin. In NAB astrocytes FLX decreased expression of H3K27ac of about 60 % after 48h and 120h (b). In HAB astrocytes the effect of FLX seems to be opposite. FLX increased the expression after 120 h to almost the same level seen in NAB C (c). ESC showed similar effects (e, f). Relative enrichment in % is calculated in respect to NAB C. All data are represented as mean +SEM. *$p<0.05$, Student's t-test with Welch´s correction (a, d), One-way ANOVA with Dunnett´s multiple comparison *post hoc test* (b, c, e, f)

3.4. Global expression of H3K27me3 under baseline conditions

Because I could show that in the cell culture model the counteracting mark H3K27me3 was affected under baseline conditions and seemed to be a pharmacological target of FLX, I subsequently analyzed the expression in the PFC of HAB and NAB rats by IF-IHC. As shown in **Fig. 32 a)** and **b)**, I identified that the overall number of cells expressing H3K27me3 in the PFC of HAB rats was significantly lower than in NAB rats under baseline conditions (NAB: n= 6, 36.05 ± 7.534 %; HAB: n= 6, 20.94 ± 2.297 %, one-tailed Student´s t-test, $t_{(10)}$= 1.918, p= 0.0420). Interestingly, I could also show that expression of H3K27me3 in the PFC of HAB animals was lower than the expression of H3K4me3 (**see Suppl. 4**). These data reflect the observation made by western blot analysis.

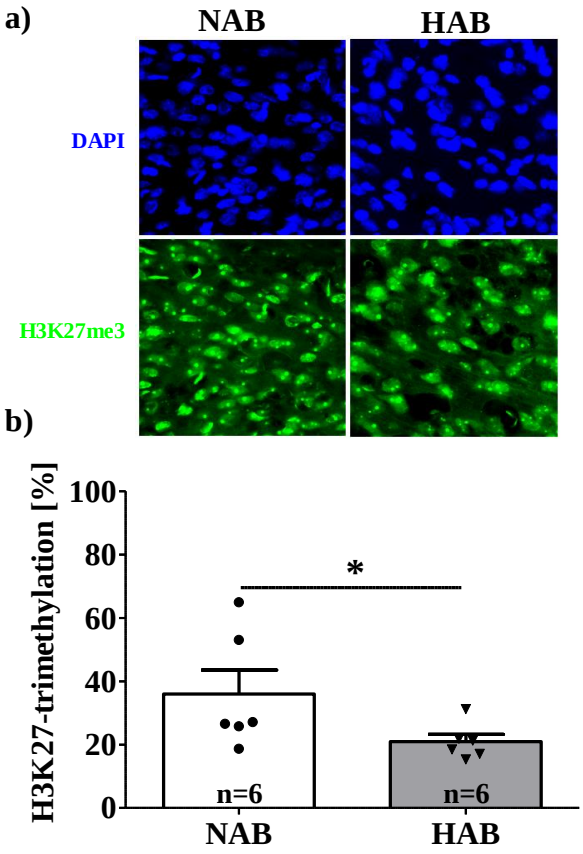

Fig. 32: Global expression of H3K27me3 in the PFC of HAB is lower than in NAB, under baseline conditions

a) Representative microphotographs (Leica SP8, Z-stack series, 20-30 µm, step size 1.23 µm). $H3K4me3^+$ cells (green), nuclear staining DAPI (blue), scale bar 10 µm

b) Quantitative IF-IHC analysis in the PFC of NAB (n= 6) and HAB (n= 6) under baseline conditions, showed that HAB have significantly less H3K27me3 than NAB. The average H3K27-trimethlyation [in %] is depicted as mean + SEM, Student´s t-test, * p< 0.05.

3.4.1. Cell-type specific expression of H3K27me3

Taking the results obtained by western blot analysis into consideration, I analyzed the cell-type specific expression of H3K27me3 in astrocytes of the PFC. In HAB rats I observed a trend towards a decrease in astrocytes colocalizing with H3K27me3 under baseline conditions (**Fig. 33, a)** and **b)** NAB: n= 6, 38.53 ± 5.724 %; HAB: n= 6, 27.60 ± 3.475 %; one-tailed Student´s t-test $t_{(10)}$= 1.633, p= 0.0668).

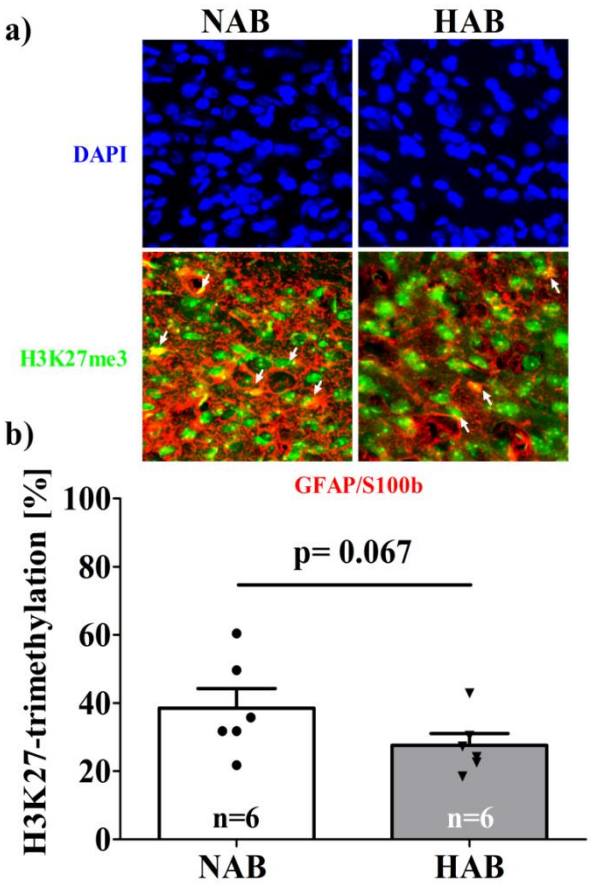

Fig. 33: Astrocyte specific expression of H3K27me3 in PFC of NAB and HAB under baseline conditions, shows a tendency towards decreased colocalization

a) Representative microphotographs (Leica SP8, Z-stack series, 20-30 µm, step size 1.23 µm). H3K4me3^{+} cells (green), nuclear staining DAPI (blue), scale bar 10 µm

b) Astrocyte specific IF-IHC analysis in the PFC of NAB (n= 6) and HAB (n= 6) under baseline conditions, showed that HAB tend to colocalize less with H3K27me3 than NAB. The average H3K27-trimethlyation [in %] is depicted as mean +SEM, one-tailed Student´s t-test, * p< 0.05.

3.5. Candidate genes

In order to establish a more specific H3K4me3-dependent target, that might be dysregulated in HAB animals, we performed a chromatin-immunoprecipitation and analyzed several candidate genes known to be differentially expressed after AD treatment and which might be affected in HAB astrocytes, among which EphA2 and GDF15 (**see 1.12**). EphA2 belongs to the EphRs, which generally display highly promiscuous binding affinities to their ligands. But from cancer studies, it is known that EphA2 preferentially interacts with the ligand ephrinA1 [215]. Especially some studies point out that there is an interaction with soluble ephrinA1, which is able to interact with EphA2, causing phosphorylation of the receptor [216, 217]. Therefore, we further investigated whether ephrinA1 might be a target in our animal model, involved in the upregulation of EphA2 after AD treatment.

3.5.1. Chromatin-immunoprecipitation

In cooperation with Dr. Mira Jakovcevski, I examined the expression of ephrinA1 in cortical astrocytes derived from HAB and NAB rats. We used a ChIP assay, with an antibody directed against H3K4me3. Subsequent qPCR, identified that *Efna1* promoter-containing DNA fragments were significantly higher in immunoprecipitates prepared from HAB astrocytes, under basal conditions (**Fig. 34**, NAB: n= 7, 1.016 ± 0.1374 %; HAB: n= 7, 1.598 ± 0.1188 %, Student´s t-test, $t_{(12)}$= 0.0076).

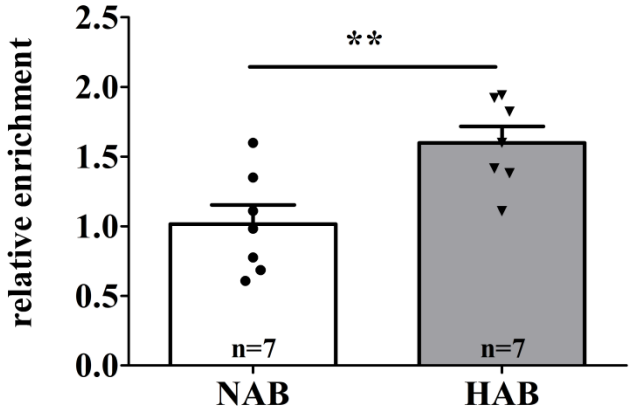

Fig. 34: EphrinA1 is regulated by H3K4me3 in HAB rat under basal conditions

mRNA expression of *Efna1* in cortical astrocytes of HAB and NAB rats, under basal conditions, were analyzed using a ChIP assay with antibodies against H3K4me3 and B2M.

3.5.2. EphrinA1 protein expression

After having established that the expression of the ligand of one of our candidate genes from the microarray, namely ephrinA1, was regulated by H3K4me3 at the promoter level, I analyzed the protein expression in our cell culture model. EphrinA1 appears in two isoforms, a 26 kDa and a 15 kDa, which have been characterized before [218]. NAB and HAB cells were treated as described before with FLX for 48 h (10 µM, once) and 120 h (5 µM, twice). The analysis revealed that under basal conditions HAB astrocytes express almost 4-times more ephrinA1 (26 kDa) than NAB astrocytes (See **Fig. 35 Fig. 36a**, 26 kDa, NAB C: n= 3, 100.00 ± 54.55 %, HAB C: n= 3, 365.1 ± 99.10 %, Student´s t-test with Welch´s correction, $t_{(6)}$= 2.344, p= 0.0576). Interestingly, in NAB cells, after FLX (48 h and 120 h) treatment, ephrinA1 increased gradually although without reaching significance (**Fig. 36b**; NAB 48: n= 3, 138.2 ± 57.81 % , NAB 120: n= 3, 216.4 ± 82.08 %, One-way ANOVA with Dunnett´s multiple comparison *post hoc test*, $F_{(3,17)}$ = 0.7574, p= 0.5333). In HAB astrocytes FLX decreased the protein expression of ephrinA1 (26 kDa) (See **Fig. 36c**: HAB 48: n= 3, 273.6 ± 134.5 %, HAB 120: n= 3, 193.2 ± 97.71 %, One-way ANOVA with Dunnett's multiple comparison *post hoc test*, $F_{(2,10)}$= 0.4687, p= 0.6389). The 15 kDa form of ephrinA1 was significantly higher expressed in HAB than in NAB astrocytes under basal conditions, showing an immense

4.5 fold increase in comparison to NAB (**Fig. 36 d**, NAB C: n= 4, 100.00 ± 38.59 %, HAB C: n= 3, 456.0 ± 118.6 %, Student´s t-test, $t_{(8)}$= 3.376, p= 0.0097). In NAB astrocytes FLX did not change the expression of ephrinA1 (15 kDa) significantly (**Fig. 36** e, NAB 48: n= 4, 120.7 ± 38.95 %, NAB 120: n= 4, 131.1 ± 61.66 %, One-way ANOVA with Dunnett´s multiple comparison *post hoc test*, $F_{(2,15)}$= 0.1170, p= 0.8960). HAB astrocytes showed a biological effect upon FLX treatment, displayed by a reduction of ephrinA1 (15 kDa) after 120 h, although the level did not show a significant difference (**Fig. 36** f, HAB 48: n= 4, 563.0 ± 136.4 %, HAB 120: n= 4, 232.0 ± 41.71 %, One-way ANOVA with Dunnett´s multiple comparison *post hoc test*, $F_{(2,14)}$= 2.518, p= 0.1164). Although the data did not reveal a significant effect after FLX treatment, it should be mentioned there, that this is probably only due to the high variances among experiments and a possible pharmacological effect should not be ruled out. Further experiments to increase the number of independent experiment (n) should be carried out.

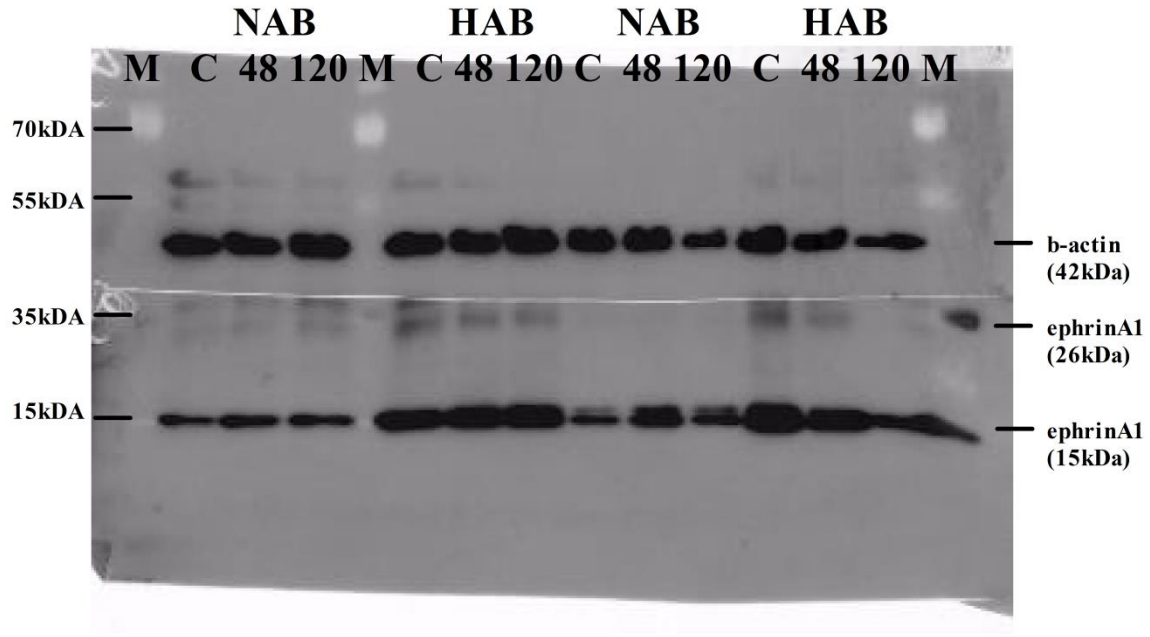

Fig. 35: Western blot analysis on primary cortical astrocytes under baseline conditions showed a 3-fold higher expression of ephrinA1 (26 kDa and 15 kDa) in HAB astrocytes

EphrinA1 level were measured in astrocytes derived from NAB and HAB rats under baseline conditions (C) *in vitro* normalized to β-actin and after FLX treatment. Relative enrichment in % is calculated in respect to NAB C.

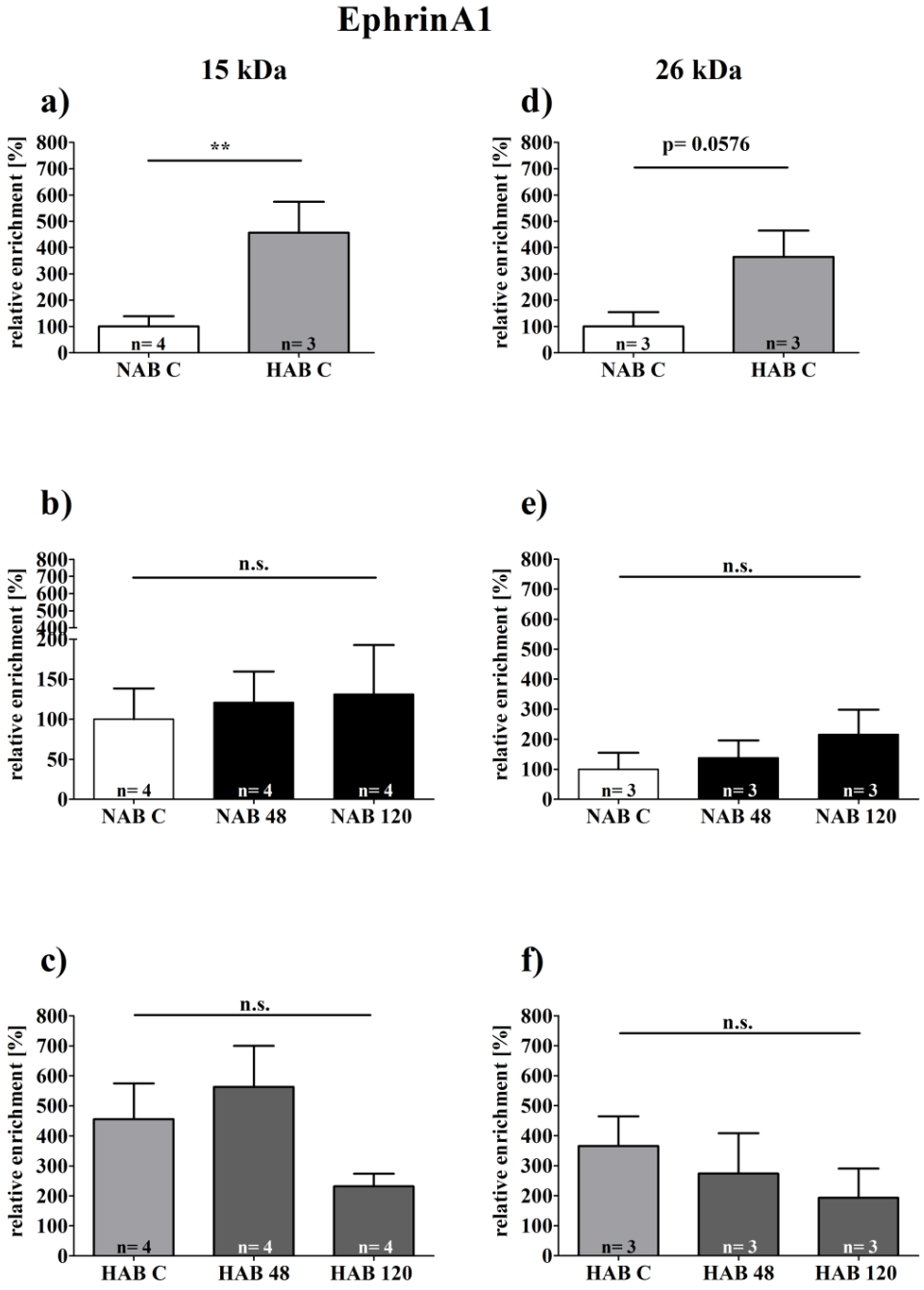

Fig. 36: Western blot analysis of primary cortical astrocytes NAB and HAB after FLX treatment

EphrinA1 levels were measured in astrocytes derived from NAB and HAB under baseline conditions (C) and after treatment with FLX (10 µM total concentration) for 48 h and 120 h *in vitro*, normalized to β-actin. Revealing a pronounce difference in both forms of EphrinA1 with increases of 3.5 and over 4-fold in HAB compared to NAB cells. NAB astrocytes seem to respond FLX by gradually increasing eprhinA1 (26 and 15 kDa, b, c) expression. In HAB astrocytes 120 h FLX treatment decreased ephrinA1 protein expression (26 kDa and 15 kDa, c, d). Relative enrichment in % is calculated in respect to NAB C. All data are represented as mean +SEM. *p<0.05, Student´s t-test with Welchs correction (a, d) One-way ANOVA with Dunnett´s multiple comparison *post hoc test* (b, c, e, f)

3.5.3. EphrinA1 knockdown via siRNA

Hence there was evidence that HAB astrocytes showed an over exaggerated ephrinA1 expression under baseline conditions, I designed siRNA against ephrinA1 mRNA (see **2.11**), and transfected HAB cells for 3d. Afterwards, I analyzed the expression of ephrinA1 (15 kDa) by means of western blotting. Preliminary data showed that siRNA 1 50 nM, si3 100 nM and si4 50 and 100 nM can knockdown ephrinA1 to less than 50 % expression in HAB astrocytes **(Fig. 37 a** and **b)**. The scr sequence showed a slight downregulation of ephrinA1 in HAB astrocytes, but it did not reach the NAB C level.

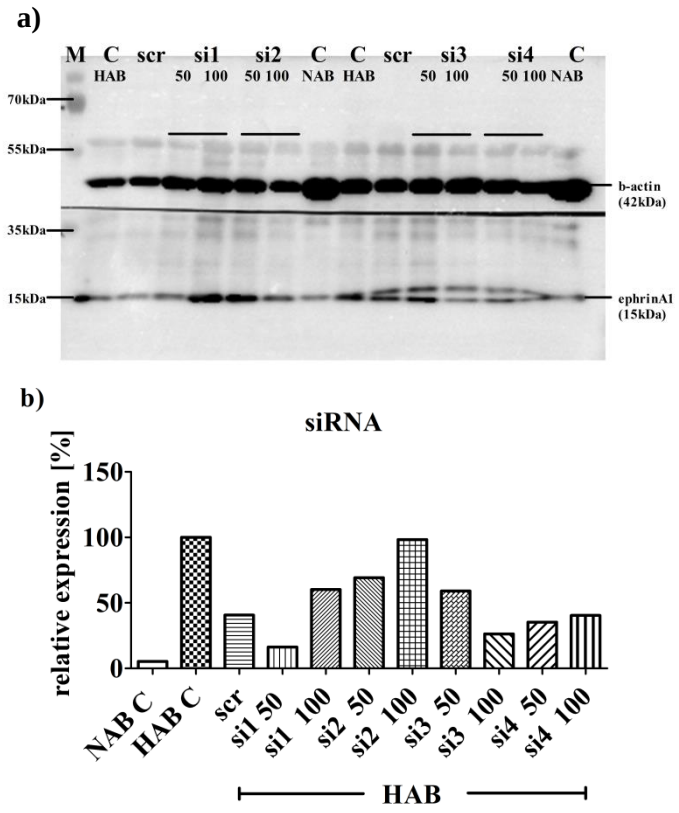

Fig. 37: Western blot analysis of primary cortical astrocytes HAB, after siRNA mediated knockdown of ephrinA1

a) Representative western blot of siRNA mediated knockdown

b) Western blot analysis (preliminary data) EphrinA1 levels were measured in astrocytes derived from NAB and HAB under baseline conditions (C) and after transfection with different siRNAs *in vitro*, normalized to β-actin. siRNA 2,3 and 4 seem to effectively decreasing ephrinA1 expression in HAB.

3.6. IF-IHC on ephrinA1 and EphA4 in PFC of untreated NAB and HAB animals

In parallel, I was interested to see, if the changes found *in vitro* represented the situation *ex vivo*. Therefore, I performed IF-IHC in the PFC of HAB and NAB animals together with Diana Haba-Schneider, during her internship under my supervision. Subsequent confocal analysis showed that the baseline differences observed in cell culture reflected the situation in the animals. IF-IHC revealed a significant higher expression of ephrinA1 in the PFC in

HAB compared to NAB animals (See **Fig. 38,** NAB: n= 4, 100.00 ± 9.125 %, HAB: n= 4, 147.7 ± 7.807 %, Student´s t-test, $t_{(27)}$= 3.992, p= 0.0005). Moreover, from the morphology of the cells which expressed ephrinA1, I could hypothesize that it was mostly expressed in astrocytes. Additionally, I analyzed the expression of EphA4, a receptor that is able to bind ephrinA1, in the PFC of these animals. The analysis revealed no differences in the expression of EphA4 in the PFC (See **Fig. 38,** NAB: n= 4, 100.00 ± 4.696 %; HAB: n= 4, 104.2 ± 5.978 %, Student´s t-test, $t_{(27)}$= 0.5292, p= 0.610).

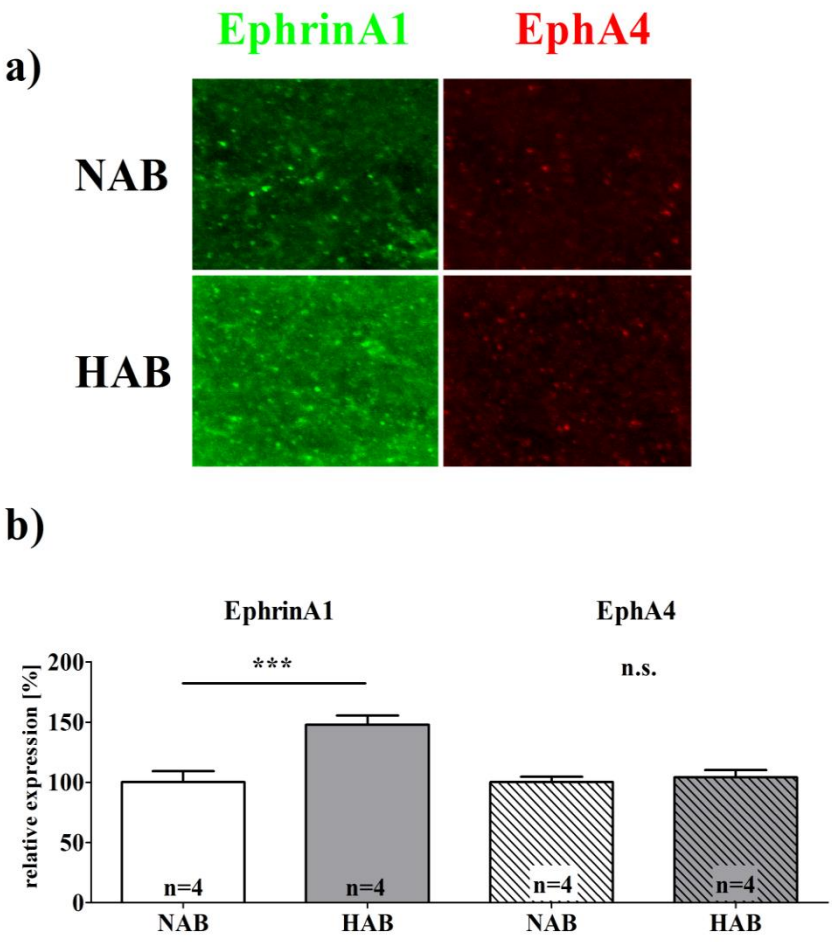

Fig. 38: Overall expression of ephrinA1 and its receptor EphA4 in HAB and NAB rats, under baseline conditions

a) Representative microphotographs (Leica SP8, Z-stack series, 20-30 µm, step size 1.23 µm). H3K4me3+ cells (green), nuclear staining DAPI (blue), scale bar 10 µm

b) Quantitative IF-IHC analysis in the PFC of NAB (n= 4 animals) and HAB (n= 4 animals) under baseline conditions, reveals not difference in EphA4, but ephrinA1 is significantly higher expressed (1.5-fold) compared to NAB. The average EphrinA1 and EphA4 expression [in %] is depicted as mean +SEM. Student´s t-test, *** p< 0.001; n.s. p> 0.05.

3.7. EphrinA1 and EphA4

Considering the previous findings showing that ephrinA1 was 1) dysregulated in HAB astrocytes (*in vitro* and *ex vivo*) and 2) downregulated by FLX treatment, I wanted to examine the functional consequences of an excess of ephrinA1 in HAB astrocytes.

Considering that ephrinA1 is highly involved in the formation of synaptic compartments, I established a co-culture model to examine HAB astrocytes together with NAB neurons and NAB astrocytes with NAB neurons. The goal was to see whether I could block an eventual effect of ephrinA1 overexpression in HAB cells on NAB neuronal synapses using its soluble ligand, the EphA4 receptor, and whether I could eventually induce an effect using the soluble ephrinA1 ligand to treat NAB neurons [196, 197]. After approximately 14 D*IV*, co-cultures were treated according to the following scheme for either 48 h or 120 h.

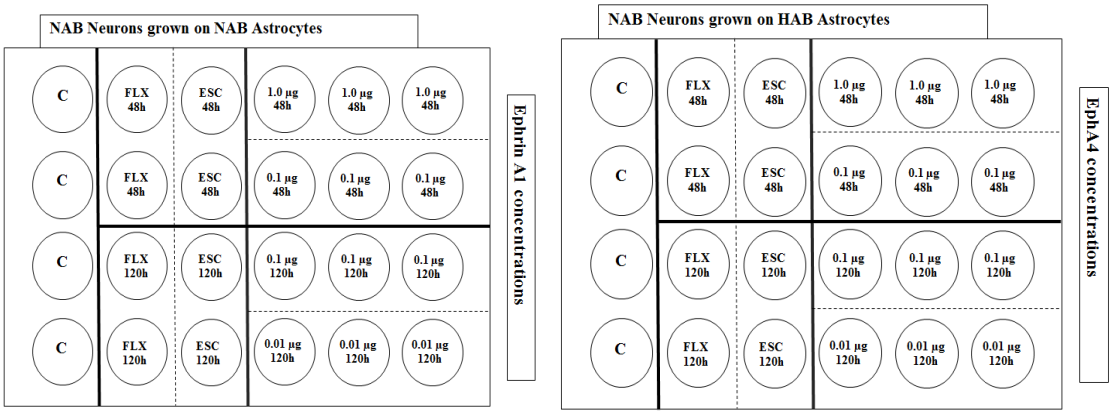

Fig. 39: Layout of Co-Cultures neurons growing on astrocytes derived from either NAB or HAB rats.

NAB-NAB co-cultures were treated with FLX, ESC and recombinant ephrinA1-Fc, at different concentrations and time points. HAB-NAB co-cultures were treated with the same way suing FLX, ESC, but with recombinant EphA4-Fc.

I performed IF-ICC with antibodies directed against MAP2 (a neuron-specific cytoskeletal protein that labels dendrites, in gray), PSD95 (a postsynaptic protein, in green) and synaptophysin (a presynaptic protein, in red) under basal conditions and after treatment with either ephrinA1-Fc or EphA4-Fc. So far, only a qualitative analysis of differences at the synaptic level was done. According to **Fig. 40**, co-cultures grown on HAB astrocytes showed a reduced expression of both synaptic markers (PSD95 and synaptophysin) as well as they showed less mature synapses (indicated by yellow color). FLX treatment apparently induced a decrease in the expression of the synaptic markers in both co-cultures (HAB-NAB, and NAB-NAB), suggesting that FLX may cause synaptic reorganization. I

applied different concentrations of ephrinA1-Fc to the NAB-NAB co-cultures in order to investigate whether the excess of ephrinA1 can cause a phenotype in NAB similar to HAB. Vice versa, I applied EphA4-Fc to block excess of ephrinA1 in HAB-NAB co-cultures to investigate possible rescue effects. These first qualitative data indeed showed a rescue effect in HAB-NAB co-cultures after treatment for 48 h with EphA4 (0.1 ng/ml), whereas on the other hand 0.1 ng/ml ephrinA1 applied for 48 h to NAB-NAB co-cultures apparently reduced the expression of synaptic proteins. The higher concentrations of 1.0 ng/ml EphA4 or ephrinA1 did not show any significant differences. This might be due to a too high concentration of the respective compounds. Treatment for 120 h was not possible in this paradigm.

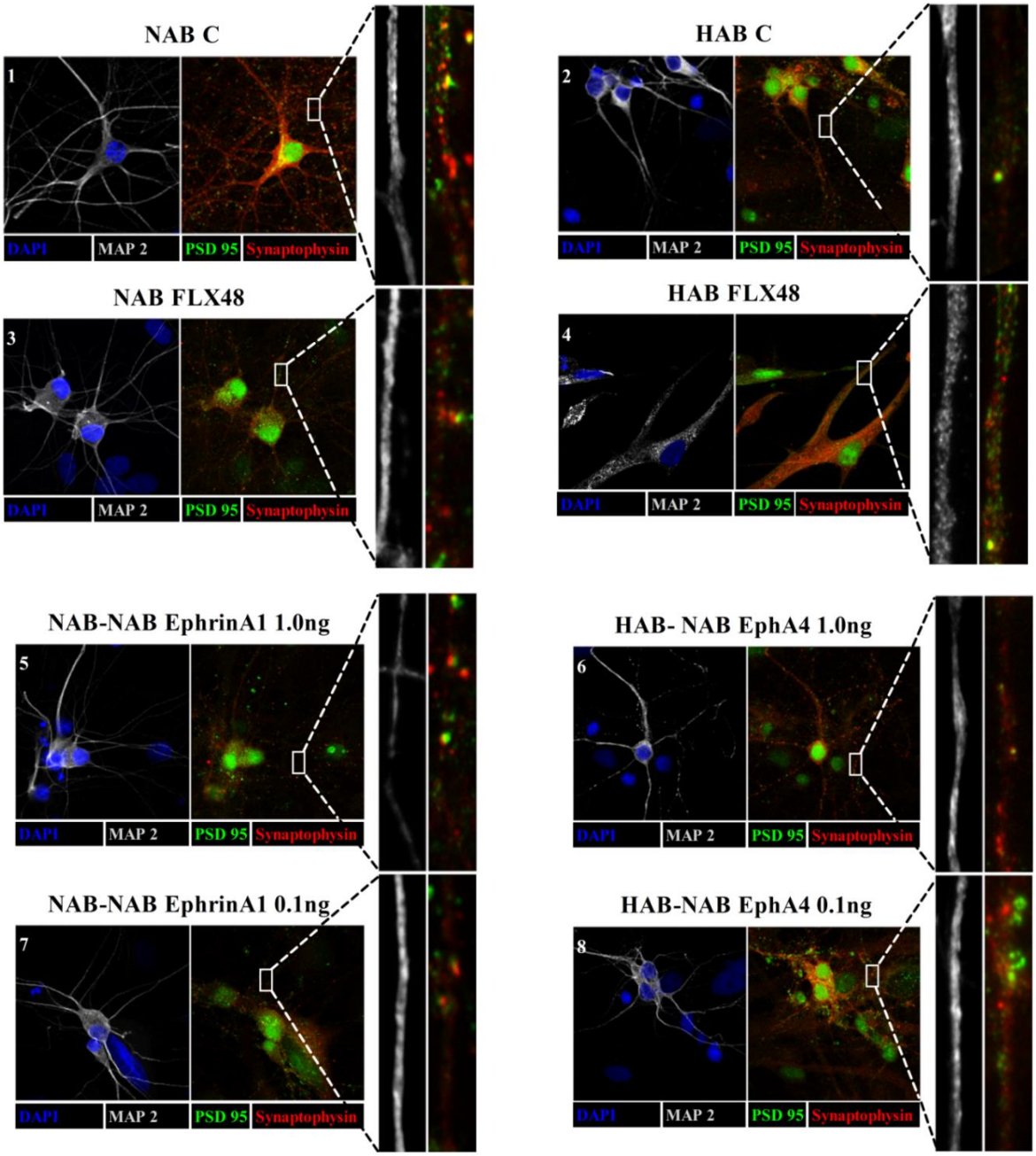

Fig. 40: C**o-Cultures of astrocytes and neurons under baseline conditions and after treatment with FLX (10 µM), ephrinA1 or EphA4 (1.0 and 0.1 ng/ml) for 48 h**

Qualitative analysis of pre- (synaptophysin, red) and post- (PSD 95, green) as well as MAP2 (gray) marker on Co-cultures of HAB astrocytes – NAB neurons (HAB-NAB) and NAB astrocytes – NAB neurons (NAB-NAB), showed less expression of synaptic markers in HAB-NAB co-cultures and seems to be rescued with EphA4 treatment. Baseline conditions (**1 and 2**), FLX treatment (**3 and 4**) and after ephrinA1-Fc (1.0 ng/ml, **5** or 0.1 ng/ml, **6**) or EphA4-Fc (1.0 ng/ml, **7**, or 0.1 ng/ml, **8**)

3.8. GDF 15

(Malik *et al*., in preparation)

As mentioned before another of our candidate genes, which came up to be regulated by ADs (FLX and desipramine)in an unbiased microarray screening, might be of potential interest in our animal model for depressive-like behavior.

3.8.1. Microarray

In previous experiments, our lab could show that several candidate genes are activated by AD treatment (FLX and DMI, 25µM both) after 2 h treatment.

We used C6 glioma cells, which serve as a model for astrocytes, and primary rat astrocytes in order to validate the findings. By means of qPCR we could validate that among these candidate genes *Gdf15* was especially activated upon AD treatment (

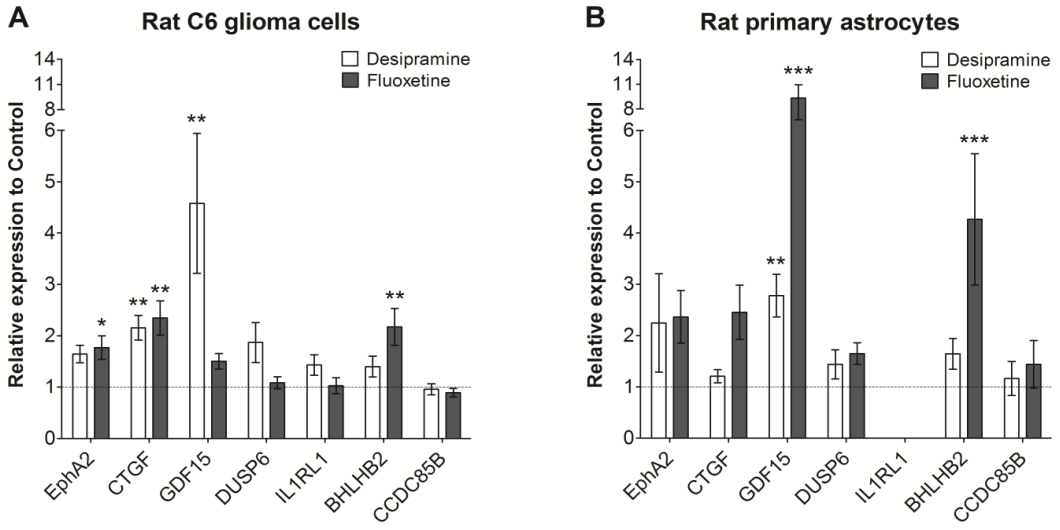

Fig. 7, n= 3, Kruskal-Wallis-test, * p< 0.05, ** p< 0.01, *** p< 0.001).

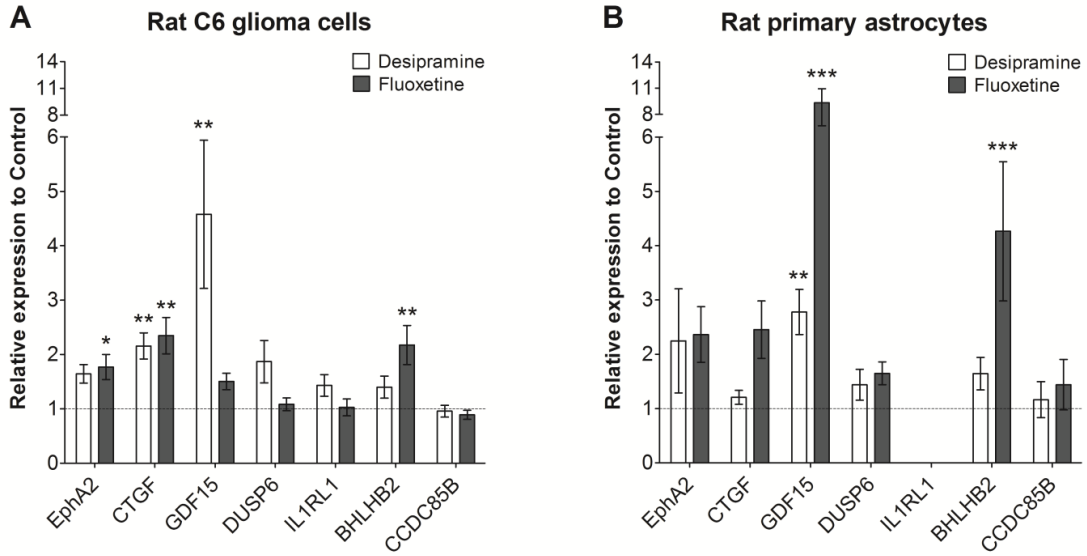

3.8.2. In situ hybridization -validation of GDF15 probe

In order to analyze the physiological role of increased GDF15 after treatment with FLX, I generated a fluorescent probe to perform *in situ* hybridization (ISH) analysis in brain slices derived from naïve CD1 mice, treated with FLX for 2 h. As previously published by Strelau *et al*. [219], I observed expression of GDF15 in the choroid plexus, thereby confirming the specificity and reliability of the ISH probe to detect *Gdf15* mRNA. Furthermore, I could show that FLX treatment decreased *Gdf15* mRNA in the same region significantly, pointing out that *Gdf15* mRNA expression is a pharmacological target of FLX. Although these results seemed to be counterintuitive, the microarray screening showed that FLX upregulated *Gdf15* mRNA expression (**Fig. 41 a)** and **b)**, C: n= 4, 1.418 ± 0.06, FLX: n= 5, 1.118 ± 0.06), in the choroid plexus different mechanism may mediate an AD effect than in the astrocytes derived from the PFC. Moreover, one needs to take into account that the choroid plexus mainly consists of ependymal cells, not astrocytes, which might react differently to AD treatment. In addition to the known region, we observed *Gdf15* expression around blood vessels in the PFC (**Fig. 41**), indicating that this factor might play a role at the glia-vasculature interface.

3.9. GDF15 in blood vessels

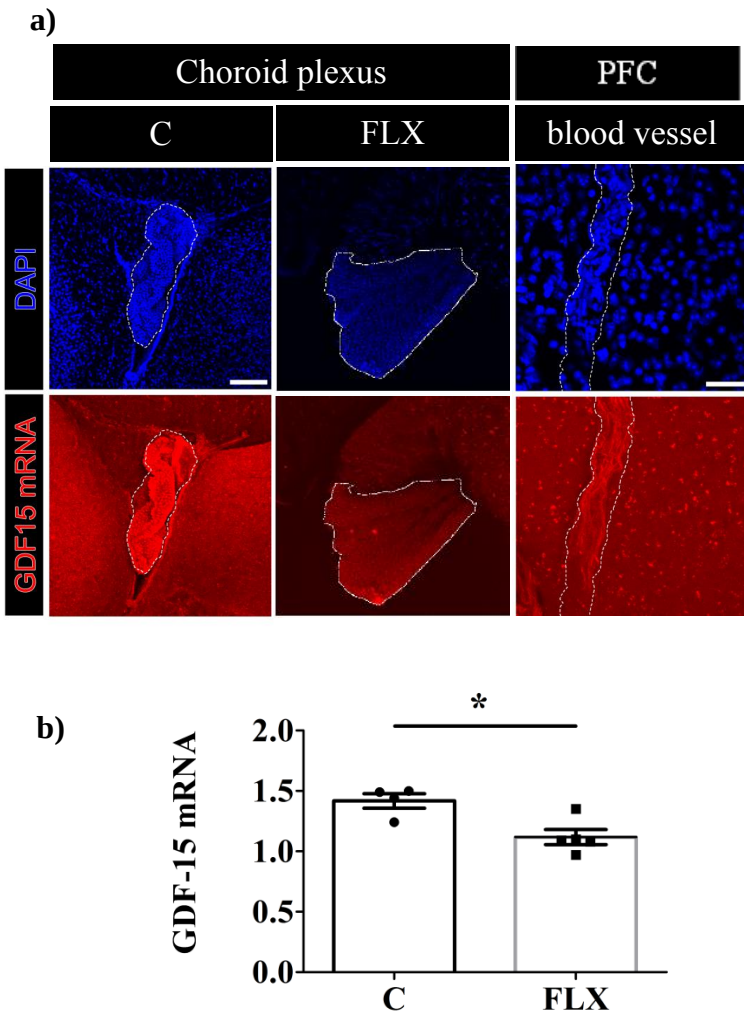

Fig. 41: Validation of the ISH probe targeting GDF15 in the choroid plexus and in blood vessel of the PFC

a) Representative microphotographs of the choroid plexus before and after treatment with FLX and around blood vessel in the PFC

b) Quantitative analysis of GDF15 mRNA in the choroid plexus showed a significant downregulation after treatment with FLX and can be detected around blood vessels in the PFC

In light of the findings that in the PFC of MDD patients and in our animal model, blood vessels show decreased coverage with astrocytic endfeet, [12, 209], we analyzed the effects of FLX treatment on *Gdf15* around blood vessels in the PFC of HAB and NAB animals (*ex vivo*). Therefore, I performed ISH-IF-IHC on brain slices derived from NAB and HAB animals treated with FLX for 2 d and respective controls. I could show that FLX increased *Gdf15* mRNA expression specifically around blood vessels in the PFC (**Fig. 42**, NAB C: n= 4, 0.0029 ± 0.0006; NAB + FLX: n= 5, 0.007 ± 0.001, Mann-Whitney test, p= 0.0317).

I also observed the formation of *Gdf15*-positive processes between the blood vessels and parenchymal cells (white arrows **Fig. 42 a^{IV}**). The extension of processes might be a reaction of astrocytes upon FLX treatment and could represent a mechanism relevant for recovering of a functional glia-vasculature interface in MDD.

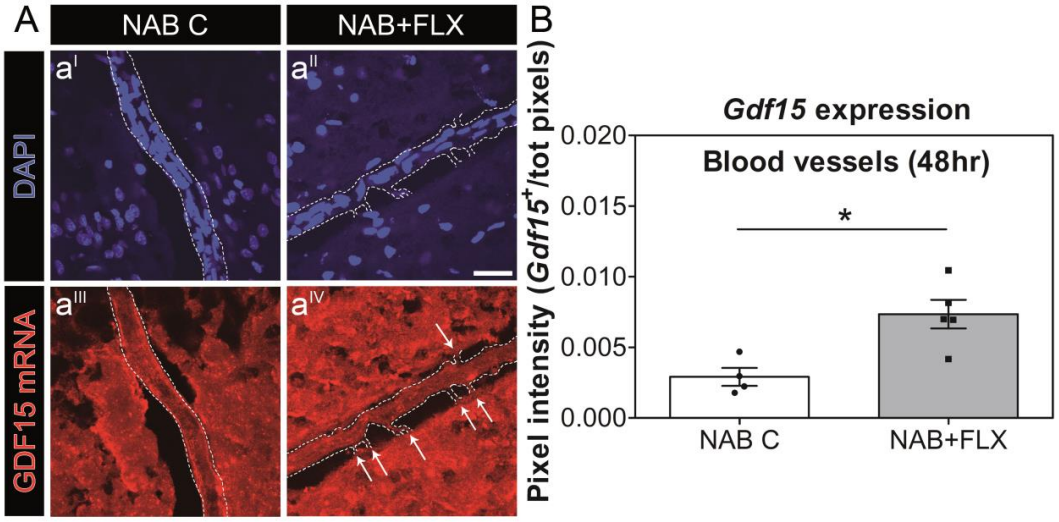

Fig. 42: FLX increases GDF15 mRNA expression around blood vessel in the PFC of NAB rats

A) Representative microphotographs show blood vessels (in blue DAPI staining a^{I}, a^{II}) and labelling with a probe targeting GDF15 mRNA (in red, a^{III}, a^{IV}) in the PFC of control and FLX treated NAB rats. Scale bar 50µM. Arrows pointing at processed between blood vessels and parenchymal cells.

B) Quantitative analysis on the fluorescence- intensity of GDF15 expression (in pixel, GDF15^{+}) normalized to the total volume of each blood vessel (total pixels) revealed a significant upregulation after FLX treatment. NAB C: n=4, NAB + FLX: n= 5, Mann-Whitney-test, *p<0.05. Data are represented as mean ± SEM,

3.9.1. GDF 15 expression around blood vessel in HAB

In a recently published paper from our lab (**[209]**), we could show that short term treatment with FLX (48 h) is sufficient to increase the reduced coverage of blood vessels by GFAP^{+} processes in the PFC of HAB animals. However, this short treatment time was only sufficient to rescue the structural deficiency seen in HAB animals, but not the coverage of blood vessels by Aqp-4^{+} processes, suggesting an involvement of different pathways, which affect structural and functional changes in astrocytic processes. Therefore, I investigated here whether GDF15 might be involved in the modulation of structural deficiencies. First we investigated the expression of GDF15 around blood vessels in the PFC of NAB and HAB animals both under basal conditions and after FLX treatment (2d).

Global *Gdf15* expression did not reveal any differences between HAB and NAB or after treatment in HAB animals (**Fig. 43 B)**, NAB C: n= 3, 0.0048 ± 0.0004, HAB C: n= 3, 0.0053 ± 0.0008, HAB + FLX: n= 3, 0.0056 ± 0.0006, One-way ANOVA with Tukey´s multiple comparison *post hoc test*, $F_{(2,6)}$= 0.38, p= 0.699). Thus, leading to the suggestion that GDF15 in endothelial cells might not be affected in depression-like behavior. However, quantification of $GFAP^+$ processes around blood vessels confirmed the reduced number of blood vessel-associated astrocytic processes, in the PFC of HAB, as previously shown. Treatment with FLX for 2d (i.p.) could rescue this deficiency (**Fig. 43 C**), NAB C: n= 3, 2.053 ± 0.259, HAB C: n= 3, 0.945 ± 0.241, HAB + FLX: n= 3, 2.378, ± 0.252. One-way ANOVA with Tukey´s multiple comparison *post hoc test*, $F_{(1,2)}$= 8.98, p= 0.0157).

I subsequently analyzed whether increased *Gdf15* expression might occur at more specific site, like astrocytic processes. Therefore changes in the relative number of *Gdf15*-enriched astrocytic processes were quantified. The results revealed no difference between NAB and HAB animals, but a tendency towards an increased amount of *Gdf15*-enriched processes after FLX treatment (**Fig. 43 D**) NAB C: n= 3, 0.049 ± 0.011, HAB C: n= 3, 0.048 ± 0.018, HAB + FLX 0.092 ± 0.0067, Kruskal-Wallis test p= 0.0500). These data suggest that a basal difference between NAB and HAB might be masked by the underlying lack of processes around blood vessels in HAB animals. Thus I conducted a more in-depth analysis, preventing this masking effect. I quantified the density of $Gdf15^+/GFAP^+$ -enriched astrocytic processes. This analysis showed that in HAB animals, not only the density of $Gdf15^+/GFAP^+$ processes was reduced, but also that FLX was able to increase this number with respect to both NAB and HAB strains (**Fig. 43 E)** NAB C: n= 3, 0.094 ± 0.019, HAB C: n= 3, 0.039 ± 0.013, HAB + FLX: n= 3, 0.201 ± 0.008, One-way ANOVA with Tukey´s multiple comparison *post hoc test*, $F_{(2,6)}$= 32.92, p= 0.0006).

3.9.2. GDF 15 protein expression

The obtained results led to the suggestion that FLX might affect the expression and localization of GDF15 around blood vessels at astrocytic processes. To further analyze the functional role of GDF15, we used our cell culture model.

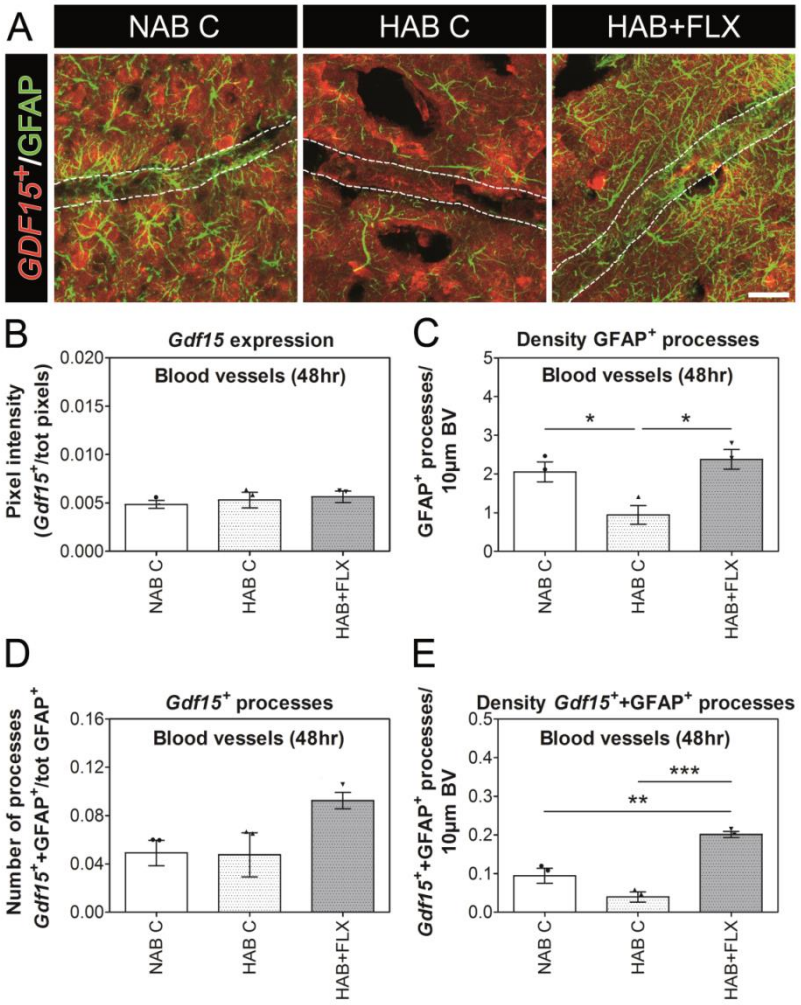

Fig. 43: Coverage of blood vessels by GDF15 $^{+}$ processes in the PFC of NAB and HAB animals under basal conditions and after FLX treatment

A) Representative microphotographs of GDF15^{+}/GFAP^{+} processes around blood vessels under basal conditions in HAB C and NAB C and after treatment with FLX (2d)

B) Quantification of GDF15^{+} processed revealed no differences between the groups, neither under basal conditions nor after FLX treatment in HAB animals

C) Analysis of GFAP^{+} processes confirmed the loss of astrocytic processes in HAB animals compared to NAB, under basal conditions. FLX treatment was able to restore the number of GFAP^{+} processed in HAB animals. One-way ANOVA, $F_{(1,2)}= 8.98$, *$p<0.05$

D) Analysis of GDF15^{+} - enriched astrocytic processes (GFAP^{+}) showed a tendency towards an increase in HAB animals after FLX treatment

E) In depth analysis of GDF15^{+}/GFAP^{+} density was significantly less in HAB animals under basal conditions and was significantly increased after FLX treatment

I then performed a preliminary western blot analysis on astrocytes treated with FLX for 48 h and 96 h. FLX treatment did not affect GDF15 protein expression, significantly, neither after 48 h nor 96 h (**Fig. 44**, NAB C: n= 3, 100.00 ± 34.18 %, NAB 48: n= 3, 96.34 ± 42.85 %, NAB 96: n= 3, 126.7 ± 18.59 %; HAB C: n= 3, 52.62 ± 9.468 %, HAB 48: n= 3, 67.07 ± 13.64 %, HAB 96: n= 1, 216.6, One-way ANOVA with Dunnett´s multiple comparison *post hoc test*, $F_{(4,24)}$= 0.8102, p= 0.5310). Suggesting that under basal conditions endogenously expressed GDF15 does not significantly differ between HAB and NAB animals. Nevertheless, FLX treatment might cause an increase of GDF15 in HAB astrocytes, but this observation still needs to be clarified.

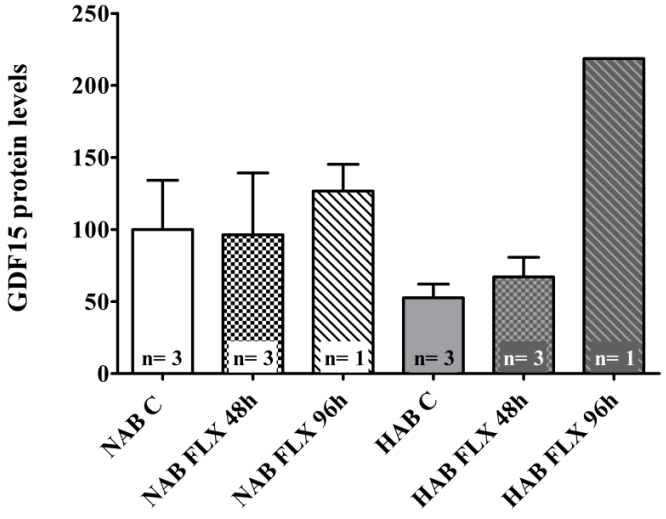

Fig. 44: GDF 15 protein expression in astrocytes derived from NAB and HAB treated with FLX for 48 h and 96 h

No differences could be observed under basal conditions between NAB and HAB astrocytes, nor did FLX treatment change the protein expression of GDF15 significantly. Data are represented as mean + SEM, One-way ANOVA with Dunnett´s multiple comparison *post hoc test.*

3.10. In depth analysis of astrocytic process

In our recently published paper [51], we observed that FLX is able to increase mainly short astrocytic processes after short-term treatment around blood vessels. Therefore, I conducted an in-depth analysis of astrocytic processes, with regard to their specific numbers and lengths, under baseline and treatment conditions. In addition, because I hypothesized that GDF15 might be responsible of the outgrowth of new processes, I analyzed how exogenous GDF15 in different concentrations might affect astrocytic process *in vitro*. The following data were obtained in the framework of a Master thesis conducted together with Laura Mittmann.

3.10.1. Number of processes in primary cortical astrocytes under baseline conditions

First, I analyzed by means of IF-ICC, whether I could reproduce the findings that HAB astrocytes display deficits in their processes, as observed in *ex vivo* experiments [51]. Indeed, I could show that the number of astrocytic processes per cell was significantly reduced in HAB cells as compared to NAB cells under baseline conditions, confirming once again the previous results (**Fig. 45:** NAB C: n= 16, 6.313 ± 0.0560; HAB C: n= 12, 4.083 ± 0.6211; Student´s t-test, $t_{(26)}$= 2.808, p= 0.0093).

Fig. 45: Under baseline conditions HAB astrocytes have significantly less processes *in vitro* than NAB

a) Representative microphotographs (Leica SP8, Z-stack series, 6-8 µm, step size 1.23 µm) of HAB and NAB astrocytes *in vitro*, using a double staining GFAP and S100β (both red).

b) IF-ICC analysis of the number of processes revealed, a significant deficit HAB astrocytes (n= 12, 4.083) compared to NAB (n= 16, 6.313). Data are represented as mean + SEM, Student´s t-test, ** p< 0.01

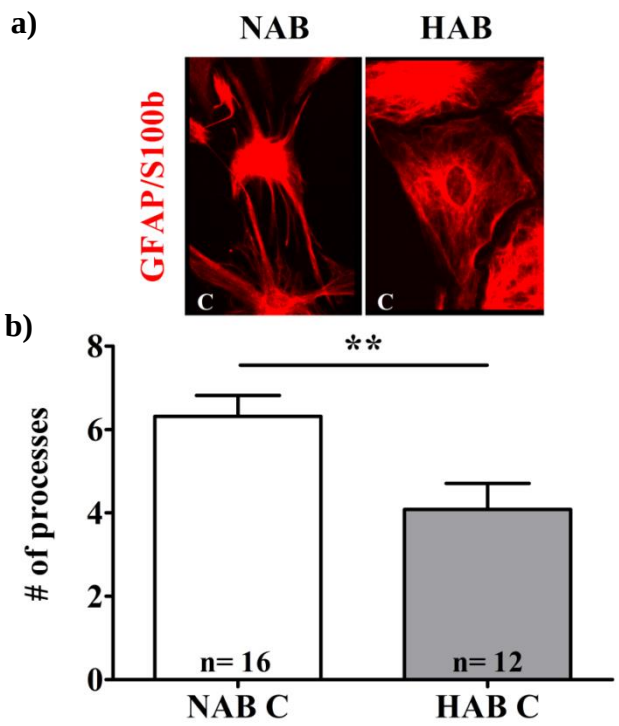

3.10.2. Number of processes in primary cortical astrocytes after treatment with FLX and exogenous GDF15

In order to investigate the hypothesis, if FLX treatment is able to increase the number of processes in astrocytes, and whether GDF15 might be a factor involved in this effect, I conducted further IF-ICC experiments using the cell culture model. Astrocytes of both strains were either treated with FLX (once 10 µM) or with different concentrations of exogenous GDF15 (1.0 ng/ml, 0.1 ng/ml or 0.01 ng/ml) in both experimental setups for 48 h and 96 h. As depicted in **Fig. 46** , I analyzed first the pharmacological effects of FLX. In both cell-types, FLX significantly increased the number of processes, already after 48 h (NAB 48 h: n= 14 , 11.43 ± 1.098, HAB 48 h: n= 12, 11.08 ± 1.500). This high increase in

the number of processes per cell seemed to display a ceiling effect, substantiated by the finding that FLX treatment for a longer time (96 h) did not further increase the numbers neither in NAB nor in HAB (NAB 96 h: n= 11, 11.18 ± 1.426; HAB 96 h: n= 12, 9.917 ± 1.228). Both one-way ANOVA with Dunnett´s multiple comparison *post hoc test*, NAB: $F_{(2,38)}$= 9.227, p= 0.0005; HAB: $F_{(82,33)}$= 9.901, p= 0.0004). I further investigated the effects of exogenous GDF15 on these cells, using three different concentrations (1.0, 0.1 and 0.01 ng/ml) at two time points (48 h and 96 h).

Treatment of the cell for 48 h revealed a significant increase in the number of processes per cell in NAB identical to the increase observed after FLX, but only with the highest concentration applied (1.0 ng/ml). (NAB 1.0: n= 12, 12.50 ± 1.936, NAB 0.1: n= 14, 6.857 ± 0.9542, NAB 0.01: n= 11, 7.091 ± 1.171, one-way ANOVA with Dunnett´s multiple comparison *post hoc test*, NAB: $F_{(3,49)}$= 5.910, p= 0.0016). HAB cells showed a higher sensitivity to exogenous GDF15, hence I observed the pronounced increase with 1.0 ng/ml but also, tough slightly less, with 0.1 ng/ml (HAB 1.0: n= 11, 10.18 ± 1.052, HAB 0.1: n=11, 8.273 ± 0.8851, HAB 0.01: n= 11, 4.909 ± 1.013, one-way ANOVA with Dunnett´s multiple comparison *post hoc test*, NAB: $F_{(3,43)}$= 10.21, p= 0.0001), indicative of a concentration-dependence in HAB cells. To investigate whether the treatment might also be time-dependent, I tested another time point (96 h). Here I observed in NAB cells a dependence on the concentration which seemed to include the time component, hence this effect was not present after 48 h treatment. The pronounced effect with 1.0 ng/ml was still present, as seen in FLX treatment, but in addition the intermediate concentration 0.1 ng/ml was able to increase the number of processes per cell to the same level (NAB 1.0: n= 12, 10.75 ± 1.805, NAB 0.1: n= 11, 10.55 ± 1.194, NAB 0.01: n= 13, 8.154 ± 0.9047, one-way ANOVA with Dunnett´s multiple comparison *post hoc test*, NAB: $F_{(3,48)}$= 3.772, p= 0.0165). HAB cells also responded in a dose- and time-dependent manner to exogenous GDF15, as we observed a significant increase in the number of processes per cell even with the intermediate concentration 0.1 ng/ml for 96 h (HAB 1.0: n= 14, 6.286 ± 0.8349, HAB 0.1: n= 10, 12.80 ± 1.769, HAB 0.01: n= 11, 5.636 ± 1.521, one-way ANOVA with Dunnett´s multiple comparison *post hoc test*, NAB: $F_{(3,43)}$= 9.356, p< 0.0001). Surprisingly, I did not observe an increase in the number of processes with the highest concentration 1.0 ng/ml. A possible explanation for this result might be that GDF15 exerts toxic effects on astrocytes, when applied at potentially unphysiological concentrations for longer times.

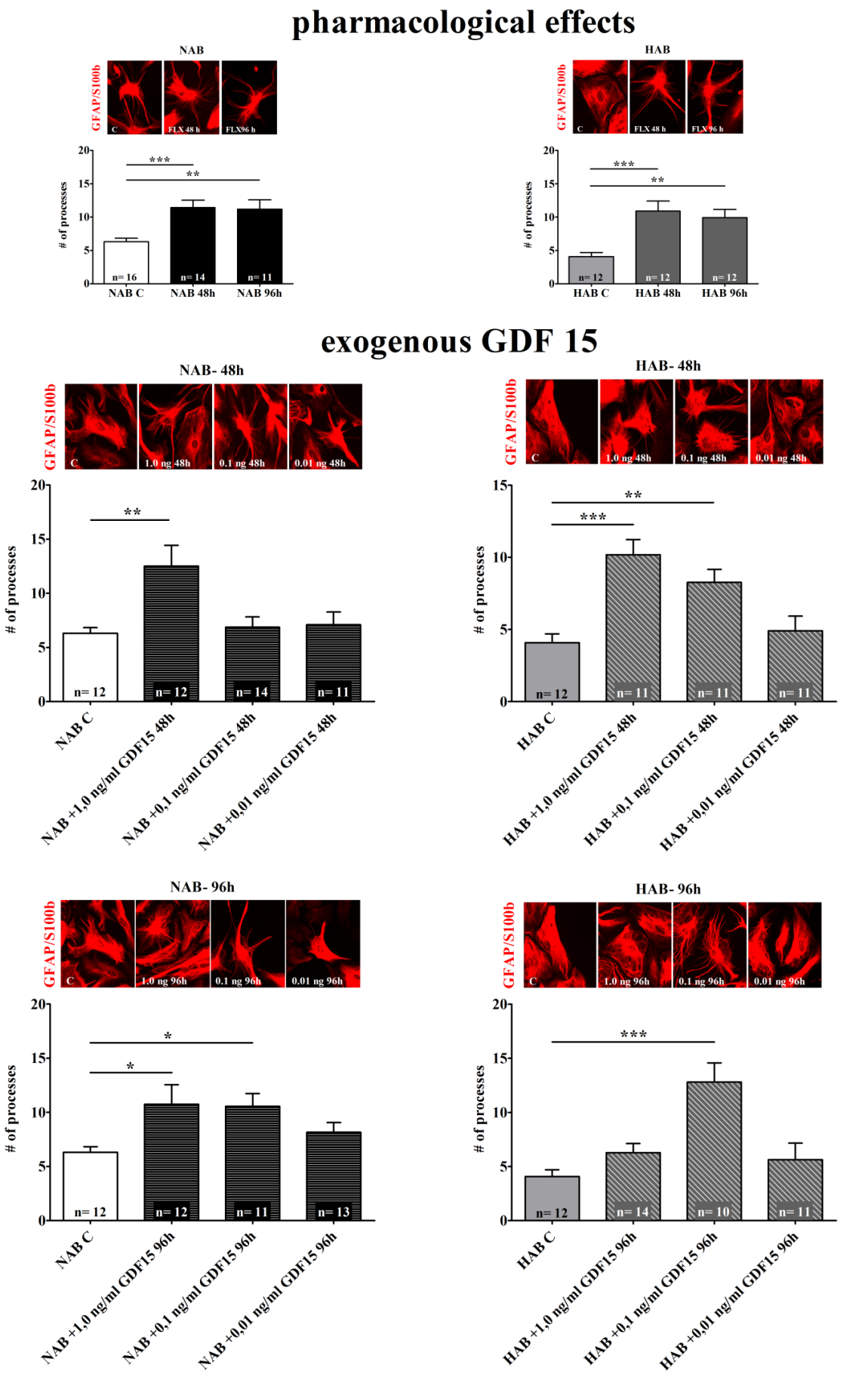
pharmacological effects
NAB
HAB
GFAP/S100b
C
FLX 48 h
FLX96 h
# of processes
n= 16
n= 14
n= 11
n= 12
NAB C
NAB 48h
NAB 96h
HAB C
HAB 48h
HAB 96h
exogenous GDF 15
NAB- 48h
HAB- 48h
1.0 ng 48h
0.1 ng 48h
0.01 ng 48h
NAB +1,0 ng/ml GDF15 48h
NAB +0,1 ng/ml GDF15 48h
NAB +0,01 ng/ml GDF15 48h
HAB +1,0 ng/ml GDF15 48h
HAB +0,1 ng/ml GDF15 48h
HAB +0,01 ng/ml GDF15 48h
NAB- 96h
HAB- 96h
1.0 ng 96h
0.1 ng 96h
0.01 ng 96h
NAB +1,0 ng/ml GDF15 96h
NAB +0,1 ng/ml GDF15 96h
NAB +0,01 ng/ml GDF15 96h
HAB +1,0 ng/ml GDF15 96h
HAB +0,1 ng/ml GDF15 96h
HAB +0,01 ng/ml GDF15 96h

Fig. 46: Pharmacological effects of FLX and exogenous GDF15 on the number of processes in astrocytes derived from HAB and NAB rats

Pharmacolgical effects: FLX increased the number of processes per cell in both NAB and HAB astrocytes significalty after 48 h. This effect persisted with proglonged treatment, indicating a possible ceiling effect

Exogenous GDF15: The highest concentraton of exogenous GDF15 (1.0 ng/ml for 48 h) increaed the number of processes in both cell types, identically to the effect observed with FLX. HAB cells seemed more sensitive to the treatment hence the intermediate concentration (0.1 ng/ml for 48 h) increased the number of processes significnatly. Prolonged treatment (96 h) revealed the same effect in NAB cell with a pronounced increase (1.0 ng/ml for 96h) and a dose- and time dependence, seen as an significant increase with intermediate concentrations (0.1 ng/ml). This dependenc is also observed in HAB cells (0.1 ng/ml for 96 h), althought the highest concentrations (1.0 ng/ml for 96 h) seemed to exert toxic effects.

Data are represented as mean + SEM, One-way ANOVA with Dunnett´s multiple comparison *post hoc test* * p< 0.05, ** p< 0.01, *** p< 0.001

3.10.3. Sprouting of processes in primary cortical astrocytes after treatment with FLX and exogenous GDF15

Following the hypothesis that an appropriate length of astrocytic processes might be necessary to mediate effects of FLX, I investigated whether the increased number of processes may correlate with differences in the length of preexisting processes or caused the sprouting of new processes. Therefore, I measured the length of processes in both cell-types after treatment with FLX and exogenous GDF 15. **Fig. 47 a)** depicts the differences in the number of processes at a specific length. NAB cells showed a very characteristic curve, with approximately three processes at a length between 0- 10 µm (**very short processes**), followed by a continuous decrease in the numbers as the length increased (approx. 2.5 processes at 10-20 µm (**short processes**) less than one process with higher length (**intermediate length** (20-30 µm, **long** 30-40 µm), whereas no **very long** (>60µm) processes were visible. On the contrary, HAB cells displayed significantly less processes at intermediate length, without changes in short or long processes under baseline conditions (NAB C: n= 16, HAB C: n= 12, 2-way ANOVA with Bonferroni´s multiple comparison *post hoc test*, $F_{(15,390)}$= 35.26, p< 0.0001). In **Fig. 47 b)**, I examined in depth the effects of FLX on the different lengths of processes. In NAB cells FLX treatment for 48 h and 96 h shifted the curve along the y-axis, which reflected an increase in the number of processes, without losing the characteristic shape of the curve. In detail, at both time points FLX increased the number of very short (0-10 µM) and short (10-20 µm) processes significantly, without changing intermediate or long processes, although in a few cells very long processes (>60µm) could be observed. Thus suggesting the generation of new

processes (sprouting) after FLX treatment with possible prolongation of preexisting ones (2-way ANOVA with Dunnett´s multiple comparison *post hoc test*, $F_{(15,570)}= 105.8$, $p<0.0001$)

For a better comparison in the graph depicting HAB cells + FLX treatment, the NAB C curve is depicted in light gray color as well. However, statistical analysis was calculated to the respective control, in this case HAB C. FLX caused a pronounced increase in very short, short and intermediate-length processes, at both time points (48 h and 96 h). Interestingly, the shape of the curve in HAB cells after FLX treatment was almost identical to the very characteristic NAB curve. The data also suggest that in HAB cells a sprouting effect might have been elicited by FLX treatment. Additionally, some processes in the very long range (>60 µm), which could not be observed under basal conditions, were visible, possibly indicating a prolongation effect (2-way ANOVA with Dunnett´s multiple comparison *post hoc test*, $F_{(15,495)}= 52.96$, $p<0.0001$)

Furthermore, hence I saw that exogenous GDF15 increases the number of processes in both cell-types, in a dose- and time-dependent manner, I analyzed the length of the processes after GDF15 treatment. **Fig. 47 c**), depicts the data for both cell-types (NAB green colors, HAB blue colors) with different concentrations of GDF15 (1.0, 0.1, 0.01 ng/ml) at both time points (48 h and 96 h). After 48 h treatment with exogenous GDF15, the number of very short (0-10 µm) and short (10-20 µm) increased significantly at the highest concentration (1.0 ng/ml) without losing the characteristic shape of the curve. Moreover, I observed some processes in the very long range that were not present under baseline conditions. The intermediate (0.1 ng/ml) and low (0.01 ng/ml) concentration did not increase the numbers at any length significantly (2-way ANOVA with Dunnett´s multiple comparison *post hoc test*, $F_{(15,735)}= 64.09$, $p<0.0001$). In HAB cells GDF15 treatment caused an astonishingly similar results. The high (1.0 ng/ml) and intermediate (0.1 ng/ml) concentration increased the number of very short, short and intermediate processes, significantly. No very long processes were present. The low concentration (0.01 ng/ml) did not seem to be effective (2-way ANOVA with Dunnett´s multiple comparison *post hoc test*, $F_{(15, 465)}= 58.78$, $p<0.0001$). A prolongation of the treatment for 96 h resulted in an increase in the number of very short processes in NAB cells with all three concentrations applied, whereas only with the intermediate and high concentration I observed a significant increase the number of short processes. These two concentrations also induced some processes in the very long range (2-way ANOVA with Dunnett´s multiple comparison *post hoc test*, $F_{(15, 720)}= 100.3$, $p<0.0001$ In HAB cells, the highest

concentration failed to increase the number of very short processes at 96 h. On the contrary I even observed a significant decrease, whereas short, intermediate and long processes were significantly increased, suggsting a possible toxicity of GDF15 at least on the sprouting effect. The intermediate concentration was able to significantly increase very short, short and intermediate length processes, as well as prolonging some of the preexisting ones in the very long range (2-way ANOVA with Dunnett´s multiple comparison *post hoc test*, $F_{(15,\ 495)}= 43.77$, $p<0.0001$).

Overall these data showed that FLX and GDF15 can cause the sprouting of new processes, in our study defined as very short (0-10 µm) and short (10-20 µm) length and seemed to be able to prolong the preexisting processes, named here “very long” processes, in a dose and time-dependent manner. Furthermore, NAB cells showed a very characteristic shape of the curve indicating defined distribution of processes along different ranges, which still persisted after FLX and GDF15 treatment. Interestingly, the distribution of HAB processes, under baseline conditions, resulted in a distinct differently shaped curve, but treatment with FLX and GDF15 was able to shift this distribution into almost the identical direction as the NAB curve.

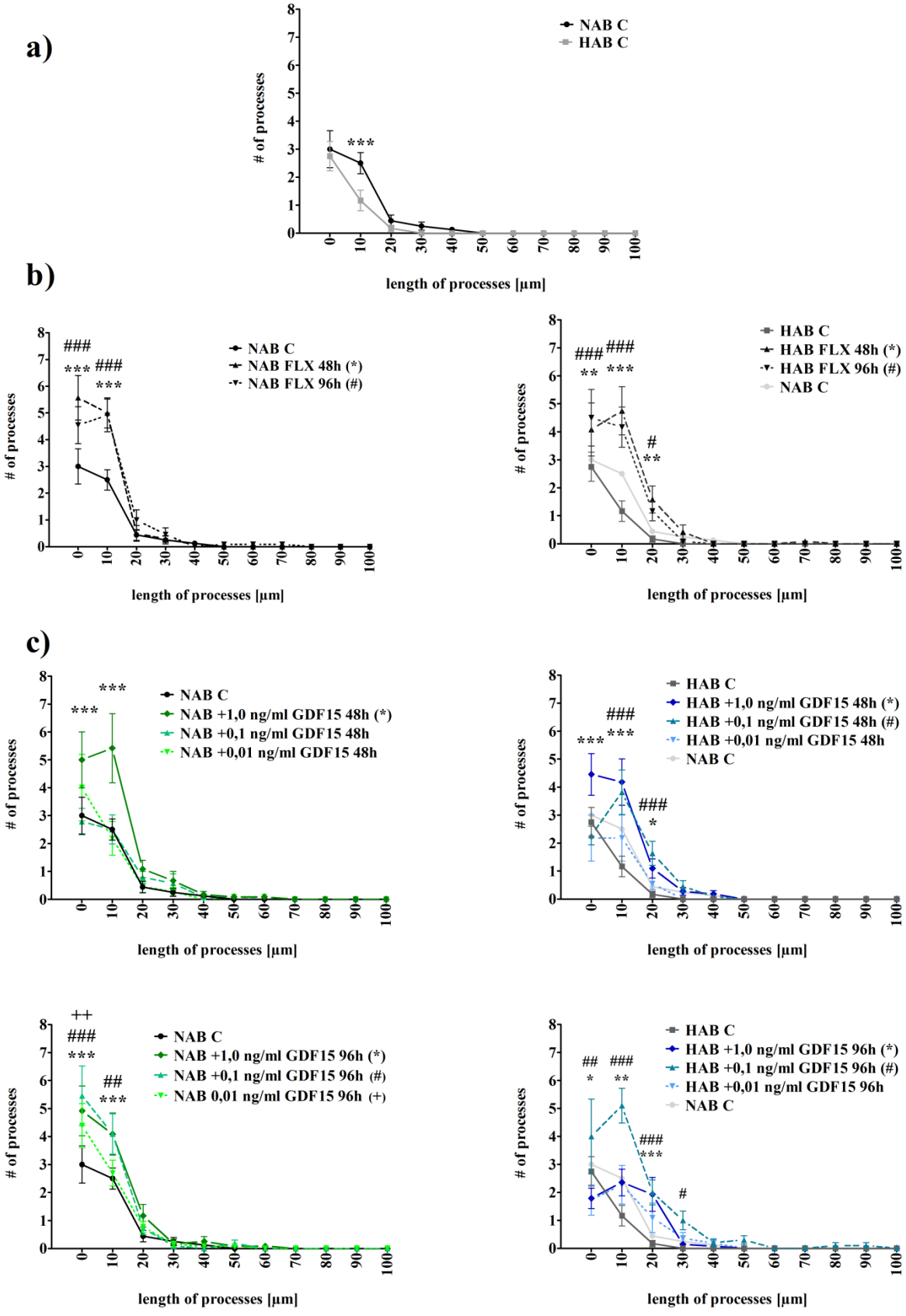
a)
NAB C
HAB C
# of processes
length of processes [µm]
***
b)
NAB C
NAB FLX 48h (*)
NAB FLX 96h (#)
HAB C
HAB FLX 48h (*)
HAB FLX 96h (#)
c)
NAB C
NAB +1,0 ng/ml GDF15 48h (*)
NAB +0,1 ng/ml GDF15 48h
NAB +0,01 ng/ml GDF15 48h
HAB C
HAB +1,0 ng/ml GDF15 48h (*)
HAB +0,1 ng/ml GDF15 48h (#)
HAB +0,01 ng/ml GDF15 48h
NAB C
NAB +1,0 ng/ml GDF15 96h (*)
NAB +0,1 ng/ml GDF15 96h (#)
NAB 0,01 ng/ml GDF15 96h (+)
HAB C
HAB +1,0 ng/ml GDF15 96h (*)
HAB +0,1 ng/ml GDF15 96h (#)
HAB +0,01 ng/ml GDF15 96h
NAB C

Fig. 47: Effects of FLX and exogenous GDF15 on the length of processes in HAB and NAB astrocytes, indicate sprouting of new processes

a) Analysis of the length of processes in HAB and NAB under baseline conditions, reveled a significant deficit in HAB cells
b) FLX treatment (48 h and 96 h) increased the number of processes at certain lengths in NAB cells (very short 0-10 µm, short 10-20 µm), as well as in HAB cells with a further increase at intermediate length (20-30 µm) processes
c) Exogenous GDF15 increased the number of very short and short processes in NAB cells in does- and time-dependent manner. Similar results were observed in HAB animals, with the addition of increases in intermediate and long processes.

Data are represented as mean ± SEM for each length, very short (0-10 µm), short (10-20 µm), intermediate (20-30 µm), long (30-40 µm), very long (>60 µm). 2-way ANOVA with Dunnett´s multiple comparison *post hoc test*. *, # $p< 0.05$, **, ##,++ $p< 0.01$,***,### $p< 0.001$

3.10.4. Knockdown of endogenous GDF15 in NAB cells

After having established the effect of exogenous GDF15, we wanted to investigate whether GDF15 is necessary to induce FLX effects. Therefore, we transfected NAB cells with siRNA specifically designed to knockdown *Gdf15* and subsequently treated them with FLX (**Fig. 49**).

The analysis of the number of processes showed that siRNA-mediated knockdown of endogenous GDF15 is able to reduce the number of processes, although not significantly (NAB C: n= 12, 6.333 ± 0.882, NAB scr: n = 10, 5.800 ± 0.359; NAB siRNA2: n= 11, 3.273 ± 1.833). However, 48 h FLX treatment restored the total number of processes in siRNA treated cells to similar amounts as not transfected and scr transfected cells (NAB FLX 48 h: n= 11, 10.82 ± 0.749, NAB scr+FLX: n= 11, 12.91 ± 1.148, NAB siRNA2+FLX: n= 5, 9.60 ± 1.833, Kruskal-Wallis test with Dunn´s multiple comparison *post hoc test*, $p<0.0001$).

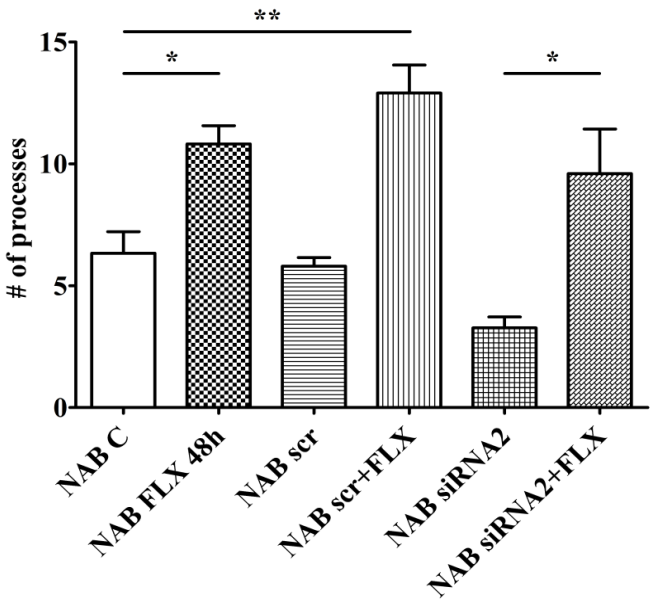

Fig. 48: Knockdown of GDF15 via siRNA with subsequent FLX treatment does not inhibit AD-mediated effects on the total number of processes in NAB cells.
NAB astrocytes were transfected with siRNA directed against GDF15 or non-targeting scr siRNA, as well as untreated (NAB C). Subsequently cells were treated with for 48 h with FLX. Data are represented as mean + SEM, Kruskal-Wallis test with Dunn´s multiple comparison *post hoc test*, *p<0.05, **p<0.01

Hence, knockdown of endogenous GDF15 did not significantly inhibit the growth of processes in NAB astrocytes or inhibited the FLX-mediated effects, but still exogenous GDF15 elicited the same effects as observed after FLX treatment, we investigated the effects of GDF15 knockdown on then specific lengths of astrocytes.

As seen in **Fig. 49,** knockdown of GDF15 decreased the number of very short processes in NAB cells below control levels. Thus, suggesting a role of GDF15 in stabilization of processes, as preexisting processes were lost when endogenous levels of GD15 were reduced. Subsequent treatment with FLX was able to increase the number of short processes, and the number of very short ones reached control levels (2-way ANOVA with Dunnett´s multiple comparison *post hoc test*, $F_{(15,480)}= 41.28$, $p< 0.0001$). Thus it might be that GDF15 is necessary to induce the sprouting of new processes upon FLX treatment.

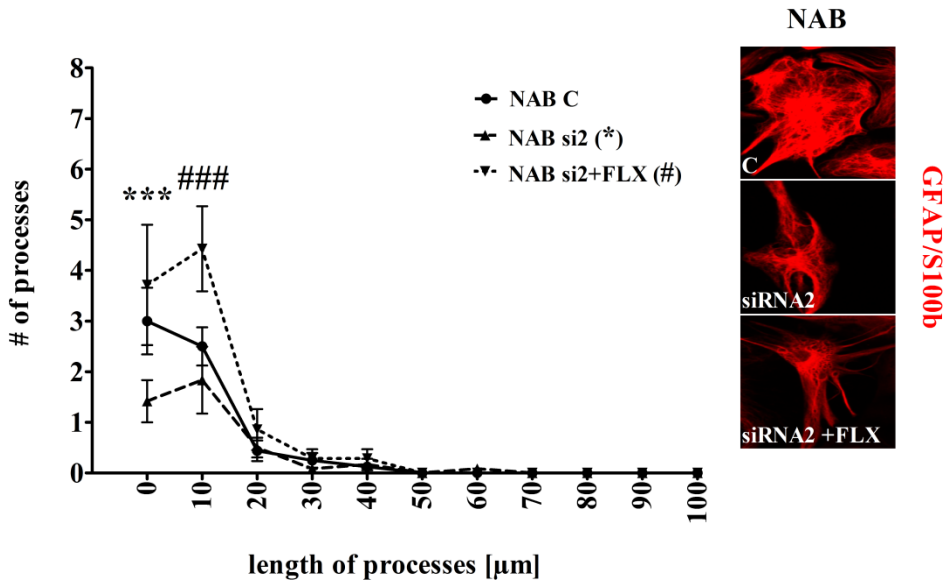

Fig. 49: Knockdown of endogenouse GDF15 in NAB astrocytes seem necessary for stabilisation of exisiting processed and FLX mediated sprouting

siRNA mediated knockdown of exogenous GDF15 caused a loss of very short (0-10 µm) processes. This loss could not be rescued by subsequent FLX treatment. FLX did significantly increase the number of short (10-20 µm) processes. Data are represented as mean ± SEM for each single length. Microphotographs depict NAB astrocytes under different treatment conditions. Data were analyzed using 2-way ANOVA with Dunnett´s multiple comparison *post hoc test*, ***,### $p < 0.001$

4. Discussion

Depression was recently estimated to be the leading cause of disability worldwide [7]. Although since the 50s antidepressant therapy options are available, the exact underlying mechanisms of MDD and the action of ADs are still poorly understood. With the development of new generations of antidepressants, the focus of research changed, from examining solely the monoaminergic system, towards more advanced and specific alternative targets.

However, the initial problems could still not be resolved. Antidepressants still require several weeks until the patients feel improvement of depressive symptoms and over 30 % of patients do not respond to the first treatment at all, thus requiring additional antidepressants. Thus, most clinical approaches are still based on trial and error, which represents a huge burden for patients, who have betaken themselves to seek medical help, although the stigmata for depression is still very present in our society. Therefore, the scientific effort should be directed to find novel, faster acting compounds and biomarkers that might predict the outcome of pharmacological treatments. A very promising approach to this type of "personalized medicine" developed with the emerging understanding of epigenetic mechanisms.

With the postulation of the histone code hypothesis [143] the focus was drawn towards an understanding how, not only eventual genetic predispositions, but also daily life events can impact such a disorder. Epigenetic modifications have been broadly implicated in the pathophysiology of mood disorders. But this research field is still in its infant shoes and mainly based on global aberrancies or misbalances in neuronal cells. Although, very striking evidence exists about depression being not primarily a neuronal, but rather a glia cell disease. Foremost, aberrancies in astrocytes have been shown to cause depressive phenotypes and many currently available antidepressants act directly on astrocytic populations. However, almost nothing is known about epigenetic modifications in glia cell, specifically in astrocytes. With the present study I was trying to shed some light on the possible underlying mechanisms that may contribute to the development of MDD, with a major focus on cell-type specific alterations in the PFC of HAB animals, which represent a very promising animal model for "endogenous" depression.

I investigated in our animal model which combination of different PTMs diverged from the "healthy" state and how antidepressant therapy impacted such modifications. Furthermore, I was able to identify a new candidate gene that was specifically regulated by PTMs, providing the first evidence that misregulation of this gene is linked to epigenetic

modifications in MDD. Moreover, using an unbiased microarray screening approach, another target of AD treatment was identified that is involved in regulating sprouting and maintenance of astrocytic processes, a mechanism that may be essential for AD responses. Astrocytic processes are known to be involved in MDD [51, 128] especially at the level of the blood-brain barrier. Improving brain plasticity by rescuing the reduced astrocytic processes might help to accelerate the uptake of antidepressants into the brain parenchyma, thus helping to establish a faster response to therapies and amelioration of symptoms.

The major questions of this study were:

1) How is the status quo in HAB animals compared to NAB animals regarding PTMs?
2) Are these differences cell-type specific?
3) How do ADs affect the misbalance?
4) Which are the downstream effects of such an aberrant epigenetic modification?
5) Can we target astrocytes at the level of processes in order to improve AD response
6) Are these factors putative targets to improve depressive symptoms

4.1. Posttranslational histonemodifications

Coming from the knowledge about histone modifications impacting the brain in MDD, I investigated in HAB animals, whether PTMs depict also a target in this model for depression.

Therefore, I investigated several PTMs in the PFC, which is one of the main regions affected in MDD [54, 62].

In the first approach, I analyzed H3K4me3, a PTM that is generally considered to be transcription activating (permissive mark) on a global level. Using IF-IHC, I analyzed the expression of H3K4me3 in the PFC of untreated HAB and NAB animals to establish a baseline between the two strains. This global analysis of H3K4me3 did not reveal any differences between the two strains. The missing global effects depicted a substantial deficit in the general epigenetic studies. Often only global differences are investigated, without taking into account that the expression of PTMs differs greatly not only among different brain regions or genes [68, 157, 220], but presumably also in different cell-types [151]. The PFC contains different cell-types, some of which might respond to ADs whereas others do not or even respond in opposite ways. These opposite effects may therefore counteract each other, ultimately leading to a nullification of the global effects. This sole investigation of global differences completely neglects existing changes in single cell-types, which might be even more important to understand the pathophysiology underlying MDD:

Thus, I decided to analyze the *ex vivo* brain slices in a cell-type specific manner. During this analysis two highly important results came up. First, I could show that HAB animals have significantly less astrocytes in the PFC, representing a further validation of HAB animals as a suitable model to study MDD, hence it was previously shown that reduced numbers of glia cells were found in the PFC of humans suffering from MDD [12, 31]. Secondly, I could reveal that the colocalization of H3K4me3 in HAB was significantly increased in astrocytes, but not in neurons, under baseline conditions. This indicated an astrocyte specific phenotype in HAB animals with regard to H3K4me3. This mark is generally thought to promote gene transcription, thus leading to the suggestion that HAB animals might display an aberrantly active expression of genes that could contribute to their behavioral phenotype. Further implicating that active gene transcription might not necessarily be beneficial in mood disorders, but rather induce a misregulation that could possibly lead to deleterious effects. With these data I provided evidence that, under baseline conditions, HAB animals do show epigenetic differences in comparison to "healthy" NAB animals and that such differences are specific to astrocytes of the PFC.

After having established that H3K4me3 in HAB animals is distinctly different than in controls, I investigated whether the misregulated H3K4me3 is a target of antidepressants. Chronic treatment with paroxetine, a SSRI, of HAB rats showed antidepressant effects, as measure by the forced swim test (FST) [221]. Following up that HAB rats beneficially respond to SSRIs, I used in this study fluoxetine (FLX), another SSRI that was shown to beneficially affect depression in humans [222] and is among the most prescribed antidepressant on the market. In first instance, to evaluate whether H3K4me3 is a pharmacological target of FLX, NAB animals were injected FLX or SAL as controls. I chose this short-term treatment, because I was interested in the early molecular effects of FLX, which supposedly start after the first administration of a drug, long before behavioral improvement might take place.

Indeed, I observed that FLX treatment in NAB rats increased the global expression of H3K4me3, showing that AD treatment upregulates H3K4me3 in the PFC already after this short-term treatment. This finding proved that H3K4me3 is targeted by FLX even under non-pathological conditions. In parallel, I investigated if a specific cell-type was affected by FLX injections and I could thereby reveal that, indeed, in NAB animals an upregulation of H3K4me3 occurred, again specifically in astrocytes, whereas neurons were not affected. Thus, emphasizing that specific cell-types might be more prone to respond differently to pharmacological treatment than others. Because astrocytes are part of the BBB, which is

the entrance for any drug into the brain, and the fact that HAB animals have less astrocytes in the PFC led to the suggestion that the delayed onset of AD efficacy might correlate with this misregulation.

It is known that epigenetic modifications change according to the environment, especially upon stressors. Hence injection of substances is always accompanied by some kind of stress, I wanted to investigate whether the injection itself caused changes in H3K4me3. To rule this possibility out, I compared injected animal to naïve animals at the level of H3K4me3 and did not find significant differences, thus implicating that no injection effect is damping the findings.

To see if HAB animals pharmacologically respond to FLX, I replicated this experiment in HAB animals injected with either SAL or FLX. The analysis of the global expression of H3K4me3 in the injected HAB animals did not show an overall difference in this mark. But the cell-type specific analysis revealed that, after the short-term treatment, H3K4me3 in HAB astrocytes was not targeted by FLX, whereas in the colocalization with neurons I observed a strong tendency towards a decrease. On first instance, this finding was very surprising, because I observed that astrocytes and not neurons were the affected cell-type in HAB animals. However, this finding went quite well in line with the fact that ADs take some time to elicit positive effects. It might be that a prolongation of the treatment, which better corresponds to a beneficial behavioral outcome, might ultimately target astrocytes to restore their functionality. Furthermore, it is not surprising that the diseased cells did not immediately respond to a pharmacological intervention, but maybe first FLX targeted the non-affected cell-type. It might also be that a proper number of astrocytes in the PFC of HAB animals first needs to be re- established before AD treatment can elicit beneficial effects in these animals, thus requiring a prolongation of FLX treatment. To investigate if a prolonged treatment with FLX might be able to restore the imbalance of H3K4me3 in HAB astrocytes, I used our cell culture model of primary cortical astrocytes, isolated from HAB and NAB pups. First, I established whether the *in vitro* model was suitable to reflect the findings obtained from *ex vivo* experiments. HAB and NAB astrocytes were treated with FLX and compared to untreated cells. Western blot analysis confirmed the basal differences in H3K4me3 protein expression that I observed in the *ex vivo* experiments, with a pronounced upregulation in untreated HAB astrocytes compared to untreated NAB astrocytes. A prolonged treatment with FLX up to 120 h significantly decreased H3K4me3 protein expression in HAB astrocytes, although this decrease was not yet visible after 48 h. These results further substantiated the suggestion that a short term treatment (48 h, or 2d *ex*

vivo) might not be sufficient to achieve beneficial effects in astrocytes yet, but a prolongation of the treatment might indeed target the diseased cells and they might have enough time to recover. To fully understand if a prolonged treatment with FLX might elicit the same effect in the PFC, it would be necessary to conduct a longitudinal study in HAB rats. To investigate if another AD, namely ESC, was also affecting H3K4me3 in HAB and NAB astrocytes, I treated the cells in the same manner as described with FLX. The baseline difference between untreated controls was persistent, confirming the strong molecular phenotype of our cell culture model. But ESC treatment did not target this methylation mark significantly, leading to the suggestion that the pharmacological effects may be specific to FLX. The differential effects of these two SSRIs, which supposedly should act in the same way, might be worth to be further investigated, in order to examine how specific ADs might target different epigenetic modifications also in light of finding putative markers for individual antidepressant responses.

As suggested by the "histone code hypothesis" [143], typically gene expression is determined by a combination of different modifications. These modifications might act synergistically or opposing to establish specific gene expression patterns [5], which might represent novel target for pharmacological intervention. To investigate if in our animal model such a combinatorial code might be involved in the underlying pathogenesis, which additionally could be unique to HAB rats, I further investigated other PTMs.

I analyzed H3K27ac, that is generally considered to be gene activating and has been implicated in MDD as well as being affected by ADs [223]. In our cell culture model, I identified that H3K27ac was downregulated under basal conditions, although this reduction was not significant. A possible explanation for this high variability in NAB astrocytes might be that because the cells are derived from outbred Wistar rats, they show a higher divergence than genetically driven HAB cells. This fact should be taken into account when interpreting such data, because, even if no significances occur, the biological effects should not be dismissed. After treating the cells with ADs, I observed a significant downregulation in NAB astrocytes after 120 h FLX treatment, speaking again for this mark also being a pharmacological target of ADs. In HAB astrocytes on the other hand, I observed an upregulation of H3K27ac after 120 h although it did not reach significance. The same biological effects were observed in HAB cells after ESC treatment, whereas in NAB animals the significant decrease of H3K27ac was not observed after 120 h ESC treatment, again speaking for different molecular pathways of these two drugs. This combination of the two PTMs might be explained by the fact that probably several genes

are impacted in different ways, emphasizing the necessity to analyze this combination at specific loci.

I further analyzed the expression of the repressive H3K27me3. This mark is supposed to counteract H3K4me3 [224]. Under baseline conditions, H3K27me3 was significantly downregulated in HAB animals, substantiating the counteracting effects of the activating H3K4me3 and repressive H3K27me3. In NAB animals this mark was not affected by FLX or ESC treatment, although an increase could be suggested upon FLX treatment. In HAB astrocytes the low expression was even further decreased after FLX treatment for 120 h, suggesting another player in the novel combination between these PTMs that could be unique to our model. ESC treatment did to affect this mark neither in NAB nor in HAB cells.

Having established the basal and pharmacological effects of H3K27me3 upon FLX treatment specifically in HAB astrocytes, I further analyzed the status quo in the PFC of NAB and HAB animals (*ex vivo*), as well as the pharmacological effects. Using brain slices derived from perfused animals represents a better possibility to analyze effects of ADs in a complex environment, than single cultures of astrocytes. Indeed, in the IF-IHC experiments I observed a significant downregulation of global H3K27me3 in the PFC of HAB animals of about 40 %.

These results substantiated the hypothesis of an existing combinatorial histone code in HAB animals. Further, I analyzed the astrocyte-specific colocalization of H3K27me3 in NAB and HAB. Among the astrocytic population again only 40 % of the cells showed a colocalization with H3K27me3 in NAB and this expression showed a tendency to decrease in HAB animals (about 28 %). Interestingly, H3K27me3 was in general very low expressed in the PFC of control animals (NAB), in which the expression levels only reached about 36 %. This might implicate that the effect size could not be high enough to be detectable in a single culture, thus not disregarding an underlying biological effect.

This combination of less repressive H327me3 together with the observed upregulation of the activating H3K4me3 provided evidence that astrocytes in the PFC of HAB animals, indeed, show a different combinatorial histone code than NAB animals under baseline conditions, further supporting the suggestion of aberrantly active gene transcription machinery involved in the behavioral phenotype. Here, I want to mention again that according to our cell culture model only a prolonged treatment might elicit significant molecular effects, emphasizing the necessity of a prolonged study in our animal model to be able to reveal possible treatment effects.

4.2. H3K4me3 regulation of ephrinA1

As already indicated from other published data [117, 147, 225], investigation of global differences is a valid starting point to identify novel targets, but to identify specific functional differences, it might be rather more important to investigate changes in specific genes. In an unbiased microarray screening approach, conducted previously in our lab, we were able to identify several candidate genes that are differentially expressed in astrocytes and C6 glioma cells treated with FLX and DMI. Among them EphA2, which belongs to the Eph receptor tyrosine kinase family [218], came up to be a target of AD treatment. Hence we went on and analyzed in cooperation with Dr. Mira Jacovcevski at the Max Planck Institute of Psychiatry, Munich, if the ephrin/EphR system might be a possible new target of ADs in astrocytes. To investigate this possibility, we conducted a chromatin-immunoprecipitation analysis (Ch-IP), to evaluate if our candidate gene might be regulated by H3K4me3. This approach confirmed that ephrinA1, a ligand of EphA2 and EphA4, was differentially regulated by the previously identified H3K4me3 in HAB astrocytes and prolonged treatment with FLX was able to decrease ephrinA1 to the baseline amounts observed in NAB. Consequently our data showed that ephrinA1 expression is specifically activated in HAB animals, probably leading to an imbalance in the ephrin/EphR system that might represent a molecular mechanism underlying the depression-like phenotype in HAB animals. These findings might open a novel approach in the field of understanding the pathophysiology of depression. Only one other study so far has implicated a misregulation in the ephrin/Eph system to MDD [199], but this study linked the ephrinB/EphB system to a misregulation on neuronal cells caused by stress-induced depressive symptoms.

Further, I went on to characterize the expression patterns of ephrinA1 upon FLX treatment in astrocytes. The cells were treated with FLX and a western blot analysis confirmed the pronounced upregulation of ephrinA1 (4-fold increase) in HAB astrocytes under baseline conditions. Interestingly, the results of western blot experiments showed two very distinct bands for ephrinA1, one at 26 kDa and one at 15 kDa. According to the manufacturer, ephrinA1 protein should be visible at roughly 30 kDa, which would indicate the 26 kDa band to be the one to look at. But there is evidence that different isoforms of ephrinA1 exist [218]. At present, I cannot rule out that these alternative spliced forms of ephrinA1 might represent a cell-type specific difference. Currently, I am examining how H3K4me3 and ephrinA1 are expressed in neurons and whether they might be modulated by AD treatment. Therefore, I decided to investigate both. Indeed, both isoforms were

differentially expressed in HAB animals, with a significant upregulation of the 15 kDa band and a strong tendency towards an upregulation of the 26 kDa band. Moreover, FLX treatment decreased the expression of both isoforms after 120 h treatment, although the effect did not reach significance, yet. In NAB astrocytes FLX caused an opposite effect, although also here no significance could be detected. A possible explanation why the effects after 120 h were not significant, might be that although we observed effects on the regulating PTM, the effects on gene specific expression, which involves the whole transcriptional and translational machinery, require longer times to be detectable. For future studies it might also be interesting to investigate if the two isoforms might play distinct roles.

Together with the pronounced upregulation of ephrinA1 in HAB astrocytes regulated by H3K4me3, and the suggestion that FLX normalized these effects again, I hypothesized that blocking the overexpression of ephrinA1 by RNA interference might have beneficial effects on the surrounding neuronal environment. Therefore, I designed siRNA directed specifically against ephrinA1 and transfected HAB astrocytes. After transfection, I observed a decreased ephrinA1 protein expression in HAB astrocytes.

With the establishment of this specific tool, I will be able further investigate, whether the knockdown of ephrinA1 is sufficient to reverse the morphological phenotype of HAB astrocytes and maybe even the depression-like behavior of HAB rats.

But first to examine whether this high ephrinA1 expression could also be observed in the PFC of HAB animals, I conducted IF-IHC experiments in the PFC of both, HAB and NAB, analyzing the expression of ephrinA1 and EphA4. Under baseline conditions, we were able to detect a significantly higher global expression of ephrinA1 in the PFC of HAB rats, whereas the expression of EphA4 did not differ, suggesting a gene specific imbalance. The finding that in ephrinA1 is overexpressed in the PFC of HAB as well as in astrocytes (*in vitro*) regulated by H3K4me3 and may be responsive to AD treatment, led me to the hypothesis that this specific gene might be highly involved in molecular phenotype of the HAB animals and is very likely involved in the pathophysiology the depressive-like behavior. However, I further need to elucidate if the overexpression in the PFC of HAB animals is specific to astrocytes, as indicated by the cell culture experiments, and whether AD treatment can reverse this expression. Furthermore, to investigate if overexpression of ephrinA1 is also sufficient to induce a depressive-like phenotype, I should induce an overexpression of ephrinA1 in the PFC of NAB rats and test their resulting behavior in the FST.

4.3. EphrinA1 and its implication it the regulation of synapses

The ephrin/EphR system is known to be involved in the regulation of synaptic compartments [203]. It is already known that a misregulation of the synaptic compartment is involved in MDD [123], and thus ephrinA1 may also play a distinct role in this regulation. In the present study, I was interested in investigating if synaptic contacts in HAB might differ from the normal phenotype. Therefore, I established a co-culture model to mimic a more "*in vivo*-like" situation.

The model consisted in the cultivation of astrocytes, either derived from HAB or NAB pups, that were plated a few days before the freshly isolated neuronal cells (only NAB) were added onto the feeder layer. The idea behind this approach was to see whether the "diseased" HAB cells were able to induce an aberrant phenotype in "healthy" neuronal cells on synaptic level and if these deficiencies could be rescued by administering the soluble Eph-receptor that binds to exaggeratedly expressed ephrinA1, thereby saturating ephrinA1 and inhibiting the binding to the native receptors with consequent rescuing effects.

Indeed, preliminary data on these co-cultures showed that neurons grown on HAB astrocytes seem to have less synapses as indicated by staining of pre- and postsynaptic terminals, as well as a reduction in the number of mature synapses. Interestingly, FLX treatment decreased the expression of synaptic markers in both co-cultures, further suggesting that ADs might cause plasticity changes into the direction of a de-differentiation of the targeted cells, thereby eliciting a remodeling of synapses. From the preliminary experiments I further observed that administration of EphA4, indeed, dampened the effects of overexpressed ephrinA1. In fact, 48 h after application of soluble EphA4-Fc HAB co-cultures showed an increased expression of synaptic proteins, indicative of a possible rescue effect. Whereas, ephrinA1 applied to NAB co-cultures showed a reduction in synapses. However, further quantitative studies are needed in order to elucidate the specific effects on pre- and postsynaptic terminals.

In a study by Nestor et al. [226] it was demonstrated that astrocytes in the rat hippocampus are able to respond to EphA receptor activation by increasing the length and number of fine processes. Furthermore, ephrins can regulate functional astrocyte-neuron communication by inhibiting Ca^{2+} oscillations in astrocytes, thereby leading to changes in glutamate release. This effect can be elicited by exogenous ephrinA-Fc application and by cleavage of the endogenous ephrinAs from their GPI anchors, indicating a cell-contact

independent mechanism. Furthermore, both, astrocytes and dendritic spines have been shown to express EphA receptors. Misregulation on both sides might cause morphological changes on the level of astrocytic processes and dendritic spines. Hence in the present study I saw a misbalance in the ligand (ephrinA1) but not in one of the receptors (EphA4), therefore it is likely that the exaggerated ligand expression is causing an inhibitory force on the normally expressed receptors, thus leading to retraction of spines and concomitantly to a reduced number in synapses. Alternatively, it might be that it also causes a repulsive force between the ephrinA1 expressing cells as it was already shown for example in gliomas [227]. Specifically, if cells which express the ligand come in close proximity to each other, they are able to sense the expression of the respective ligands and if the same ligand is expressed in the cell surface this elicits a repulsion force causing probably a transendocytosis of the complex into either cells, ultimately leading to cell rounding and retraction of processes. To clarify this aspect, it would be necessary to investigate the exact set of EphA receptors expressed by HABs in the PFC to determine whether other EphA receptors, like EphA2, might be misregulated. The high promiscuity of EphA receptors binding literally all ephrinA ligands requires a laborious experimental set up to investigate which specific combinations elicit these effects. Nonetheless, the fact that HAB astrocytes endogenously overexpress ephrinA1 in comparison to NAB astrocytes opens a new exciting possibility to identify novel mechanisms underlying MDD as an astrocytic pathology.

4.4. Summary and outlook on PTMS and ephrinA1

Interestingly, these data further suggested that the beneficial effects of blocking ephrinA1 at the synaptic level might be faster acting that the regulation by ADs. Short-term AD treatment did not restore synapses. It rather seems like the ADs elicited general readjustment processes on synaptic levels as seen by decrease in synaptic compartments in NAB-NAB cultures after 48 h treatment, whereas EphA4-Fc seems to increase at least pre- and postsynaptic protein expression already in this short time frame. It needs to be elucidated whether the 48 h EphA4 treatment is sufficient to induce an increase in the number of functional, mature synapses. Taken together my data indicate: 1) a unique combinatorial histone code in HAB animals with a pronounced upregulation of H3K4me3 specifically in astrocytes and not in neurons, H3K27me3 (repressive) being downregulated in HAB astrocytes and H3K27ac (permissive) which was downregulated in HAB astrocytes as well;

2) upon FLX treatment H3K4me3 was downregulated almost to control levels, H3K27me3 is downregulated as well, and H3K27ac was upregulated although not significantly, altogether indicating a novel mechanism of FLX treatment via PTMs.
3) H3K4me3 at the promoter caused a pronounced overexpression of ephrinA1 in HAB astrocytes that can be counteracted by FLX treatment after 120 h but the downregulation did not reach significance, which might be dependent on the time that transcriptional machinery requires to be restored. Hence we see the significant effect in the PTM but the gene expression might require longer time to reveal the differences on protein level. We are currently examining the effects of FLX on ephrinA1 regulated by H3K4me3 at the promoter level via ChIP.
4) knockdown of ephrinA1 was sufficient to reduce the protein expression in HAB astrocytes. Further analysis in needed to investigate if ephrinA1 is necessary for the FLX mediated effects. If this is the case, we will further investigate if siRNA mediated knockdown in HAB astrocytes might be able to rescue the deficiencies at the synaptic level and ultimately if virus mediated knockdown of ephrinA1 in the PFC might provide a mechanism to reverse the depressive-like phenotype in HAB animals, hence we see the pronounced upregulation in IF-IHC, corresponding to the changes observed *in vitro*.

This study provides interesting new findings of deregulated PTMs in astrocytes, causing aberrant gene expression of a novel target, the Eph/ephrin system, in HAB animals that ultimately might contribute to the depressive-like phenotype. Preliminary data on synaptic levels also indicate a misregulation on synaptic plasticity at the astrocyte-neuron communication. EphrinA1 might account, at least in part, for the readjustment of synaptic contacts in HAB animals, letting me to speculate that a concomitant misregulation in synaptic transmission might further be involved in the depressive phenotype. For example, a decrease in the glutamate system may be correlated with our findings, causing too high concentrations of glutamate in the synaptic cleft that cannot be properly removed and therefore may exhibit deficits in cognitive functions, as seen by reduced long-term potentiation in the hippocampus of animal models for depression. Furthermore, I might speculate that the Eph/ephrin system could also play a role on the vascularization, as it is the case in many cancers, specifically at the level of the BBB, at which HAB animals display aberrant coverage of blood vessels by astrocytes under baseline conditions. But further studies are needed to investigate these implications of the Eph/ephrin system.

4.5. GDF15

Among the 7 candidate genes in our microarray analysis, *Gdf15*, a member of the TGF-β superfamily came up to be highly upregulated after treatment in primary astrocytes and C6 glioma cells. Therefore, I investigated how this factor might be involved in MDD. GDF15 was previously identified as a biomarker for cardiovascular disease [184] and serum levels of GDF15 are a highly reliable predictor of disease progression. In the CNS GDF15 has been implicated to play an essential role in the maintenance of neurons and promotes survival of developing and lesioned neurons [187]. By identifying GDF15 as novel pharmacological target of antidepressants I was interested in investigating the potential of this factor as a new putative marker for antidepressant response.

So, I examined how GDF15 expression is modulated by FLX in primary cortical astrocytes and if HAB animals display a misregulation of this trophic factor, which might subsequently be restored by AD treatment. I especially focused on morphological alterations of astrocyte in the PFC of HAB animals as well as in our *in vitro* cell culture model to identify if GDF15 participates in the aberrant morphology of astrocytic processes specifically at the level of the BBB as previously shown [51].

GDF15 is known to be expressed in the CNS, especially at the choroid plexus where it is released into the CSF, from which it can penetrate the brain parenchyma.

By in situ hybridization, I could first verify the specificity and reliability of the generated *in situ* probe for *Gdf15*, and secondly observed that *Gdf15* mRNA is also expressed around blood vessel in the PFC of NAB and HAB rats. This observation led to the suggestion that GDF15 might play a role at the glia-vasculature interface, which we recently have shown to be misregulated in HAB animals [51].

By combining the ISH followed by IF-IHC in the PFC of HAB animals I identified that 2 h of FLX treatment was sufficient to significantly increase GDF15 expression around blood vessels in NAB rats, substantiating the hypothesis that it is a pharmacological target of FLX *ex vivo*. Furthermore, in the brain slices I observed the formation of *Gdf15* positive protrusions between surrounding astrocytes and parenchymal cells of the blood vessels, implying a possible connection between FLX treatment and formation of astrocytic processes. Although, in HAB animals 2 d of AD treatment did not reveal differences in global *Gdf15* expression around blood vessels of the PFC neither under basal conditions nor after FLX treatment.

Indicating that changes of *Gdf15* might upon FLX treatment, as seen in the microarray, could be restricted to more specific sites. However, by quantifying $GFAP^+$ processes around blood vessels, which represent processes derived from astrocytes, I confirmed the reduced number of blood vessel-associated astrocytic processes in HAB animals, which were be restored by FLX treatment, further suggesting that astrocytic processes around blood vessels, as part of the BBB, are impaired in HAB animals.

Following these observations, I investigated whether increased GDF15 expression might occur on more specialized compartments like $GFAP^+$ processes around blood vessels. Therefore, I quantified the relative number of $GFAP^+/Gdf15^+$ processes to total $GFAP^+$ processes, which also did not reveal major differences between HAB and NAB, but in HABs FLX seemed to slightly increase this proportion. Given the fact that HAB animals show a deficiency in astrocytic processes at the BBB, it is very likely that basal differences between NAB and HAB could be masked by this underlying deficiency. To avoid a possible masking effect of the reduced number of astrocytic processes, I performed a more in depth analysis. I quantified the density of $GFAP^+/Gdf15^{+-}$enriched astrocytic processes. Using this analysis I identified that in the HAB PFC not only the density of $GFAP^+/Gdf15^+$ processes is reduced, but this reduction can be increased by FLX treatment with respect to both stains. These data indicated that in the PFC of HAB animals GDF15 expression is reduced at very specific sites such as astrocytic processes surrounding blood vessels, which might further indicate that GDF15 could play an important role in establishing and/or maintenance of the BBB. As well as that the deficient expression of GDF15 at astrocytic processes can be targeted by FLX treatment, thereby possibly mediating beneficial effects for the uptake of AD into the brain parenchyma.

To investigate a potential functional role of GDF15 in astrocytes, I performed a preliminary western blot analysis using our cell culture model of primary astrocytes (HAB/NAB) under basal conditions and after treatment with FLX for 48 h and 96 h. As indicated by the global GDF15 expression in astrocytes from the PFC, I did not observe significant differences in protein expression of GDF15, although HAB astrocytes might tend to express less GDF15 under basal conditions and FLX might be able to increase the expression again. These findings might substantiate the hypothesis that a deficiency in astrocytic GDF15 expression might lead to an improper glia-vasculature interface in HAB animals, which could be restored by AD treatment.

With respect to our recently published paper, in which we found that FLX seems to sufficient to increase structural aberrancies on shorter astrocytic processes, I decided to

investigate in a more sophisticated analysis how FLX might act on astrocytic processes of different lengths and whether GDF15 participates in these morphological changes. By means of IF-ICC I wanted to establish if our cell culture model reflectd the deficits in terms of reduced number of processes. Indeed, I observed that also *in vitro* HAB astrocytes have significantly less processes under baseline conditions, indicating the cell culture as a suitable model to investigate how GDF15 might be involved in the establishment of astrocytic processes and whether it is necessary to mediate effects of FLX on astrocytes.

After treatment with FLX the number of processes per cell increased significantly, proving that FLX is sufficient to target outgrowth of astrocytic processes presumably by inducing a sprouting of new processes, an effect that could be observed in both cell-types. Moreover, these findings show that the deficiencies of astrocytic processes can be reversed by AD treatment. This increase in astrocytic processes could by a possible mechanism by which a proper glia-vasculature interface is reestablished, that is needed in order to mediate further AD effects, like changes in gene expression.

The increase in the total number caused by FLX treatment remained stable after prolonged treatment, indicating a possible ´ceiling effect´ in astrocytes, meaning that a single cell can only establish a certain amount of processes. One could speculate that this ceiling effect might be involved in treatment resistance to ADs, either because the astrocytes of treatment resistant patients somehow lost their ability to form new processes, or they already reached the maximal capacity of possible processes without a beneficial effect on the pathophysiology of MDD. However, to investigate such an implication further studies would be needed examining the astrocytic morphology in treatment resistant animal models, or patients.

Nevertheless, to investigate how GDF15 is involved in morphology of astrocytic processes I administered exogenous GDF15, hence GDF15 is a trophic factor that might be released from internal stores and is able to intact with distant cells. I applied three different concentrations at two time points in order to determine if the effects might be concentrations and/or time dependent. Indeed, after application of the highest concentration of GDF15, I observed an increase in the number of processes that reached the same amount as FLX, in both HAB and NAB astrocytes. NAB astrocytes did not respond to lower doses of GDF15, whereas HAB astrocytes are more sensitive to exogenous GDF15, hence they responded also to the intermediate dosage. These finding showed that GDF15 is able to elicit the same morphological changes in astrocytes as FLX, indicating GDF15 might be a new putative drug eliciting antidepressant effects.

Prolongation of the treatment with exogenous GDF15 resulted in a time and concentration dependence in NAB and HAB cells, but prolonged treatment with the highest concentration of GDF15 seemed to be toxic to HAB cells, further showing the higher sensitivity of HAB astrocyte to this trophic factor. Together these data strongly indicated that exogenous GDF15 is able to induce sprouting of astrocytic processes in a strikingly similar manner as FLX and this effect seems to be time- and concentration-dependent. A member of the TGF-β family, GDF10, has been implicated in axonal sprouting in the cortex after infarction and is able to activate a coordinated up- or down-regulation in specific pathways involved in axonal outgrowth [228]. Therefore, it can be speculated that GDF15 displays similar roles in astrocytes, although so far nothing is known about the effects of sprouting in astrocytes and GDF15.

Driven by our previous findings that a certain length of astrocytic processes might be necessary to elicit beneficial effects at the BBB upon FLX treatment [51], I further investigated the specific effect of FLX and exogenous GDF15 on the length of astrocytic processes *in vitro*. Under baseline conditions I observed that NAB astrocytes displayed a very characteristic curve of different lengths of processes, whereas the distribution of processes at certain lengths in HAB astrocytes differed greatly from NAB especially at shorter lengths, providing evidence that HAB astrocytes not only have deficits in the total numbers of processes but also that these deficits are specific to certain subsets of processes. FLX treatment increased the length of processes in both cell-types, further implicating a sprouting effect.

Interestingly, in HAB cells FLX caused an increase in the different lengths of processes, which resulted in almost identical shape of the curve as seen in NAB astrocytes. Moreover, I observed that especially after prolonged FLX treatment some processes occurred at the very long range, pointing towards an additional prolongation effect on preexisiting astrocytic processes, thereby supporting the hypothesis that prolonged FLX treatment might be able to restore the morphological alterations and might be implicated in further improving astrocytic connections around blood vessels, maybe even to reinstate a proper BBB.

To establish if GDF15 might act specifically on a subset of astrocytic processes, I also analyzed the different concentrations of exogenous GDF15. NAB and HAB astrocyte both responded to the highest concentration of GDF15 with increase at the different lengths of processes, but HAB astrocytes were more sensitive, since they also responded to the intermediate concentration after short-term treatment. Additionally, I observed some

processes in the very long range in HAB astrocyte after GDF15 treatment, which were not detectable after FLX treatment. Given the higher sensitivity of HAB astrocytes to exogenous GDF15, it can be suggested that GDF15 might be a more potent factor acting on the prolongation of preexisiting processes than FLX, indicating that exogenous GDF15 might be a faster acting pharmacological compound which could be tested for putative AD properties.

Overall these data strongly indicated that FLX and exogenous GDF15 elicit the sprouting of new astrocytic processes as well as prolongation of preexisting ones, indicative for structural alterations that might be beneficial, especially at the glia-vasculature interface, and GDF15 is sufficient to induce similar effects as FLX. To establish whether there might be causal link between the effects of FLX and exogenous GDF15, I used siRNA designed to target specifically *Gdf15* in order to investigate whether GDF15 is necessary to mediate the effects of FLX. Knockdown of *Gdf15* is able to reduce the number of processes, although not significantly. However, subsequent FLX treatment of these cells restored the numbers of processes to baseline levels, showing that endogenous GDF15 is not necessary to mediate FLX effects on astrocytic processes. Nevertheless, I was interested to investigate also here whether GDF15 might be essential at specific subsets of processes. Therefore, I analyzed in detail the effects on siRNA-mediated knockdown of endogenous GDF15 on the sprouting and prolongation effects observed. In NAB cells knockdown of GDF15 decreases the numbers of very short processes even below the control levels indicating a role of endogenous GDF15 in sprouting of astrocytic processes, although also here subsequent treatment with FLX restored the numbers.

Taken together the data indicate FLX is able to activate an intrinsic program that results in the sprouting of $GDF15^{+}$ astrocytic processes and this effect is particularly significant around blood vessels. Indicating that there might be a connection between the effects of FLX and the formation of $GDF15^{+}$ astrocytic processes in the PFC of HAB rats. These data indicate that GDF15 could be involved in restoring a proper glia-vasculature interface, especially at the level of the BBB. Administration of FLX increased the numbers significantly in both cell-types, an effect that remained stable also after prolonged treatment, hinting to a possible ´ceiling effect´, that might be worth to be further analyzed. In addition, although the endogenous protein levels do not significantly vary between HAB and NAB astrocyte *in vitro*, administration of exogenous GDF15 was sufficient to elicit the same increase of astrocytic processes in HAB and NAB cells in a dose- and time dependent manner, suggesting a beneficial role of GDF15 in HAB cells on restoring a

proper set of astrocytic processes. With the previously published data that FLX is able to restore the structural deficiencies of astrocytic processes but a short term treatment might not be sufficient to restore a proper glia-vasculature interface [51], we conducted a more in depth analysis whether specific subset of processes might be specifically targeted and whether this effects might be mediated by GDF15. This analysis revealed that FLX enhanced sprouting of new processes as well as prolonged preexisting ones, an effect that could also be observed by application of exogenous GDF15, pointing towards a functional role of GDF15 in the morphology of astrocytes, possibly by interactions with other structural factors, like actin of GFAP. However, endogenous GDF15 is not necessary to mediate the effects of FLX. Although with respect to the different lengths of processes it might be that GDF15 is responsible for the stabilization of astrocytic processes, hence knockdown of causes a significant reduction in very short processes. Ongoing experiments on this subject point into the direction that endogenous GDF15 might not be necessary for the response of astrocytes to FLX but that the release of GDF15 might be impaired in HAB astrocytes, which may be restored upon FLX treatment. However, further studies on this subject are necessary to define the mechanism by which GDF15 (endogenous or exogenous) affect astrocytic processes. Therefore, I am going to conduct an ELISA assay to examine supernatants and cell lysates derived from FLX- and GDF15-treated cells as wells with serum samples of HAB and NAB rats to further clarify the possibility of GDF15 as a potential diagnostic or treatment biomarker.

Supplementary

Absolute number of cells in PFC of HAB and NAB

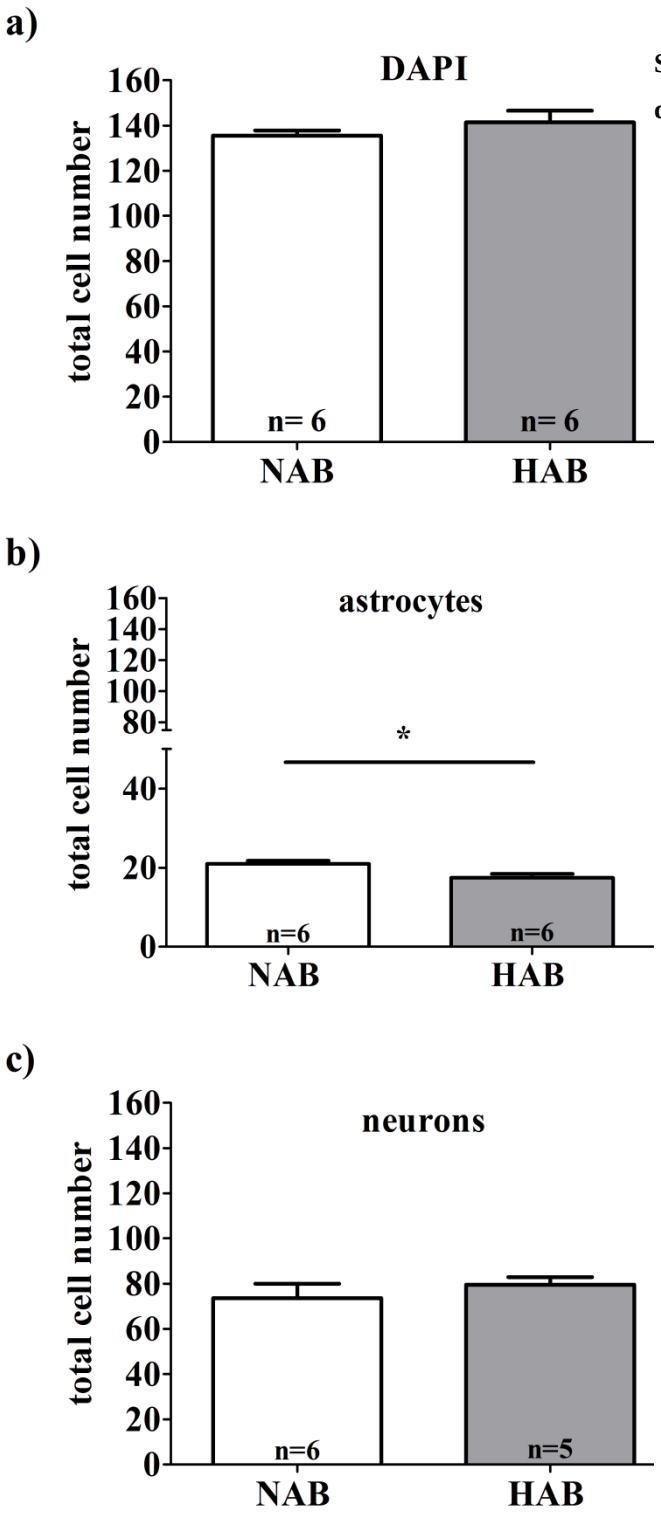

Suppl. 1: absolute numbers of cells do not differ between NAB and HAB

a) Quantitative IF-IHC analysis for total cell number (DAPI) in the PFC of NAB (n= 6 animals, 135.5 ± 2.275) and HAB (n= 6 animals, 141.4 ± 5.237) under baseline conditions

The total cell number is depicted as mean +SEM. Student´s t-test, $t_{(10)}$= 1.026, p= 0.3293, n.s.

b) Total counts of astrocytes in the PFC NAB (n= 6, 20.98 ± 0.8083) and HAB. (n= 6, 17.49 ± 0.9501) Student´s t-test, $t_{(10)}$= 0.2.796, p= 0.0.0189

c) Total counts of neurons in the PFC NAB (n= 6, 73.63 ± 6.336) and HAB (n= 5, 79.48 ± 3.388), Student´s t-test, $t_{(9)}$= 0.7654, p= 0.4636

Effects of the injection itself on H3K4me3

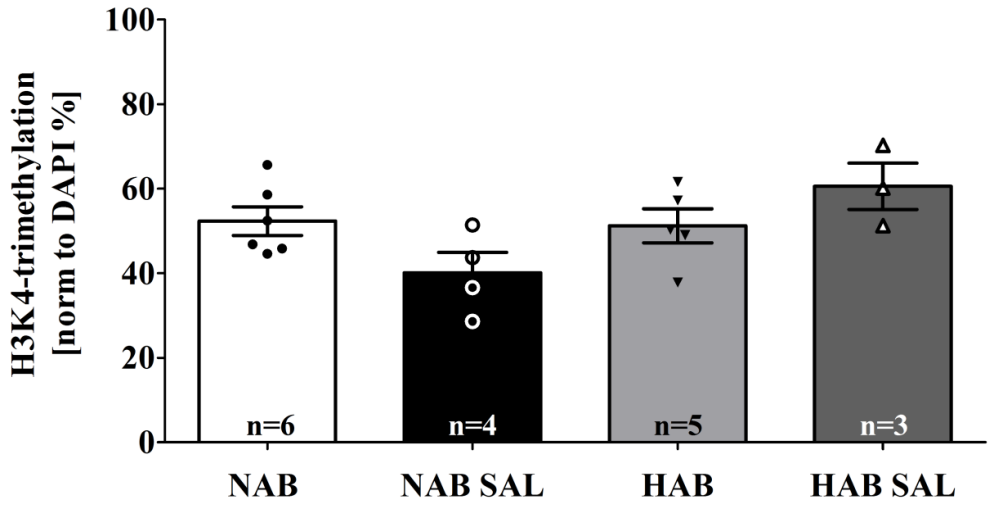

Suppl. 2: Analysis of possible effects on H3K4me3 cause by the injection itself

Comparison of NAB and HAB rats under basal conditions and after injection with SAL, did not affect the expression of H3K4me3 in the PFC, neither in NAB, nor in HAB animals. NAB: n= 6, 52.32 ± 3.409%; NAB SAL: n= 4, 40.07 ± 4.880%; HAB: n= 5, 51.21 ± 4.049%; HAB SAL: n=3, 60.56 ± 5.480%.One-way ANOVA with Tukey *post hoc* test $F_{(3, 14)}$= 3.107, p= 0.0607. All data are represented in [%] H3K4me3 normalized to DAPI and depicted as mean +SEM

Effects of the injection itself on H3K4me3- cell-type specific

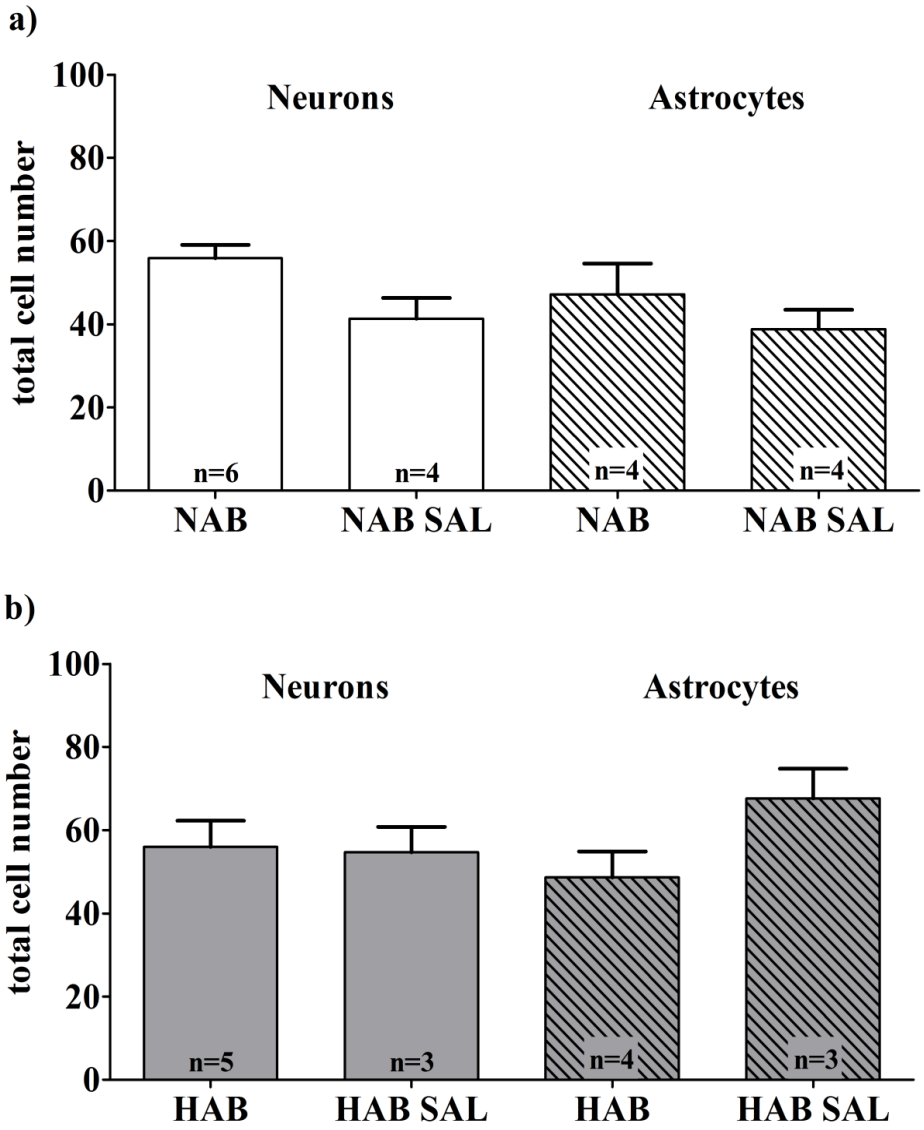

Suppl. 3: Cell type specific analysis- injection effects

Cell type specific comparison of NAB and HAB rats under basal conditions and after injection with SAL. The injection did not affect the expression of H3K4me3 in the PFC, neither in NAB, nor in HAB animals. NAB neurons: n= 6, 55.90 ± 3.204%; NAB SAL neurons: n= 4, 41.34 ± 5.003%; NAB astrocytes: n= 4, 47.21 ± 7.336%, NAB SAL astrocytes: n= 4, 38.81 ± 4.699%; One-way ANOVA with Tukey *post hoc* test $F_{(3, 11)}$= 2.677, p= 0.0873

HAB neurons: n= 5, 55.98 ± 6.300%; HAB SAL neurons: n=3, 54.72 ± 6.072%; HAB astrocytes: n=4, 48.67 ± 6.214%, HAB SAL astrocytes: 67.61 ± 7.183%; One-way ANOVA with Tukey´s post hoc test $F_{(3, 11)}$= 1.280, p= 0.3293. All data are represented in [%] H3K4me3 normalized to DAPI and depicted as mean +SEM

Proportional expression of H3K4me3 and H3K27me3

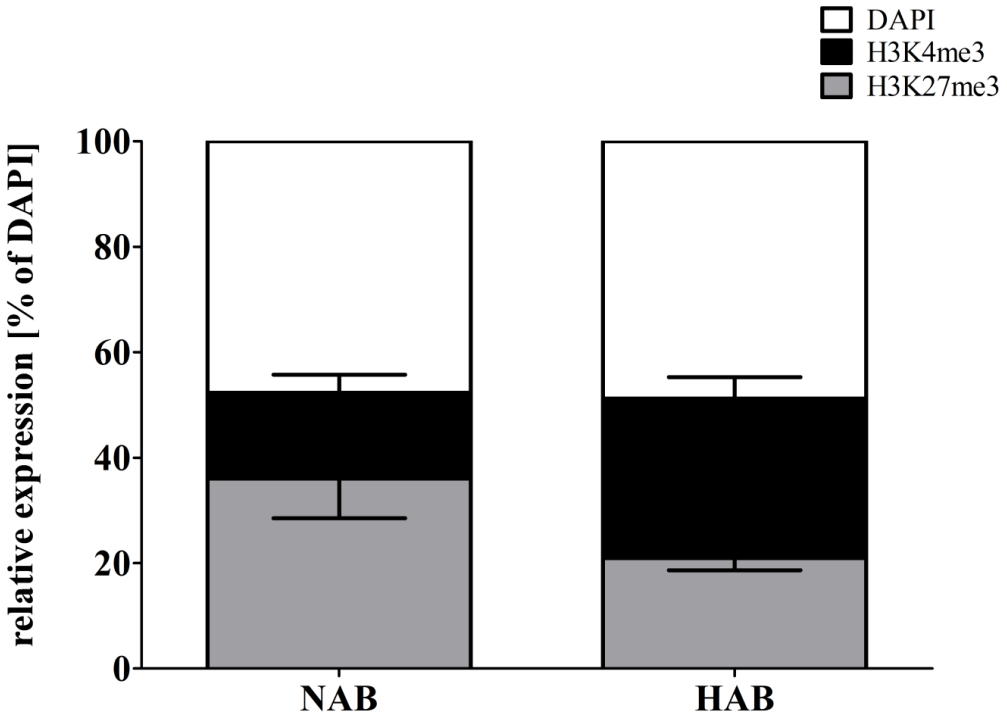

Suppl. 4: Proportional expression of H3K4me3 and H3K27me in NAB and HAB

This figure shows the proportions of the activating mark H3K4me3 and H3K27me3 in HAB and NAB animals. Depicted here is DAPI, set as 100 % for both, NAB and HAB, and the proportional expression of H3K4me3 (in black; NAB: 52.32 %, HAB: 51.21 %) and H3K27me3 (in grey; NAB: 36.05 %, HAB: 20.94 %).

List of abbreviations

WHO	world health organization
MDD	major depressive disorder
DSM-V	Diagnostic and Statistical Manual of Mental Disorders, Fifth Edition
AD	antidepressant
VTA	ventral tegmental area
NAc	nucleus accumbens
HIPPO	hippocampus
(m)PFC	(medial) prefrontal cortex
AMY	amygdala
Cg25	subcallosal cingulate gyrus
DR	dorsal raphe nucleus
5-HT	5- hydroxytryptamine = serotonin
GABA	γ-Aminobutyric acid
HPA axis	hypothalamic-pituitary-adrenal axis
SSRI	selective serotonin reuptake inhibitor
FLX	fluoxetine
LC	locus coereleus
IMI	imipramine
NA	noradrenalin
NRI	selective noradrenalin reuptake inhibitor
SNRI	serotonin and noradrenaline reuptake inhibitor
MAOI	monoamine oxidase A inhibitor
VEGF	vascular endothelial growth factor
IGF-2	insulin-like growth factor-2
FGF-1	fibroblast growth factor-1
GDNF	glia-cell derived neurotrophic factor
BDNF	brain-derived neurotrophic factor
SVZ	subventricular zone
SGZ	subgranular zone
L-AAA	L-alpha-aminoadipic acid
ERK	extracellular signal–regulated kinases
MAPK	mitogen-activated protein kinase
BBB	blood brain barrier

Aqp-4	aquaporin-4
PTM	posttranslational histonemodification
GR	glucocorticoid receptor
HDAC(i)	histone-deacetylase (inhibitor)
H3K4me3	histone 3- lysine 4- trimethylation
H3K27me3	histone 3- lysine 27- trimethylation
CNS	central nervous system
VZ	ventricular zone
GFAP	glia fibrillary acidic protein
GLAST-1	glutamate aspartate transporter -1
GLT-1	glutamate transporter -1
GS	glutamine synthase
AldhL1	aldehyde dehydrogenase family member 1
EGF	ependymal growth factor
ECM	extracellular matrix
NCAM	neural cell adhesion molecule
MMP(s)	matrix metalloprotease(s)
NGF	nerve growth factor
NT-3	neurotrophin-3
TGF-β	transforming growth factor- β
IL-6	interleukin -6
CUS	chronic unpredictable stress
ECS	extracellular space
RNAi	RNA- interference
CpG	cytosine-guanine dyads
DNMT	DNA-methyltransferase
MeCP	methyl-CpG-binding proteins
5-hmC	5-hydroxymethylcytosine
TET	ten-eleven-translocation
K	Lysine
HAT	histone-acetyltransferases
NAD	Nicotinamide adenine dinucleotide
R	Arginine
H	Histidine
H3K9	histone 3- lysine 9

H3K36	histone 3- lysine 36
H3K79	histone 3- lysine 79
H4K29	histone 4- lysine 29
HMT	histone-methyltransferase
SAM	S-adenosyl-methionine
HMD	histone-demethylase
KMT	lysine methyltransferase
MLL	mixed lineage leukemia
PRC2	polycomb repressive chromatin remodeling complex 2
KMD	lysine demethylase
HG	high grooming
LG	low grooming
GRIK2	glutamate receptor, ionotropic kainate 2
BEGAIN	brain-enriched guanylate kinase-associated protein
HAB	high anxiety-related behavior
LAB	low anxiety-related behavior
EPM	elevated plus maze
PND	post-natal day
FST	forced swim test
CRH	corticotrophin-releasing hormone
AVP	arginine vasopressin
ACTH	adrenocorticotropic hormone
DEX/CRH test	dexamethasone-suppression/CRH challenge test
GDF15	growth differentiation factor 15
CSF	cerebrospinal fluid
shRNA	short hairpin RNA
NAB	non-selectively bred
Eph(R)	erythropoietin-producing-heptaocellular carcinoma (receptor)
RTK	receptor tyrosine kinases
ephrins	Eph receptor-interacting-signals
NAB	non-selectively bred
RT	room temperature
h	hours
E18	embryonic day 18
ESC	escitalopram

PBS	phosphate buffered saline
i.p.	intraperitoneal
HBSS	Hank´s balanced salt solution
SN	supernatant
min	minutes
DMEM	Dulbecco´s modified eagle medium
FCS	fetal calf serum
PDL	poly-D-lysine
D*IV*	days *in vitro*
DMSO	dimethylsulfoxide
d	days
P4	passage 4
rpm	rounds per minute
IF	immunofluorescence
IF-IHC	immunofluorescent-immunohistochemistry
PFA	paraformaldehyde
O.N.	over night
NGS	normal goat serum
IF-ICC	immunofluorescent-immunocytochemistry
SEM	standard error of means
SDS	sodium duodecyl-sulfate
PVDF	polyvinylidene fluoride
BSA	bovine serum albumine
siRNA	short interfering RNA
ChIP	chromatin-immunoprecipitation
PBST	PBS + tween
H3K27ac	histone 3-lysine 4-acetylation

List of figures

List of figures – supplementary

List of tables

References

1. Barquilla, A. and E.B. Pasquale, *Eph receptors and ephrins: therapeutic opportunities.* Annu Rev Pharmacol Toxicol, 2015. **55**: p. 465-87.
2. Vialou, V., et al., *Epigenetic mechanisms of depression and antidepressant action.* Annu Rev Pharmacol Toxicol, 2013. **53**: p. 59-87.
3. Peña, C.J., et al., *Epigenetic Signaling in Psychiatric Disorders.* Journal of Molecular Biology, 2014. **426**(20): p. 3389-3412.
4. Linkert, M., et al., *Metadata matters: access to image data in the real world.* J Cell Biol, 2010. **189**(5): p. 777-82.
5. Graff, J. and I.M. Mansuy, *Epigenetic codes in cognition and behaviour.* Behav Brain Res, 2008. **192**(1): p. 70-87.
6. Schindelin, J., et al., *Fiji: an open-source platform for biological-image analysis.* Nat Meth, 2012. **9**(7): p. 676-682.
7. WHO, *World health organisation.* http://www.who.int/mental_health/management/depression/en/, accessed 27.04.2013 10:36h.
8. Klengel, T. and E.B. Binder, *Gene x environment interactions in the prediction of response to antidepressant treatment.* Int J Neuropsychopharmacol, 2013. **16**(3): p. 701-11.
9. Kruijshaar, M.E., et al., *Lifetime prevalence estimates of major depression: an indirect estimation method and a quantification of recall bias.* Eur J Epidemiol, 2005. **20**(1): p. 103-11.
10. Kessler, R.C., et al., *Twelve-month and lifetime prevalence and lifetime morbid risk of anxiety and mood disorders in the United States.* Int J Methods Psychiatr Res, 2012. **21**(3): p. 169-84.
11. Di Benedetto, B., R. Rupprecht, and G. Rammes, *Beyond the monoamine hypothesis: The quest for an integrative etiology of depression and new therapeutic strategies*, in *Antidepressants: Types, Efficiency and Possible Side Effects Chapters*, J.T.V. Leeuwen, Editor. 2010, Nova Science Publisher, Inc.
12. Rajkowska, G. and C.A. Stockmeier, *Astrocyte pathology in major depressive disorder: insights from human postmortem brain tissue.* Curr Drug Targets, 2013.
13. Rush, A.J., et al., *Comorbid psychiatric disorders in depressed outpatients: demographic and clinical features.* J Affect Disord, 2005. **87**(1): p. 43-55.
14. Nemeroff, C.B. and P.J. Goldschmidt-Clermont, *Heartache and heartbreak--the link between depression and cardiovascular disease.* Nat Rev Cardiol, 2012. **9**(9): p. 526-39.
15. Schulberg, H.C., et al., *Treating major depression in primary care practice: an update of the Agency for Health Care Policy and Research Practice Guidelines.* Arch Gen Psychiatry, 1998. **55**(12): p. 1121-7.
16. Nestler, E.J., et al., *Epigenetic Basis of Mental Illness.* Neuroscientist, 2015.
17. Heshmati, M. and S.J. Russo, *Anhedonia and the brain reward circuitry in depression.* Curr Behav Neurosci Rep, 2015. **2**(3): p. 146-153.
18. Heller, A.S., *Cortical-Subcortical Interactions in Depression: From Animal Models to Human Psychopathology.* Front Syst Neurosci, 2016. **10**: p. 20.
19. Malone, D.A., Jr., et al., *Deep brain stimulation of the ventral capsule/ventral striatum for treatment-resistant depression.* Biol Psychiatry, 2009. **65**(4): p. 267-75.
20. Mayberg, H.S., et al., *Deep brain stimulation for treatment-resistant depression.* Neuron, 2005. **45**(5): p. 651-60.

21. Von Der Heide, R.J., et al., *Dissecting the uncinate fasciculus: disorders, controversies and a hypothesis,* in *Brain*. 2013. p. 1692-707.
22. Price, J.L., *Comparative aspects of amygdala connectivity.* Ann N Y Acad Sci, 2003. **985**: p. 50-8.
23. Phillips, M.L., et al., *Identifying predictors, moderators, and mediators of antidepressant response in major depressive disorder: neuroimaging approaches.* Am J Psychiatry, 2015. **172**(2): p. 124-38.
24. Challis, C. and O. Berton, *Top-Down Control of Serotonin Systems by the Prefrontal Cortex: A Path toward Restored Socioemotional Function in Depression.* ACS Chem Neurosci, 2015. **6**(7): p. 1040-54.
25. Bao, A.M. and D.F. Swaab, *The stress systems in depression: a postmortem study.* Eur J Psychotraumatol, 2014. **5**: p. 26521.
26. Krishnan, V. and E.J. Nestler, *The molecular neurobiology of depression.* Nature, 2008. **455**(7215): p. 894-902.
27. Lopez-Munoz, F. and C. Alamo, *Monoaminergic neurotransmission: the history of the discovery of antidepressants from 1950s until today.* Curr Pharm Des, 2009. **15**(14): p. 1563-86.
28. Schildkraut, J.J., *The catecholamine hypothesis of affective disorders: a review of supporting evidence.* Am J Psychiatry, 1965. **122**(5): p. 509-22.
29. van Praag, H.M., *Neuroendocrine disorders in depressions and their significance for the monoamine hypothesis of depression.* Acta Psychiatr Scand, 1978. **57**(5): p. 389-404.
30. Ruhe, H.G., N.S. Mason, and A.H. Schene, *Mood is indirectly related to serotonin, norepinephrine and dopamine levels in humans: a meta-analysis of monoamine depletion studies.* Mol Psychiatry, 2007. **12**(4): p. 331-59.
31. Rajkowska, G., et al., *Morphometric evidence for neuronal and glial prefrontal cell pathology in major depression.* Biol Psychiatry, 1999. **45**(9): p. 1085-98.
32. Hercher, C., G. Turecki, and N. Mechawar, *Through the looking glass: examining neuroanatomical evidence for cellular alterations in major depression.* J Psychiatr Res, 2009. **43**(11): p. 947-61.
33. Duman, R.S. and N. Li, *A neurotrophic hypothesis of depression: role of synaptogenesis in the actions of NMDA receptor antagonists.* Philos Trans R Soc Lond B Biol Sci, 2012. **367**(1601): p. 2475-84.
34. Duman, R.S. and L.M. Monteggia, *A neurotrophic model for stress-related mood disorders.* Biol Psychiatry, 2006. **59**(12): p. 1116-27.
35. Castren, E., *Is mood chemistry?* Nat Rev Neurosci, 2005. **6**(3): p. 241-6.
36. Duclot, F. and M. Kabbaj, *Epigenetic mechanisms underlying the role of brain-derived neurotrophic factor in depression and response to antidepressants.* J Exp Biol, 2015. **218**(Pt 1): p. 21-31.
37. Manji, H.K. and R.S. Duman, *Impairments of neuroplasticity and cellular resilience in severe mood disorders: implications for the development of novel therapeutics.* Psychopharmacol Bull, 2001. **35**(2): p. 5-49.
38. Castren, E. and T. Rantamaki, *The role of BDNF and its receptors in depression and antidepressant drug action: Reactivation of developmental plasticity.* Dev Neurobiol, 2010. **70**(5): p. 289-97.
39. Jeon, S.W. and Y.K. Kim, *Molecular Neurobiology and Promising New Treatment in Depression.* Int J Mol Sci, 2016. **17**(3).
40. Sharma, A.N., et al., *Role of trophic factors GDNF, IGF-1 and VEGF in major depressive disorder: A comprehensive review of human studies.* J Affect Disord, 2016. **197**: p. 9-20.

41. Sen, S., R. Duman, and G. Sanacora, *Serum brain-derived neurotrophic factor, depression, and antidepressant medications: meta-analyses and implications.* Biol Psychiatry, 2008. **64**(6): p. 527-32.
42. Shirayama, Y., et al., *Brain-derived neurotrophic factor produces antidepressant effects in behavioral models of depression.* J Neurosci, 2002. **22**(8): p. 3251-61.
43. Eisch, A.J., et al., *Brain-derived neurotrophic factor in the ventral midbrain-nucleus accumbens pathway: a role in depression.* Biol Psychiatry, 2003. **54**(10): p. 994-1005.
44. Monteggia, L.M., et al., *Brain-derived neurotrophic factor conditional knockouts show gender differences in depression-related behaviors.* Biol Psychiatry, 2007. **61**(2): p. 187-97.
45. Sahay, A. and R. Hen, *Hippocampal neurogenesis and depression.* Novartis Found Symp, 2008. **289**: p. 152-60; discussion 160-4, 193-5.
46. Castren, E. and R. Hen, *Neuronal plasticity and antidepressant actions.* Trends Neurosci, 2013.
47. Santarelli, L., et al., *Requirement of hippocampal neurogenesis for the behavioral effects of antidepressants.* Science, 2003. **301**(5634): p. 805-9.
48. Rajkowska, G. and J.J. Miguel-Hidalgo, *Gliogenesis and glial pathology in depression.* CNS Neurol Disord Drug Targets, 2007. **6**(3): p. 219-33.
49. Cotter, D.R., C.M. Pariante, and I.P. Everall, *Glial cell abnormalities in major psychiatric disorders: the evidence and implications.* Brain Res Bull, 2001. **55**(5): p. 585-95.
50. Cotter, D., et al., *Reduced neuronal size and glial cell density in area 9 of the dorsolateral prefrontal cortex in subjects with major depressive disorder.* Cereb Cortex, 2002. **12**(4): p. 386-94.
51. Di Benedetto, B., et al., *Fluoxetine Requires the Endfeet Protein Aquaporin-4 to Enhance Plasticity of Astrocyte Processes.* Front Cell Neurosci, 2016. **10**: p. 8.
52. Torres-Platas, S.G., et al., *Astrocytic hypertrophy in anterior cingulate white matter of depressed suicides.* Neuropsychopharmacology, 2011. **36**(13): p. 2650-8.
53. Schroeter, M.L., et al., *Mood disorders are glial disorders: evidence from in vivo studies.* Cardiovasc Psychiatry Neurol, 2010. **2010**: p. 780645.
54. Banasr, M. and R.S. Duman, *Glial loss in the prefrontal cortex is sufficient to induce depressive-like behaviors.* Biol Psychiatry, 2008. **64**(10): p. 863-70.
55. Perez-Alvarez, A. and A. Araque, *Astrocyte-neuron interaction at tripartite synapses.* Curr Drug Targets, 2013. **14**(11): p. 1220-4.
56. Araque, A., G. Carmignoto, and P.G. Haydon, *Dynamic signaling between astrocytes and neurons.* Annu Rev Physiol, 2001. **63**: p. 795-813.
57. Hisaoka, K., et al., *Antidepressants increase glial cell line-derived neurotrophic factor production through monoamine-independent activation of protein tyrosine kinase and extracellular signal-regulated kinase in glial cells.* J Pharmacol Exp Ther, 2007. **321**(1): p. 148-57.
58. Kugaya, A. and G. Sanacora, *Beyond monoamines: glutamatergic function in mood disorders.* CNS Spectr, 2005. **10**(10): p. 808-19.
59. Kodama, M., T. Fujioka, and R.S. Duman, *Chronic olanzapine or fluoxetine administration increases cell proliferation in hippocampus and prefrontal cortex of adult rat.* Biol Psychiatry, 2004. **56**(8): p. 570-80.
60. Paratcha, G., et al., *Released GFRalpha1 potentiates downstream signaling, neuronal survival, and differentiation via a novel mechanism of recruitment of c-Ret to lipid rafts.* Neuron, 2001. **29**(1): p. 171-84.

61. Garcia-Martinez, J.M., et al., *Glial cell line-derived neurotrophic factor promotes the arborization of cultured striatal neurons through the p42/p44 mitogen-activated protein kinase pathway.* J Neurosci Res, 2006. **83**(1): p. 68-79.
62. Di Benedetto, B., et al., *Acute antidepressant treatment differently modulates ERK/MAPK activation in neurons and astrocytes of the adult mouse prefrontal cortex.* Neuroscience, 2012.
63. Mercier, G., et al., *MAP kinase activation by fluoxetine and its relation to gene expression in cultured rat astrocytes.* J Mol Neurosci, 2004. **24**(2): p. 207-16.
64. Bagot, R.C., et al., *Epigenetic signaling in psychiatric disorders: stress and depression.* Dialogues Clin Neurosci, 2014. **16**(3): p. 281-95.
65. Akbarian, S. and H.S. Huang, *Epigenetic regulation in human brain-focus on histone lysine methylation.* Biol Psychiatry, 2009. **65**(3): p. 198-203.
66. Kendler, K.S., et al., *A Swedish national twin study of lifetime major depression.* Am J Psychiatry, 2006. **163**(1): p. 109-14.
67. Weaver, I.C., et al., *Epigenetic programming by maternal behavior.* Nat Neurosci, 2004. **7**(8): p. 847-54.
68. Cruceanu, C., et al., *H3K4 tri-methylation in synapsin genes leads to different expression patterns in bipolar disorder and major depression.* Int J Neuropsychopharmacol, 2013. **16**(2): p. 289-99.
69. Wang, D.D. and A. Bordey, *The astrocyte odyssey.* Prog Neurobiol, 2008. **86**(4): p. 342-67.
70. Kimelberg, H.K., *The problem of astrocyte identity.* Neurochem Int, 2004. **45**(2-3): p. 191-202.
71. Sofroniew, M.V. and H.V. Vinters, *Astrocytes: biology and pathology.* Acta Neuropathol, 2010. **119**(1): p. 7-35.
72. Pelvig, D.P., et al., *Neocortical glial cell numbers in human brains.* Neurobiol Aging, 2008. **29**(11): p. 1754-62.
73. Malatesta, P., et al.
74. Schmechel, D.E. and P. Rakic, *A Golgi study of radial glial cells in developing monkey telencephalon: morphogenesis and transformation into astrocytes.* Anat Embryol (Berl), 1979. **156**(2): p. 115-52.
75. Aguirre, A. and V. Gallo, *Postnatal neurogenesis and gliogenesis in the olfactory bulb from NG2-expressing progenitors of the subventricular zone.* J Neurosci, 2004. **24**(46): p. 10530-41.
76. Levison, S.W. and J.E. Goldman, *Multipotential and lineage restricted precursors coexist in the mammalian perinatal subventricular zone.* J Neurosci Res, 1997. **48**(2): p. 83-94.
77. Ganong and W. F, *Review of Medical Physiology*. Vol. 22nd edition. 2005: Lange medical books/ McGraw-Hill.
78. Miller, R.H. and M.C. Raff, *Fibrous and protoplasmic astrocytes are biochemically and developmentally distinct.* J Neurosci, 1984. **4**(2): p. 585-92.
79. Ventura, R. and K.M. Harris, *Three-dimensional relationships between hippocampal synapses and astrocytes.* J Neurosci, 1999. **19**(16): p. 6897-906.
80. Bushong, E.A., et al., *Protoplasmic astrocytes in CA1 stratum radiatum occupy separate anatomical domains.* J Neurosci, 2002. **22**(1): p. 183-92.
81. Gomes, F.C., D. Paulin, and V. Moura Neto, *Glial fibrillary acidic protein (GFAP): modulation by growth factors and its implication in astrocyte differentiation.* Braz J Med Biol Res, 1999. **32**(5): p. 619-31.
82. Liu, X., et al., *GFAP-expressing cells in the postnatal subventricular zone display a unique glial phenotype intermediate between radial glia and astrocytes.* Glia, 2006. **54**(5): p. 394-410.

83. Donato, R., *Functional roles of S100 proteins, calcium-binding proteins of the EF-hand type.* Biochim Biophys Acta, 1999. **1450**(3): p. 191-231.
84. Bezzi, P., et al., *Astrocytes contain a vesicular compartment that is competent for regulated exocytosis of glutamate.* Nat Neurosci, 2004. **7**(6): p. 613-20.
85. Toro, C.T., et al., *Glial fibrillary acidic protein and glutamine synthetase in subregions of prefrontal cortex in schizophrenia and mood disorder.* Neurosci Lett, 2006. **404**(3): p. 276-81.
86. Pav, M., et al., *Neurobiological aspects of depressive disorder and antidepressant treatment: role of glia.* Physiol Res, 2008. **57**(2): p. 151-64.
87. Liu, B. and A.H. Neufeld, *Activation of epidermal growth factor receptors in astrocytes: from development to neural injury.* J Neurosci Res, 2007. **85**(16): p. 3523-9.
88. Cornell-Bell, A.H., et al., *Glutamate induces calcium waves in cultured astrocytes: long-range glial signaling.* Science, 1990. **247**(4941): p. 470-3.
89. Wang, X., T. Takano, and M. Nedergaard, *Astrocytic calcium signaling: mechanism and implications for functional brain imaging.* Methods Mol Biol, 2009. **489**: p. 93-109.
90. Perea, G., M. Navarrete, and A. Araque, *Tripartite synapses: astrocytes process and control synaptic information.* Trends Neurosci, 2009. **32**(8): p. 421-31.
91. Czeh, B. and B. Di Benedetto, *Antidepressants act directly on astrocytes: evidences and functional consequences.* Eur Neuropsychopharmacol, 2013. **23**(3): p. 171-85.
92. Lu, P., et al., *Extracellular matrix degradation and remodeling in development and disease.* Cold Spring Harb Perspect Biol, 2011. **3**(12).
93. Brown, A.M. and B.R. Ransom, *Astrocyte glycogen and brain energy metabolism.* Glia, 2007. **55**(12): p. 1263-71.
94. Su, S., et al., *Inhibition of astroglial inwardly rectifying Kir4.1 channels by a tricyclic antidepressant, nortriptyline.* J Pharmacol Exp Ther, 2007. **320**(2): p. 573-80.
95. Guglielmi, L., et al., *Update on the implication of potassium channels in autism: K(+) channelautism spectrum disorder.* Front Cell Neurosci, 2015. **9**: p. 34.
96. Ballabh, P., A. Braun, and M. Nedergaard, *The blood-brain barrier: an overview: structure, regulation, and clinical implications.* Neurobiol Dis, 2004. **16**(1): p. 1-13.
97. Yoon, B.E. and C.J. Lee, *GABA as a rising gliotransmitter.* Front Neural Circuits, 2014. **8**: p. 141.
98. Schipke, C.G., I. Heuser, and O. Peters, *Antidepressants act on glial cells: SSRIs and serotonin elicit astrocyte calcium signaling in the mouse prefrontal cortex.* J Psychiatr Res, 2011. **45**(2): p. 242-8.
99. Haber, M. and K.K. Murai, *Reshaping neuron-glial communication at hippocampal synapses.* Neuron Glia Biol, 2006. **2**(1): p. 59-66.
100. Allen, N.J. and B.A. Barres, *Signaling between glia and neurons: focus on synaptic plasticity.* Curr Opin Neurobiol, 2005. **15**(5): p. 542-8.
101. Piet, R., et al., *Physiological contribution of the astrocytic environment of neurons to intersynaptic crosstalk.* Proc Natl Acad Sci U S A, 2004. **101**(7): p. 2151-5.
102. Seil, F.J., F.P. Eckenstein, and P.J. Reier, *Induction of dendritic spine proliferation by an astrocyte secreted factor.* Exp Neurol, 1992. **117**(1): p. 85-9.
103. Nishida, H. and S. Okabe, *Direct astrocytic contacts regulate local maturation of dendritic spines.* J Neurosci, 2007. **27**(2): p. 331-40.
104. Ongur, D., W.C. Drevets, and J.L. Price, *Glial reduction in the subgenual prefrontal cortex in mood disorders.* Proc Natl Acad Sci U S A, 1998. **95**(22): p. 13290-5.

105. Flügge, G. and Fuchs, *E. Social stress in tree shrews: Effects on physiology, brain function, and behavior in subordinate individuals.* Pharm. Biochem. and Behav. 2002. **73**(1): p: 247-258
106. D'Sa, C. and R.S. Duman, *Antidepressants and neuroplasticity.* Bipolar Disord, 2002. **4**(3): p. 183-94.
107. Maes, M., *The cytokine hypothesis of depression: inflammation, oxidative & nitrosative stress (IO&NS) and leaky gut as new targets for adjunctive treatments in depression.* Neuro Endocrinol Lett, 2008. **29**(3): p. 287-91.
108. Miller, A.H., V. Maletic, and C.L. Raison, *Inflammation and its discontents: the role of cytokines in the pathophysiology of major depression.* Biol Psychiatry, 2009. **65**(9): p. 732-41.
109. Czeh, B., et al., *Astroglial plasticity in the hippocampus is affected by chronic psychosocial stress and concomitant fluoxetine treatment.* Neuropsychopharmacology, 2006. **31**(8): p. 1616-26.
110. Jansson, L., et al., *Glial cell activation in response to electroconvulsive seizures.* Prog Neuropsychopharmacol Biol Psychiatry, 2009. **33**(7): p. 1119-28.
111. Conti, B., et al., *Region-specific transcriptional changes following the three antidepressant treatments electro convulsive therapy, sleep deprivation and fluoxetine.* Mol Psychiatry, 2007. **12**(2): p. 167-89.
112. Sillaber, I., et al., *Profiling of behavioral changes and hippocampal gene expression in mice chronically treated with the SSRI paroxetine.* Psychopharmacology (Berl), 2008. **200**(4): p. 557-72.
113. Fatemi, S.H., et al., *Chronic psychotropic drug treatment causes differential expression of connexin 43 and GFAP in frontal cortex of rats.* Schizophr Res, 2008. **104**(1-3): p. 127-34.
114. Liu, Q., et al., *Chronic clomipramine treatment restores hippocampal expression of glial cell line-derived neurotrophic factor in a rat model of depression.* J Affect Disord, 2012. **141**(2-3): p. 367-72.
115. Allaman, I., et al., *Fluoxetine regulates the expression of neurotrophic/growth factors and glucose metabolism in astrocytes.* Psychopharmacology (Berl), 2011. **216**(1): p. 75-84.
116. Di Benedetto, B., et al., *N-desalkylquetiapine activates ERK1/2 to induce GDNF release in C6 glioma cells: a putative cellular mechanism for quetiapine as antidepressant.* Neuropharmacology, 2012. **62**(1): p. 209-16.
117. Uchida, S., et al., *Epigenetic status of Gdnf in the ventral striatum determines susceptibility and adaptation to daily stressful events.* Neuron, 2011. **69**(2): p. 359-72.
118. Ohno, Y., et al., *Inhibition of astroglial Kir4.1 channels by selective serotonin reuptake inhibitors.* Brain Res, 2007. **1178**: p. 44-51.
119. Lodge, N.J. and Y.W. Li, *Ion channels as potential targets for the treatment of depression.* Curr Opin Drug Discov Devel, 2008. **11**(5): p. 633-41.
120. Bernard, R., et al., *Altered expression of glutamate signaling, growth factor, and glia genes in the locus coeruleus of patients with major depression.* Mol Psychiatry, 2011. **16**(6): p. 634-46.
121. Bechtholt-Gompf, A.J., et al., *Blockade of astrocytic glutamate uptake in rats induces signs of anhedonia and impaired spatial memory.* Neuropsychopharmacology, 2010. **35**(10): p. 2049-59.
122. Banasr, M., et al., *Glial pathology in an animal model of depression: reversal of stress-induced cellular, metabolic and behavioral deficits by the glutamate-modulating drug riluzole.* Mol Psychiatry, 2010. **15**(5): p. 501-11.

123. Kang, H.J., et al., *Decreased expression of synapse-related genes and loss of synapses in major depressive disorder.* Nat Med, 2012. **18**(9): p. 1413-7.
124. Maya Vetencourt, J.F., et al., *The antidepressant fluoxetine restores plasticity in the adult visual cortex.* Science, 2008. **320**(5874): p. 385-8.
125. Karpova, N.N., et al., *Fear erasure in mice requires synergy between antidepressant drugs and extinction training.* Science, 2011. **334**(6063): p. 1731-4.
126. Magarinos, A.M., et al., *Chronic psychosocial stress causes apical dendritic atrophy of hippocampal CA3 pyramidal neurons in subordinate tree shrews.* J Neurosci, 1996. **16**(10): p. 3534-40.
127. Ampuero, E., et al., *Chronic fluoxetine treatment induces structural plasticity and selective changes in glutamate receptor subunits in the rat cerebral cortex.* Neuroscience, 2010. **169**(1): p. 98-108.
128. Rajkowska, G., et al., *Coverage of blood vessels by astrocytic endfeet is reduced in major depressive disorder.* Biol Psychiatry, 2013. **73**(7): p. 613-21.
129. Nielsen, S., et al., *Specialized membrane domains for water transport in glial cells: high-resolution immunogold cytochemistry of aquaporin-4 in rat brain.* J Neurosci, 1997. **17**(1): p. 171-80.
130. Papadopoulos, M.C. and A.S. Verkman, *Aquaporin water channels in the nervous system.* Nat Rev Neurosci, 2013. **14**(4): p. 265-77.
131. Kong, H., et al., *Aquaporin-4 knockout exacerbates corticosterone-induced depression by inhibiting astrocyte function and hippocampal neurogenesis.* CNS Neurosci Ther, 2014. **20**(5): p. 391-402.
132. Zheng, G.Q., et al., *Beyond water channel: aquaporin-4 in adult neurogenesis.* Neurochem Int, 2010. **56**(5): p. 651-4.
133. Waddington, Conrad, and Hal, *Organisers and Genes*. 1940, Cambridge University Press: Cambridge.
134. Russo and VEA, *Epigenetic mechanisms of gene regulation*. 1996, Woodbury: Cold Spring Harbour Laboratory Press.
135. Bird, A., *DNA methylation patterns and epigenetic memory.* Genes Dev, 2002. **16**(1): p. 6-21.
136. Weber, M. and D. Schubeler, *Genomic patterns of DNA methylation: targets and function of an epigenetic mark.* Curr Opin Cell Biol, 2007. **19**(3): p. 273-80.
137. Hervouet, E., F.M. Vallette, and P.F. Cartron, *Dnmt3/transcription factor interactions as crucial players in targeted DNA methylation.* Epigenetics, 2009. **4**(7): p. 487-99.
138. Tan, M., et al., *Identification of 67 histone marks and histone lysine crotonylation as a new type of histone modification.* Cell, 2011. **146**(6): p. 1016-28.
139. Zhang, Z., et al., *Identification of lysine succinylation as a new post-translational modification.* Nat Chem Biol, 2011. **7**(1): p. 58-63.
140. Izzo, A. and R. Schneider, *Chatting histone modifications in mammals.* Brief Funct Genomics, 2010. **9**(5-6): p. 429-43.
141. Peter, C.J. and S. Akbarian, *Balancing histone methylation activities in psychiatric disorders.* Trends Mol Med, 2011. **17**(7): p. 372-9.
142. Latham, J.A. and S.Y.R. Dent, *Cross-regulation of histone modifications.*
143. Jenuwein, T. and C.D. Allis, *Translating the histone code.* Science, 2001. **293**(5532): p. 1074-80.
144. Tsankova, N.M., et al., *Sustained hippocampal chromatin regulation in a mouse model of depression and antidepressant action.* Nat Neurosci, 2006. **9**(4): p. 519-25.
145. Schmauss, C., *An HDAC-dependent epigenetic mechanism that enhances the efficacy of the antidepressant drug fluoxetine.* Sci Rep, 2015. **5**: p. 8171.

146. Covington, H.E., 3rd, et al., *Antidepressant action of HDAC inhibition in the prefrontal cortex.* Neuroscience, 2015. **298**: p. 329-35.
147. Covington, H.E., 3rd, et al., *Antidepressant actions of histone deacetylase inhibitors.* J Neurosci, 2009. **29**(37): p. 11451-60.
148. Renthal, W., et al., *Histone deacetylase 5 epigenetically controls behavioral adaptations to chronic emotional stimuli.* Neuron, 2007. **56**(3): p. 517-29.
149. Benton, C.S., et al., *Evaluating genetic markers and neurobiochemical analytes for fluoxetine response using a panel of mouse inbred strains.* Psychopharmacology (Berl), 2012. **221**(2): p. 297-315.
150. Gupta, S., et al., *Histone methylation regulates memory formation.* J Neurosci, 2010. **30**(10): p. 3589-99.
151. Jakovcevski, M., et al., *Neuronal Kmt2a/Mll1 histone methyltransferase is essential for prefrontal synaptic plasticity and working memory.* J Neurosci, 2015. **35**(13): p. 5097-108.
152. Huang, H.S., et al., *Prefrontal dysfunction in schizophrenia involves mixed-lineage leukemia 1-regulated histone methylation at GABAergic gene promoters.* J Neurosci, 2007. **27**(42): p. 11254-62.
153. Tahiliani, M., et al., *The histone H3K4 demethylase SMCX links REST target genes to X-linked mental retardation.* Nature, 2007. **447**(7144): p. 601-5.
154. Pereira, J.D., et al., *Ezh2, the histone methyltransferase of PRC2, regulates the balance between self-renewal and differentiation in the cerebral cortex.* Proc Natl Acad Sci U S A, 2010. **107**(36): p. 15957-62.
155. Burgold, T., et al., *The histone H3 lysine 27-specific demethylase Jmjd3 is required for neural commitment.* PLoS One, 2008. **3**(8): p. e3034.
156. Kuzumaki, N., et al., *Hippocampal epigenetic modification at the brain-derived neurotrophic factor gene induced by an enriched environment.* Hippocampus, 2011. **21**(2): p. 127-32.
157. Ernst, C., E.S. Chen, and G. Turecki, *Histone methylation and decreased expression of TrkB.T1 in orbital frontal cortex of suicide completers*, in *Mol Psychiatry*. 2009: England. p. 830-2.
158. Tsankova, N.M., A. Kumar, and E.J. Nestler, *Histone modifications at gene promoter regions in rat hippocampus after acute and chronic electroconvulsive seizures.* J Neurosci, 2004. **24**(24): p. 5603-10.
159. Karpova, N.N., et al., *Long-lasting behavioural and molecular alterations induced by early postnatal fluoxetine exposure are restored by chronic fluoxetine treatment in adult mice.* Eur Neuropsychopharmacol, 2009. **19**(2): p. 97-108.
160. Zhang, X., et al., *Electroconvulsive therapy increases glial cell-line derived neurotrophic factor (GDNF) serum levels in patients with drug-resistant depression.* Psychiatry Res, 2009. **170**(2-3): p. 273-5.
161. Nagy, C., et al., *Astrocytic abnormalities and global DNA methylation patterns in depression and suicide.* Mol Psychiatry, 2015. **20**(3): p. 320-8.
162. Shaltiel, G., et al., *Evidence for the involvement of the kainate receptor subunit GluR6 (GRIK2) in mediating behavioral displays related to behavioral symptoms of mania.* Mol Psychiatry, 2008. **13**(9): p. 858-72.
163. Li, B., et al., *Down-regulation of GluK2 kainate receptor expression by chronic treatment with mood-stabilizing anti-convulsants or lithium in cultured astrocytes and brain, but not in neurons.* Neuropharmacology, 2009. **57**(4): p. 375-85.
164. Neumann, I.D., A.H. Veenema, and D.I. Beiderbeck, *Aggression and anxiety: social context and neurobiological links.* Front Behav Neurosci, 2010. **4**: p. 12.

165. Neumann, I.D., et al., *Animal models of depression and anxiety: What do they tell us about human condition?* Prog Neuropsychopharmacol Biol Psychiatry, 2011. **35**(6): p. 1357-75.
166. Crawley, J. and F.K. Goodwin, *Preliminary report of a simple animal behavior model for the anxiolytic effects of benzodiazepines.* Pharmacol Biochem Behav, 1980. **13**(2): p. 167-70.
167. Landgraf, R. and A. Wigger, *High vs low anxiety-related behavior rats: an animal model of extremes in trait anxiety.* Behav Genet, 2002. **32**(5): p. 301-14.
168. Landgraf, R., et al., *Candidate genes of anxiety-related behavior in HAB/LAB rats and mice: focus on vasopressin and glyoxalase-I.* Neurosci Biobehav Rev, 2007. **31**(1): p. 89-102.
169. Liebsch, G., et al., *Behavioural profiles of two Wistar rat lines selectively bred for high or low anxiety-related behaviour.* Behav Brain Res, 1998. **94**(2): p. 301-10.
170. Ohl, F., et al., *Cognitive performance in rats differing in their inborn anxiety.* Behav Neurosci, 2002. **116**(3): p. 464-71.
171. Salome, N., et al., *Reliability of high and low anxiety-related behaviour: influence of laboratory environment and multifactorial analysis.* Behav Brain Res, 2002. **136**(1): p. 227-37.
172. Slattery, D.A. and J.F. Cryan, *The ups and downs of modelling mood disorders in rodents.* Ilar j, 2014. **55**(2): p. 297-309.
173. Slattery, D.A. and I.D. Neumann, *Chronic icv oxytocin attenuates the pathological high anxiety state of selectively bred Wistar rats.* Neuropharmacology, 2010. **58**(1): p. 56-61.
174. Keck, M.E., et al., *Vasopressin mediates the response of the combined dexamethasone/CRH test in hyper-anxious rats: implications for pathogenesis of affective disorders.* Neuropsychopharmacology, 2002. **26**(1): p. 94-105.
175. Keck, M.E., et al., *The anxiolytic effect of the CRH(1) receptor antagonist R121919 depends on innate emotionality in rats.* Eur J Neurosci, 2001. **13**(2): p. 373-80.
176. Landgraf, R., et al., *Hyper-reactive hypothalamo-pituitary-adrenocortical axis in rats bred for high anxiety-related behaviour.* J Neuroendocrinol, 1999. **11**(6): p. 405-7.
177. Ising, M., et al., *The combined dexamethasone/CRH test as a potential surrogate marker in depression.* Prog Neuropsychopharmacol Biol Psychiatry, 2005. **29**(6): p. 1085-93.
178. Keck, M.E., et al., *Differences in serotonergic neurotransmission between rats displaying high or low anxiety/depression-like behaviour: effects of chronic paroxetine treatment.* J Neurochem, 2005. **92**(5): p. 1170-9.
179. Miguel-Hidalgo, J.J., et al., *Morphometric analysis of vascular pathology in the orbitofrontal cortex of older subjects with major depression.* Int J Geriatr Psychiatry, 2013. **28**(9): p. 959-70.
180. Fairlie, W.D., et al., *MIC-1 is a novel TGF-beta superfamily cytokine associated with macrophage activation.* J Leukoc Biol, 1999. **65**(1): p. 2-5.
181. Subramaniam, S., J. Strelau, and K. Unsicker, *Growth differentiation factor-15 prevents low potassium-induced cell death of cerebellar granule neurons by differential regulation of Akt and ERK pathways.* J Biol Chem, 2003. **278**(11): p. 8904-12.
182. Bottner, M., et al., *Characterization of the rat, mouse, and human genes of growth/differentiation factor-15/macrophage inhibiting cytokine-1 (GDF-15/MIC-1).* Gene, 1999. **237**(1): p. 105-11.

183. Bauskin, A.R., et al., *The TGF-beta superfamily cytokine MIC-1/GDF15: secretory mechanisms facilitate creation of latent stromal stores.* J Interferon Cytokine Res, 2010. **30**(6): p. 389-97.
184. Wollert, K.C. and T. Kempf, *Growth differentiation factor 15 in heart failure: an update.* Curr Heart Fail Rep, 2012. **9**(4): p. 337-45.
185. Xu, X., Z. Li, and W. Gao, *Growth differentiation factor 15 in cardiovascular diseases: from bench to bedside.* Biomarkers, 2011. **16**(6): p. 466-75.
186. Strelau, J., et al., *Growth/differentiation factor-15/macrophage inhibitory cytokine-1 is a novel trophic factor for midbrain dopaminergic neurons in vivo.* J Neurosci, 2000. **20**(23): p. 8597-603.
187. Unsicker, K., B. Spittau, and K. Krieglstein, *The multiple facets of the TGF-beta family cytokine growth/differentiation factor-15/macrophage inhibitory cytokine-1.* Cytokine Growth Factor Rev, 2013. **24**(4): p. 373-84.
188. Frye, M.A., et al., *Feasibility of investigating differential proteomic expression in depression: implications for biomarker development in mood disorders.* Transl Psychiatry, 2015. **5**: p. e689.
189. Teunissen, C.E., et al., *The inflammatory marker GDF-15 is not independently associated with late-life depression.* J Psychosom Res, 2016. **83**: p. 46-9.
190. Lisabeth, E.M., G. Falivelli, and E.B. Pasquale, *Eph receptor signaling and ephrins.* Cold Spring Harb Perspect Biol, 2013. **5**(9).
191. Pasquale, E.B., *Eph receptor signalling casts a wide net on cell behaviour.* Nat Rev Mol Cell Biol, 2005. **6**(6): p. 462-75.
192. Pasquale, E.B., *Eph-ephrin bidirectional signaling in physiology and disease.* Cell, 2008. **133**(1): p. 38-52.
193. Xu, N.J. and M. Henkemeyer, *Ephrin-B3 reverse signaling through Grb4 and cytoskeletal regulators mediates axon pruning.* Nat Neurosci, 2009. **12**(3): p. 268-76.
194. Hattori, M., M. Osterfield, and J.G. Flanagan, *Regulated cleavage of a contact-mediated axon repellent.* Science, 2000. **289**(5483): p. 1360-5.
195. Goldshmit, Y., et al., *EphA4 blockers promote axonal regeneration and functional recovery following spinal cord injury in mice.* PLoS One, 2011. **6**(9): p. e24636.
196. Fu, A.K., et al., *Blockade of EphA4 signaling ameliorates hippocampal synaptic dysfunctions in mouse models of Alzheimer's disease.* Proc Natl Acad Sci U S A, 2014. **111**(27): p. 9959-64.
197. Jing, X., et al., *Ephrin-A1-mediated dopaminergic neurogenesis and angiogenesis in a rat model of Parkinson's disease.* PLoS One, 2012. **7**(2): p. e32019.
198. Day, B.W., et al., *EphA3 maintains tumorigenicity and is a therapeutic target in glioblastoma multiforme.* Cancer Cell, 2013. **23**(2): p. 238-48.
199. Zhang, R.-X., et al., *EphB2 in the Medial Prefrontal Cortex Regulates Vulnerability to Stress.*
200. Murai, K.K., et al., *Control of hippocampal dendritic spine morphology through ephrin-A3/EphA4 signaling.* Nat Neurosci, 2003. **6**(2): p. 153-60.
201. Guellmar, A., J. Rudolph, and J. Bolz, *Structural alterations of spiny stellate cells in the somatosensory cortex in ephrin-A5-deficient mice.* J Comp Neurol, 2009. **517**(5): p. 645-54.
202. Hruska, M. and M.B. Dalva, *Ephrin regulation of synapse formation, function and plasticity.* Mol Cell Neurosci, 2012. **50**(1): p. 35-44.
203. Murai, K.K. and E.B. Pasquale, *Eph receptors and ephrins in neuron-astrocyte communication at synapses.* Glia, 2011. **59**(11): p. 1567-78.
204. Filosa, A., et al., *Neuron-glia communication via EphA4/ephrin-A3 modulates LTP through glial glutamate transport.* Nat Neurosci, 2009. **12**(10): p. 1285-92.

205. Carmona, M.A., et al., *Glial ephrin-A3 regulates hippocampal dendritic spine morphology and glutamate transport.* Proc Natl Acad Sci U S A, 2009. **106**(30): p. 12524-9.
206. Allen, J.W., L.A. Mutkus, and M. Aschner, *Isolation of neonatal rat cortical astrocytes for primary cultures.* Curr Protoc Toxicol, 2001. **Chapter 12**: p. Unit12 4.
207. Bressler, J.P., R. Cole, and J. de Vellis, *Cell culture systems to study glial transformation.* Dev Toxicol Environ Sci, 1980. **8**: p. 187-92.
208. Schneider, C.A., W.S. Rasband, and K.W. Eliceiri, *NIH Image to ImageJ: 25 years of image analysis.* Nat Meth, 2012. **9**(7): p. 671-675.
209. Di Benedetto, B., et al., *Fluoxetine requires the endfeet protein aquaporin-4 to enhance plasticity of astrocyte processes.*
210. Collas, P., *The current state of chromatin immunoprecipitation.* Mol Biotechnol, 2010. **45**(1): p. 87-100.
211. Cheung, I., et al., *Developmental regulation and individual differences of neuronal H3K4me3 epigenomes in the prefrontal cortex.* Proceedings of the National Academy of Sciences, 2010. **107**(19): p. 8824-8829.
212. Tanasic, S., et al., *Desipramine targets astrocytes to attenuate synaptic plasticity via modulation of the ephrinA3/EphA4 signalling.* Neuropharmacology, 2016. **105**: p. 154-163.
213. Meijering, E., et al., *Design and validation of a tool for neurite tracing and analysis in fluorescence microscopy images.* Cytometry A, 2004. **58**(2): p. 167-76.
214. Meijering, E., *Neuron tracing in perspective.* Cytometry A, 2010. **77**(7): p. 693-704.
215. Parri, M., et al., *EphrinA1 repulsive response is regulated by an EphA2 tyrosine phosphatase.* J Biol Chem, 2005. **280**(40): p. 34008-18.
216. Wu, D., et al., *Prognostic value of EphA2 and EphrinA-1 in squamous cell cervical carcinoma.* Gynecol Oncol, 2004. **94**(2): p. 312-9.
217. Kinch, M.S. and K. Carles-Kinch, *Overexpression and functional alterations of the EphA2 tyrosine kinase in cancer.* Clin Exp Metastasis, 2003. **20**(1): p. 59-68.
218. Finne, E.F., E. Munthe, and H.C. Aasheim, *A new ephrin-A1 isoform (ephrin-A1b) with altered receptor binding properties abrogates the cleavage of ephrin-A1a.* Biochem J, 2004. **379**(Pt 1): p. 39-46.
219. Strelau, J., et al., *Expression and putative functions of GDF-15, a member of the TGF-beta superfamily, in human glioma and glioblastoma cell lines.* Cancer Lett, 2008. **270**(1): p. 30-9.
220. Robison, A.J., et al., *Fluoxetine epigenetically alters the CaMKIIalpha promoter in nucleus accumbens to regulate DeltaFosB binding and antidepressant effects.* Neuropsychopharmacology, 2014. **39**(5): p. 1178-86.
221. Muigg, P., et al., *Altered brain activation pattern associated with drug-induced attenuation of enhanced depression-like behavior in rats bred for high anxiety.* Biol Psychiatry, 2007. **61**(6): p. 782-96.
222. Gibbons, R.D., et al., *Who Benefits from Antidepressants?: Synthesis of 6-Week Patient-Level Outcomes from Double-Blind Placebo Controlled Randomized Trials of Fluoxetine and Venlafaxine.* Arch Gen Psychiatry, 2012. **69**(6): p. 572-9.
223. Nasca, C., et al., *Stress dynamically regulates behavior and glutamatergic gene expression in hippocampus by opening a window of epigenetic plasticity.* Proc Natl Acad Sci U S A, 2015. **112**(48): p. 14960-5.
224. Vastenhouw, N.L. and A.F. Schier, *Bivalent histone modifications in early embryogenesis.* Curr Opin Cell Biol, 2012. **24**(3): p. 374-86.

225. Fass, D.M., et al., *Epigenetic mechanisms in mood disorders: targeting neuroplasticity.* Neuroscience, 2014. **264**: p. 112-30.
226. Nestor, M.W., et al., *Plasticity of neuron-glial interactions mediated by astrocytic EphARs.* J Neurosci, 2007. **27**(47): p. 12817-28.
227. Liu, D.P., et al., *Ephrin-A1 is a negative regulator in glioma through down-regulation of EphA2 and FAK.* Int J Oncol, 2007. **30**(4): p. 865-71.
228. Li, S., et al., *GDF10 Is a Signal for Axonal Sprouting and Functional Recovery after Stroke.* Nat Neurosci, 2015. **18**(12): p. 1737-45.